Bulletin
of
The Geological Society of America

VOLUME 62 | April 1951 | NUMBER 4

CONTENTS

	Pages
Global strain accumulation and release as revealed by great earthquakes. By Hugo Benioff	331–338
Geology of the Barrilla Mountains, Texas. By G. K. Eifler, Jr.	339–354
Mechanical basis for certain familiar geologic structures. By M. King Hubbert	355–372
Stress distributions and faulting. By W. Hafner	373–398
Measurement of paleotemperatures and temperatures of the Upper Cretaceous of England, Denmark, and the Southeastern United States. By H. C. Urey, H. A. Lowenstam, S. Epstein, and C. R. McKinney	399–416
Carbonate-water isotopic temperature scale. By Samuel Epstein, Ralph Buchsbaum, Heinz Lowenstam, and Harold C. Urey	417–426

Subscription $15 per year.

Publication Office: Mt. Royal & Guilford Aves., Baltimore 2, Md.

Communications for publication should be addressed to The Geological Society of America, Dr. H. R. Aldrich, Secretary, 419 West 117th Street, New York 27, N. Y.

NOTICE.—Four weeks notice of change of address is necessary. In accordance with the rules established by the Council, claims for non-receipt of the preceding number of the Bulletin must be sent to the Secretary of the Society within three months of the date of the receipt of this number in order to be filled gratis.

Entered as second-class matter in the Post-Office at Baltimore, Md., under the Act of Congress of July 16, 1894.

Accepted for mailing at special rate of postage provided for in Section 1103, Act of October 3, 1917, authorized on July 8, 1918

PAPERS IN PRESS FOR FORTHCOMING ISSUES

Sedimentary Basins of Arizona and Adjoining Areas. By E. D. McKee

Alteration Features at Silver Bell, Arizona. By Paul F. Kerr

Geology of the Cedar Hills, Utah. By Stuart L. Schoff

Submarine Topography in the North Atlantic. By Ivan Tolstoy

Crustal Layers of the Continents and Oceans. By B. Gutenberg

Form and Structure of Sills near Pando, Colorado. By Ogden Tweto

Younger Intrusive Rocks of Plateau Province, Nigeria, Compared with the Alkalic Rocks of New England. By Robert Greenwood

Metamorphosed Igneous Rocks of the Merrimac Area in Plumas National Forest, California. By Anna Hietanen

Analogy between Diffusion and Electrical Conductivity in Porous Rocks. By L. J. Klinkenberg

Barite Concretions from the Ocean Floor. By Roger Revelle and K. O. Emery

BULLETIN OF THE GEOLOGICAL SOCIETY OF AMERICA
VOL. 62, PP. 331-338, 7 FIGS. APRIL 1951

GLOBAL STRAIN ACCUMULATION AND RELEASE AS REVEALED BY GREAT EARTHQUAKES

By Hugo Benioff

Abstract

The strain-rebound characteristic of the sequence of all great shallow earthquakes of magnitudes 8.0 and greater which have occurred since 1904 exhibits a saw-tooth shape with very nearly linear segments. The serration amplitudes and periods have been decreasing linearly with time since the beginning of the sequence. If a proposed interpretation is correct, the characteristic indicates the following conclusions: (1) Earthquakes in this magnitude range are not independent events, but are related in some form of world-wide stress system. (2) From 1908 (and presumably 1904) to 1950 the rate of total secular strain generation in the crustal layer in which these earthquakes originate was remarkably constant. (3) The strain was released in five active periods of decreasing lengths separated by quiescent intervals of very small or no activity during which crustal strain accumulated at a constant rate. (4) During the active periods the strain release proceeded at approximately twice the rate of secular strain generation.

The strain-rebound characteristic of the sequence of all great earthquakes of intermediate depth (h = 70-300 km) exhibits no resemblance to that of the shallow sequence.

The strain-rebound characteristic of the sequence of all great deep earthquakes ($h \geq 300$ km) can be represented by the equation $S = a + b \log t$ indicating that activity at this depth has been falling off continuously since 1904.

The different behavior of the three sequences is considered evidence for the existence of three layers in the earth's crust having different relative movements in the tectonic sense.

Heretofore evidence for layering in the earth's crust has been derived from studies of the propagation of seismic waves and is thus limited to short-time mechanical properties (less than 5 minutes) only. The world strain-rebound characteristics presented herein provide the first evidence for layering on the basis of secular tectonic mechanical properties. From this point of view, the crust is made up of three distinct layers each with its own proper movement, the shallow 0–70 km, intermediate 70–300 km, and deep 300–680 km approximately.

CONTENTS

	Page
Introduction	332
Sequence of great shallow earthquakes	332
Sequence of great earthquakes of intermediate depth	336
Sequence of great deep earthquakes	336
Crustal structure of the earth	338
References cited	338

ILLUSTRATIONS

Figure	Page
1. Strain-rebound characteristic. Sequence of all great shallow earthquakes magnitudes ≥ 8.0	333
2. Observed periods in strain-rebound characteristic. Sequence of all great shallow earthquakes	334
3. Origin times of terminating shocks of active intervals in the sequence of great shallow earthquakes	334
4. Epicenters of terminating earthquakes of active intervals in the sequence of great shallow earthquakes	335
5. Strain-rebound characteristic. Sequence of all shallow earthquakes magnitudes $\geq 7\frac{1}{4}$	336
6. Strain rebound characteristic. Sequence of all intermediate depth (70–300 km) earthquakes magnitudes ≥ 7.0	337
7. Strain rebound characteristic. Sequence of all deep (300–680 km) earthquakes magnitudes ≥ 7.0	337

Introduction

The elastic strain-rebound accompanying or producing an earthquake can be calculated from the seismic energy by means of a method described in an earlier paper (Benioff, 1949). The energy J is derived from the earthquake magnitude M in accordance with the following relation due to Gutenberg and Richter (1942).

$$\log J = 12 + 1.8\,M \tag{1}$$

Briefly, the method assumes that an earthquake is generated by the elastic rebound of a volume V of rock having an average elastic constant μ, and an average elastic strain ϵ preceding the earthquake. The energy stored in the rock as elastic strain is therefore

$$J = \tfrac{1}{2}\mu\epsilon^2 V \tag{2}$$

Assuming the conversion efficiency of strain energy into seismic waves is unity—which cannot be far wrong—J is then also the energy of the earthquake and ϵ is also the strain rebound. Taking the square root of equation (2) we may write

$$J^{\frac{1}{2}} = (\tfrac{1}{2}\mu V)^{\frac{1}{2}}\epsilon \tag{3}$$

In general it is not possible to determine μ and V but for any given active fault it may be assumed that they are constant so that

$$J^{\frac{1}{2}} = \epsilon C \tag{4}$$

where $C = (\frac{1}{2}\mu V)^{\frac{1}{2}}$. The square root of the earthquake energy is thus proportional to the elastic strain-rebound. Consequently, for a sequence of shocks occurring on a given fault, a graph of the accumulated sum S of the increments $J_i^{\frac{1}{2}}$ plotted against time, represents the elastic strain-rebound characteristic (times C) of the sequence.

A study of the elastic strain-rebound characteristics of a number of aftershocks indicated that aftershocks are produced by elastic afterworking of the fault rock (Benioff, 1950). Applied to a sequence of earthquakes other than aftershocks, the method has provided evidence that oceanic deeps are the surface expressions of great faults which dip under the neighboring continents (Benioff, 1949).

Sequence of Great Shallow Earthquakes

In this paper the method is applied to three world sequences of great earthquakes extending back to 1904 when reliable instrumental observations first became available. Attention will be directed first to the sequence of great shallow earthquakes (h <70 km) of magnitudes 8 and larger. The data for this sequence are taken from the catalog of Gutenberg and Richter (1949) and represent a total of 48 shocks[1]. Since the earthquakes of this sequence occurred on many different faults having presumably different values of μ and V, it was not anticipated that a plot of the strain-rebound characteristic would be of significance. However, when the graph was constructed (Fig. 1), its singular form and regularity indicated that this pessimistic view was not justified. Presumably μ and V or the product μV are substantially constant for all faults on which these great shocks occur. The characteristic approximates a saw-tooth curve with amplitudes and periods which decrease linearly with the time. Thus, beginning in 1904, the shocks were occurring frequently and the magnitudes were so related that the strain-rebound increments formed a large, nearly linear curve-segment of relatively long duration. The activity representing this segment of the curve ceased abruptly with the earthquake of 1907 October 21. Thereafter, except for the two shocks of 1911 January 3, and 1912 May 23, all of the faults were relatively quiescent for some 9½ years until the earthquake of 1917 May 1 initiated the next active period. In this period, the average strain release continued at a nearly constant rate for 7 years and ended with the shock of 1924 April 14. Except for 3 earthquakes, the faults again remained relatively quiescent until the new cycle of activity began 1931 August 10. Similar alternate intervals of activity and quiescence, but with decreasing durations and amplitudes, have been continuing up to the date of this writing.

The initial points A, B, C, and D of the active intervals mark the times when the accumulated world strain was maximum. The end points a, b, c, d, and e of the active intervals mark the

[1] Data for the last 3 shocks which occurred since the catalogue went to press were kindly given to me directly by Dr. Gutenberg.

times at which the accumulated world strain passed through minima. The upper dashed line drawn through the points of minimum strain must therefore represent the total secular strain generation (times C of equation (4)) of the system. The small spread of points on this line indicates that the rate of strain generation has been remarkably constant since 1907 and presumably since 1904. For any given date, the vertical separation between corresponding points on the generation line and the strain-rebound characteristic is a measure of the accumulated world strain (times C) available for the production of earthquakes in the magnitude range here studied. Since during the active intervals the average strain-release segment is very nearly linear, it may be concluded that earthquakes in this magnitude range are not independent events, in that the release of strain by one shock effects the time and presumably the amount of strain-release of following shocks. In order to explain the alternating intervals of activity and quiescence, it is necessary to assume the existence of some world-wide mechanism which locks all of the faults simultaneously, possibly through variations in the normal stress on the fault surfaces. Thus, although global strain is being generated at a constant rate given by the slope of the upper dotted line, it is released only during the intervals when the fault-locking is reduced.

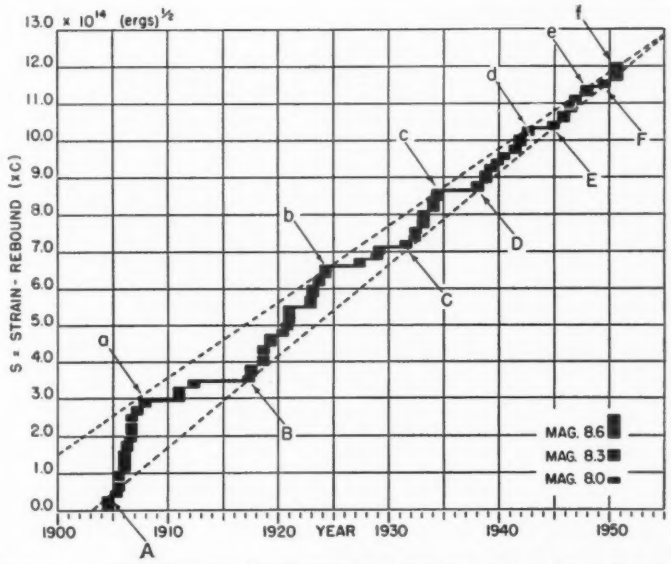

FIGURE 1. STRAIN-REBOUND CHARACTERISTIC. SEQUENCE OF ALL GREAT SHALLOW EARTHQUAKES MAGNITUDES $\geq$ 8.0

Each black rectangle represents the elastic strain-rebound increment accompanying a particular earthquake sequence. The height of the rectangle is proportional to the size of the increment and is related to the earthquake magnitude as shown in the legend. Blank spaces between rectangles have been provided in the few cases where the time-interval between two shocks is so small as to make the two corresponding rectangles appear as one.

At the present date, the oscillatory amplitude of the characteristic is so small that there is no effective secular accumulation, and strain is being released substantially as fast as it is being generated. Referring again to Figure 1, it may be seen that the serration amplitudes of the strain-rebound curve decrease linearly with the time, since they define the two converging dashed lines (Fig. 1). The consecutive periods also decrease linearly with time as shown by the curve (Fig. 2).

Figure 3 is a plot of the origin times of the terminating earthquakes of the active intervals.

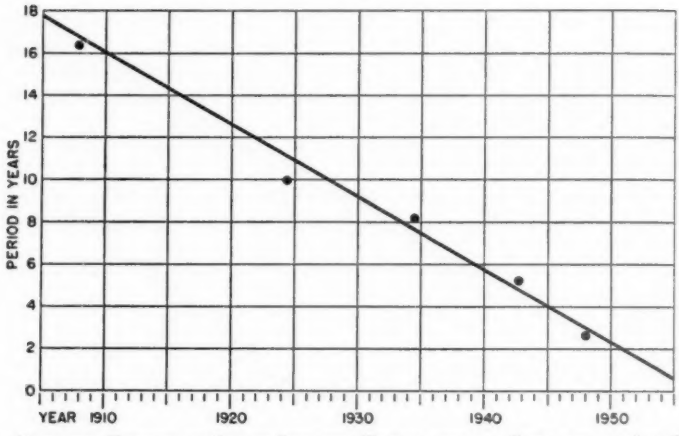

FIGURE 2. OBSERVED PERIODS IN STRAIN-REBOUND CHARACTERISTIC. SEQUENCE OF ALL GREAT SHALLOW EARTHQUAKES

The time-intervals ab, bc, cd, and de (Fig. 1) between accumulated world strain minima are plotted as ordinates and the times of the beginnings of the intervals as abscissas.

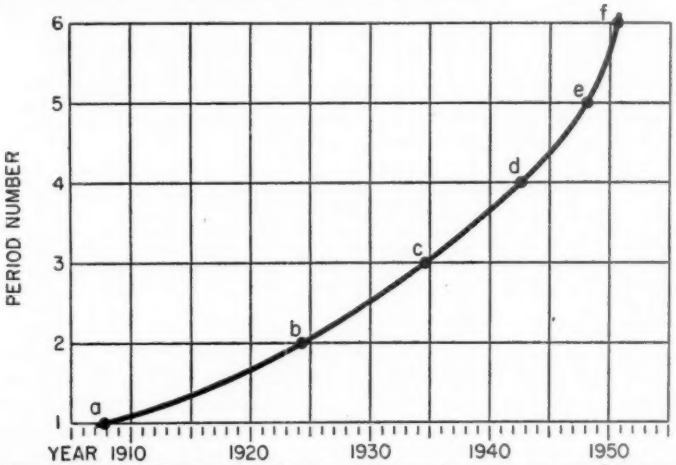

FIGURE 3. ORIGIN TIMES OF TERMINATING SHOCKS OF ACTIVE INTERVALS IN THE SEQUENCE OF GREAT SHALLOW EARTHQUAKES.

The shocks are designated a, b, c, d, e, and f to correspond with Figs. 1 and 2.

It appears that the great earthquake of 1950 August 15, designated f on the figure, marks not only the end of the minor active interval with which it is associated, but also the end of the whole secular period which began prior to 1904.

Epicenters of the terminating earthquakes are plotted on a world map in Figure 4. The dashed circle drawn to fit the points is very nearly a great circle and hence defines a plane passing through the center of the earth. The pole of this circle, indicated by the two small concentric circles on the map, is situated approximately at $\phi = 55°$ N, $\lambda = 127°$ W. It may be mere chance that the six epicenters fall so nearly on a plane. If not, then this plane may define some fundamental shearing surface which divides the earth into hemispheres.

In view of the short interval during which observations have been available, it is not possible to determine whether or not the characteristic is cyclic in nature. If it is, the amplitudes

and periods should begin to increase within a short time. On the other hand, if the characteristic represents a transient oscillation, there may be a long quiescent interval during which strain is accumulated, before the oscillatory activity begins again.

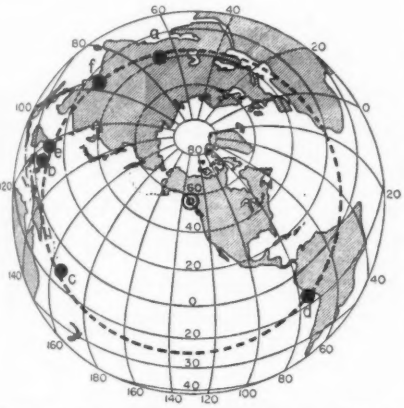

FIGURE 4. EPICENTERS OF TERMINATING EARTHQUAKES OF ACTIVE INTERVALS IN THE SEQUENCE OF GREAT SHALLOW EARTHQUAKES
The shocks are designated a, b, c, d, e, and f in accordance with Figs. 1 and 2.

A possible cause of the simultaneous locking of all the great faults is a variation in the dimension of the earth's radius such as has been postulated by astronomers to explain the observed changes in the length of the day. On this basis, to account for the shape of the strain-rebound characteristic, it would be necessary to assume that the earth is executing some form of radial relaxation oscillation in which both the period and the amplitude have been decreasing since 1904 or earlier. During the phases of oscillation when the radius is short, the normal stress on the faults is increased and they become quiescent. Likewise, when the radius is long, the normal stress is reduced and the faults become active.

Another possible interpretation of the origin of the sawtooth-shaped characteristic is suggested by its similarity to the motion of a bowed string. Thus the constant speed of the bow corresponds with a constant rate of strain generation within the crust. At the conclusion of an active period the faults all become locked corresponding with the phase in the bowed-string cycle when the string becomes attached to the bow. During the quiescent period, the strain accumulates at a constant rate in the same way that the string is displaced by the bow at a constant rate. Finally, when the stress becomes greater than the locking friction, the faults begin to slip and this corresponds with the condition in the string cycle when the bow loses hold of the string. The constant rate of strain relief during the active periods would thus be determined by some form of solid friction involving the whole shallow crustal layer of the earth. The change in period and amplitude with time can be attributed to a secular change in normal force on the faults rather than a short-time variation determined by the saw-tooth period as suggested in the preceding hypothesis. In the string analogy, a change in bow pressure changes the amplitude of string vibration but not the period. This results from the fact that the string period is determined by mass and elastic reactions. On the other hand, in the general crustal movements of the earth, the mass effects are negligible, and the period is determined by elastic and frictional forces only. In this type of oscillation it should be possible to set up conditions in which period is proportional to amplitude.

By either hypothesis, it is difficult to explain the fact that the magnitudes of the shocks appear to be independent of the total accumulated crustal strains. When the strain is large it is relieved by a large number of shocks occurring during an active interval of long duration rather than by a small number of larger shocks occurring in a short active period.

If the shallow sequence is extended to include all of the world class A shocks of Gutenberg and Richter by adding the remaining shocks of magnitudes $7\frac{3}{4}$ to 8.0, the characteristic loses most of its saw-tooth form and, except for the 1904–1908 segment, becomes approximately linear (Fig. 5). It appears therefore that the great earthquakes of magnitude 8 and larger differ in kind from those of lesser magnitude. Apparently the larger earthquakes are produced by a primary strain pattern whereas the smaller shocks represent some form of auxiliary strain-relief.

Sequence of Great Earthquakes of Intermediate Depth

The data for this sequence also taken from Gutenberg and Richter (1949, p. 133–139), represent all world earthquakes of magnitude ≥ 7 in the depth range 70–300 kilometers. There is some uncertainty as to the eligibility of some shocks in this range, since, in some regions such as Tonga-Kermadec, shocks in the 70–300 km depth range belong with the deep shocks (Benioff, 1949). Consequently, in this region there should be only two classes, shallow, 0–70 km and deep, 70–680 km. However, until a more extended study is made of this distribution, it will suffice to use the present classification. The strain-rebound characteristic of this sequence (Fig. 6) bears no resemblance to that of the shallow sequence (Fig. 1). It suggests a long term periodicity, but since less than two cycles are represented, no definite conclusions can be drawn.

Sequence of Great Deep Earthquakes

The data for this sequence are also taken from Gutenberg and Richter (1949, pp. 140–141). The sequence includes all earthquakes of magnitudes ≥ 7.0 with focal depths of 300 km and over. The uncertainty as to classification of some of the intermediate shocks mentioned in the preceding paragraph affects this sequence also.

The elastic strain-rebound characteristic of this sequence is shown in Figure 7, plotted on semi-logarithmic coordinates. This characteristic resembles neither the shallow nor the intermediate sequences. In 1904 when observations first began the rate of strain release was maximum and it has been decreasing continuously since that date. The straight line is calculated from the equation shown on the figure and is of the form of a compressional elastic (recoverable) creep-strain. The fact that the observed points fit the curve so well suggests that the

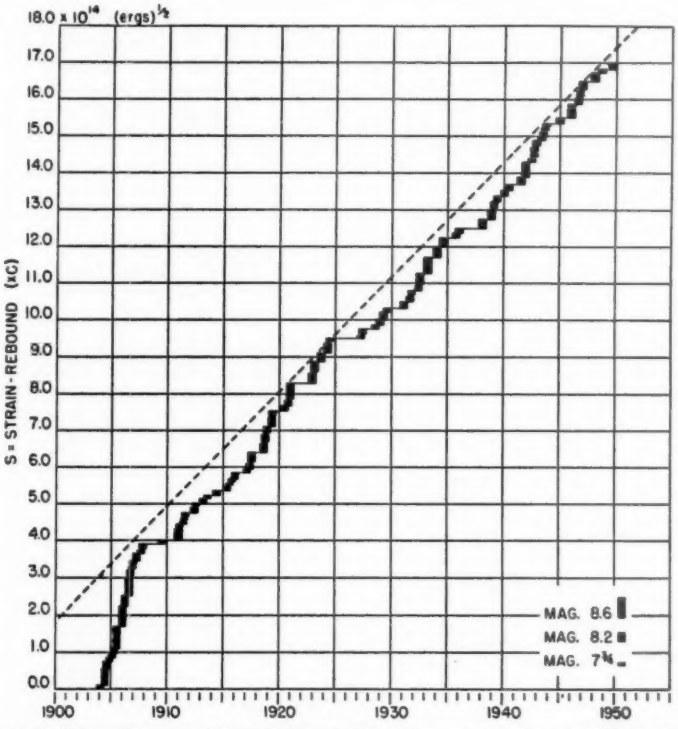

Figure 5. Strain-Rebound Characteristic. Sequence of all Shallow Earthquakes Magnitudes ≥ 7¾

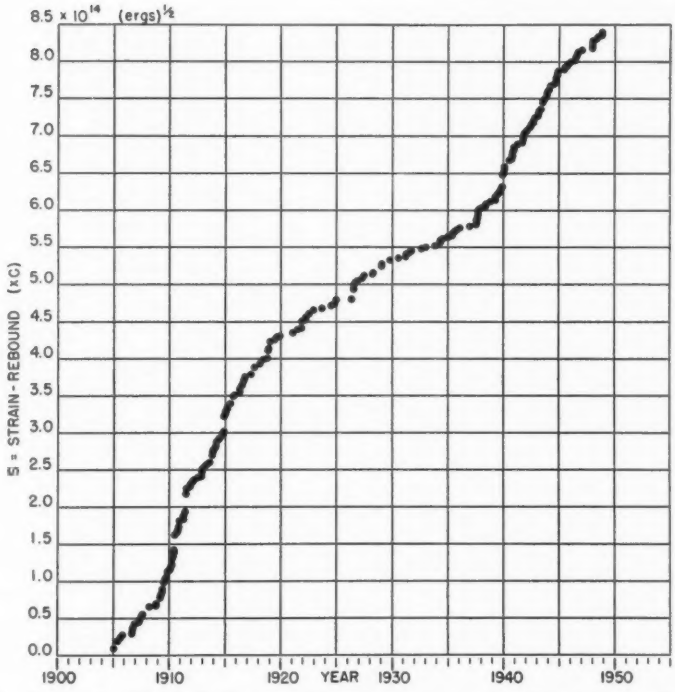

FIGURE 6. STRAIN-REBOUND CHARACTERISTIC. SEQUENCE OF ALL INTERMEDIATE DEPTH (70–300 KM) EARTHQUAKES MAGNITUDES $\geq$ 7.0

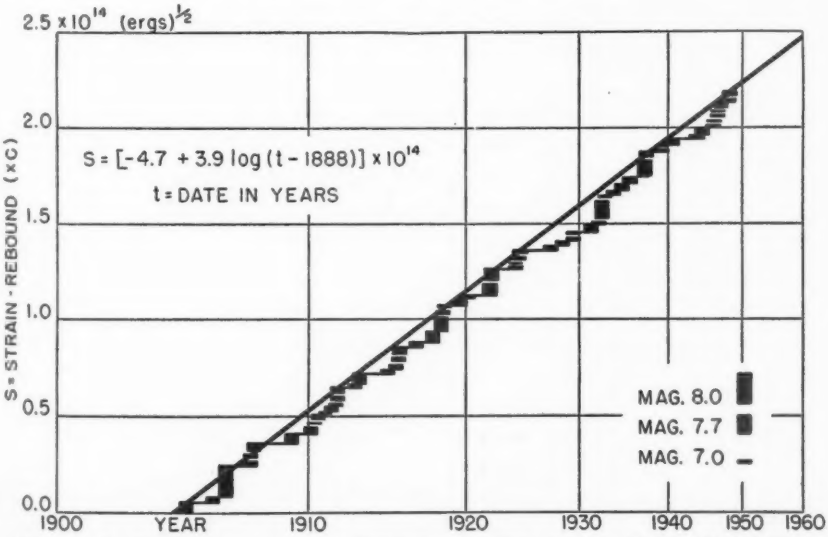

FIGURE 7. STRAIN-REBOUND CHARACTERISTIC. SEQUENCE OF ALL DEEP (300–680 KM) EARTHQUAKES MAGNITUDES $\geq$ 7.0

great deep earthquakes also are related in a single stress system and that in this system compressional elastic creep strain has been accumulating or releasing since 1888. In any case the curve shows definitely that the rate of elastic strain-rebound in this sequence has been decreasing as 1/t since 1904.

Crustal Structure of the Earth

Heretofore knowledge of the interior of the earth has been derived principally from the behavior of seismic waves. Since the largest observed periods in these waves do not exceed several minutes, the properties of the medium exhibited by these observations must be limited to short-time characteristics only. A medium can transmit shear waves and behave otherwise as a solid for waves of such short duration and yet be incapable of maintaining a shearing stress for as long as several hours or days. Thus the properties of the crust defined by waves do not necessarily refer to its tectonic or secular properties. On the other hand, elastic strain-rebound characteristics of earthquake sequences do provide information as to the tectonic cha - acteristics of the crust. Thus (Benioff, 1949) in the region covered by the Tonga-Kermadec sequence and the South American sequences, there exists a profound tectonic discontinuity at the base of the shallow layer some 60–70 km from the surface and; in the region of the South American sequences, there is an additional secular discontinuity at approximately 300 km depth. The fact that the three world-strain-rebound characteristics of Figures 1, 4, and 5 are so strikingly different is evidence that two at least of the three tectonic discontinuities found for South America and Tonga are in general world-wide. Since the tectonic movements in these separate layers appear to be unrelated, it must be concluded that they actually move relative to each other.

References Cited

Benioff, Hugo (1949) *Seismic evidence for the fault origin of oceanic deeps*, Geol. Soc. Am., Bull., vol. 60, pp. 1837–1856.

—— (1951) *Earthquakes and rock creep*, Part 1: *Creep characteristics of rocks and the origin of aftershocks*, Seismol. Soc. Am., Bull. (in press).

Gutenberg, B. and Richter, C. F., (1942) *Earthquake magnitude, intensity, energy and acceleration*, Seismol. Soc. Am., Bull., vol. 32, p. 163–191.

—— (1949) *Seismicity of the Earth and associated phenomena*, Princeton Univ. Press, p. 119–121; 133–139; 140–141.

Seismological Laboratory, 220 N. San Rafael Ave., Pasadena, Calif. May 16, 1950

Publications of the Division of the Geological Sciences, California Institute of Technology, Pasadena, California. Contribution No. 540.

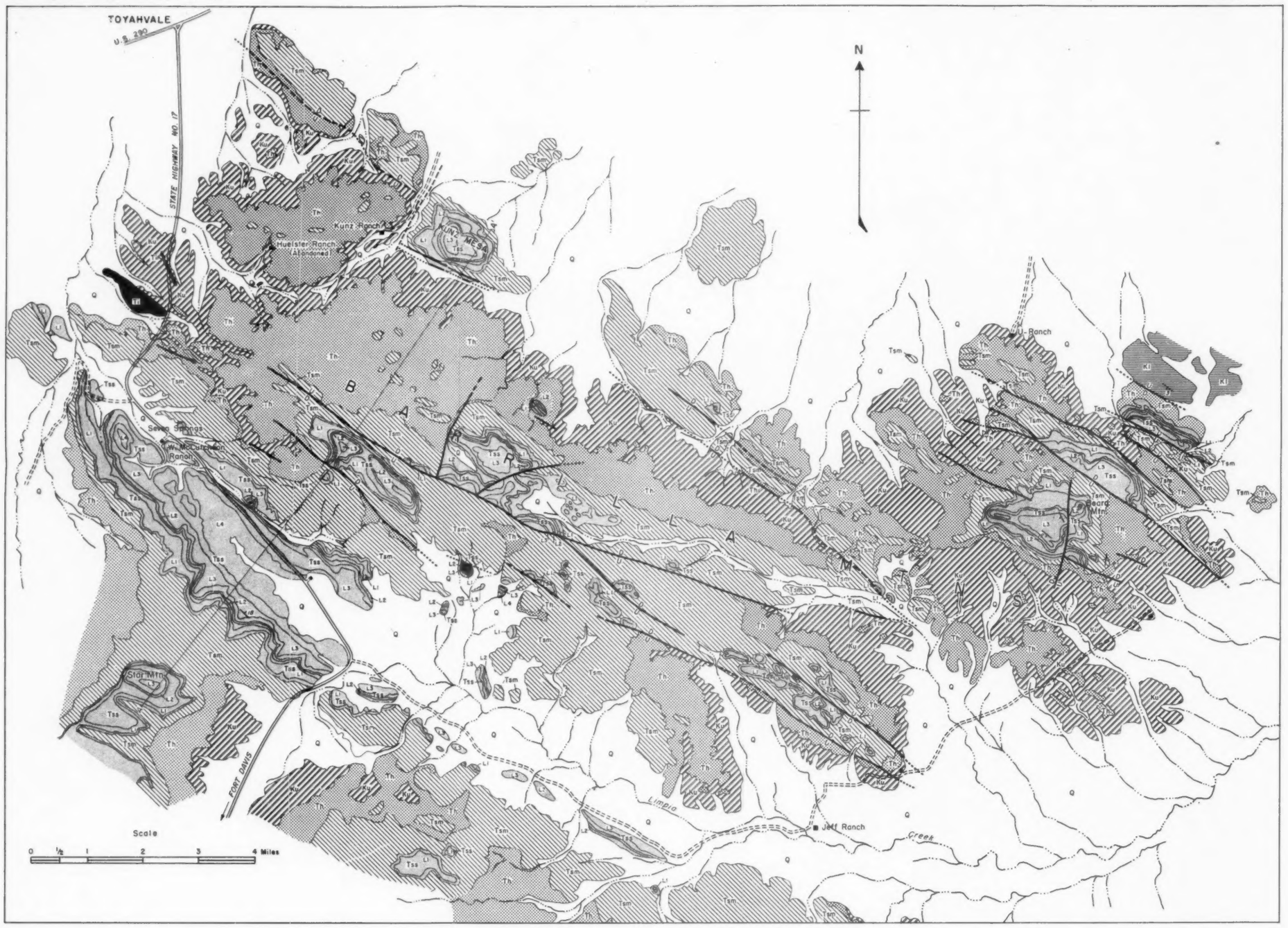

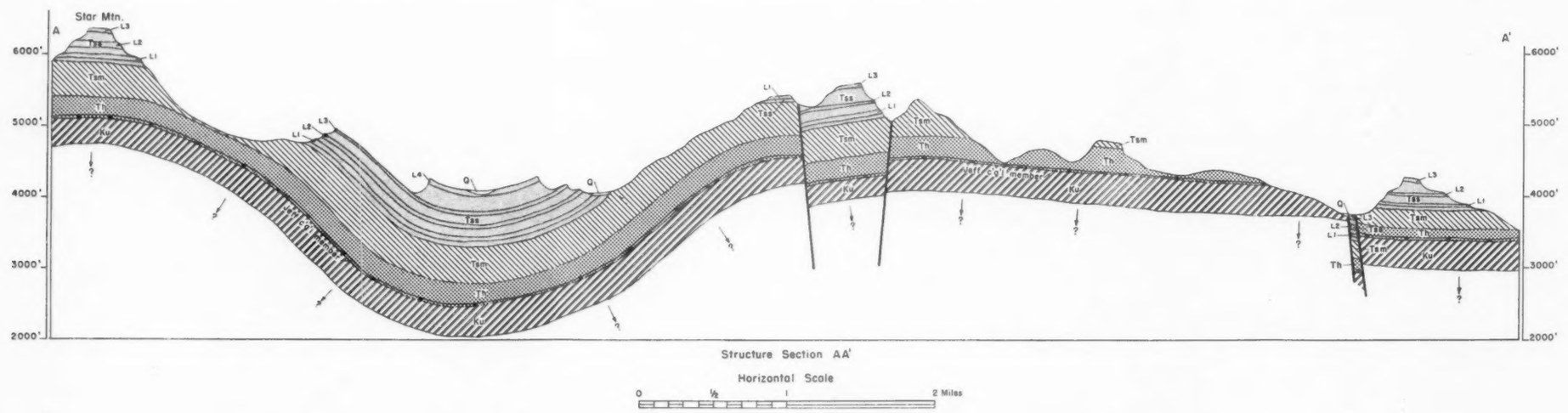

EXPLANATION

- Q — Alluvium and gravel
- Ti — Intrusive igneous rocks
- Tss — Seven Springs formation (Tuff members shown but not numbered)
  - L4 = Lava #4
  - L3 = Lava #3
  - L2 = Lava #2
  - L1 = Lava #1
- Tsm — Star Mountain rhyolite
- Th — Huelster formation (Jeff conglomerate shown in cross section only)
- Ku — Upper Cretaceous: Mostly Taylor marl; some Austin chalk.
- Kl — Lower Cretaceous: Probably Georgetown group

McCutcheon Volcanic Series

QUATERNARY
TERTIARY
CRETACEOUS

- Fault (Dashed where inferred; dotted where concealed; U, upthrown side; D, downthrown side)
- Strike and dip of beds
- Landslide Mass

GEOLOGIC MAP AND STRUCTURE SECTION OF BARRILLA MOUNTAINS, TEXAS

BULLETIN OF THE GEOLOGICAL SOCIETY OF AMERICA
VOL. 62, PP. 339-363, 1 FIG., 2 PLS. APRIL 1951

GEOLOGY OF THE BARRILLA MOUNTAINS, TEXAS

By G. K. Eifler, Jr.

Abstract

The Barrilla Mountains, in the northeastern part of the Davis Mountains of Trans-Pecos Texas, are composed of Tertiary volcanic materials. Five tuffs and five lava flows, 1500 feet thick occurring throughout the mountains, persist in thickness and lithologic characteristics. Their upper surfaces show little erosion. The lavas are chiefly Silicic and soda rich.

The volcanic succession is underlain by a Tertiary sandstone above Upper Cretaceous marine formations. These were slightly deformed by the Laramide revolution, subsequently beveled, and everywhere covered by the sands of coalescing streams. The sandstone contains well-rounded chert and quartzite pebbles.

Broad folds and normal faults succeeded the extrusions of the youngest lava.

CONTENTS

	Page
Introduction and acknowledgments	339
General stratigraphy	341
Permian system	341
Cretaceous system	341
Comanche series	341
Georgetown group	341
Gulf series	341
Austin group	341
Taylor group	342
Tertiary system	342
McCutcheon volcanic series	342
Introduction	342
Age and correlation	342
Huelster formation	342
Star Mountain rhyolite	345
Seven Springs formation	345
Possible intrusions	346
Structural features	347
Introduction	347
Folds	347
Faults	347
Geomorphology	348
Economic geology	348
Petrography. By Kathryn O. Dickson	348
General statement	348
Riebeckite soda rhyolite porphyry	349
Spherulitic riebeckite soda granophyre	349
Granophyric rhyolite porphyry	349
Soda rhyolitic vitrophyre	349
Soda trachyte porphyry	351
Porphyritic olivine trachydolerite	352
Basalt and trachybasalt porphyry	352
Vitric rhyolite porphyry or vitrolithic tuff	353
References cited	353

ILLUSTRATIONS

Figure	Page
1. Index map showing location of Barrilla Mountains	340

Plate	Facing page
1. Geologic map and structure section of Barrilla Mountains, Texas	339
2. Jeff conglomerate southwest of Jeff ranch	344

TABLE

Table	Page
1. Petrography of igneous rocks, Barrilla Mountains	350

Introduction and Acknowledgments

The Barrilla Mountains comprise a thick mass of Tertiary lavas and tuffs (Fig. 1) whose north and northeastern edges rise in bold cliffs, 2000 feet high in places. Structurally the mountains are a broad, locally domed anticlinal uplift. Longitudinal faults cut the folds.

Stratigraphically and structurally the moun-

tains resemble the more extensive Davis Mountains, which comprise alternating tuffs and lavas, and overlie marine Upper Cretaceous strata in a structurally low area. Uplifts on the north, east, and west expose Lower Creataceous and Permian rocks. Southward the Davis Mountains merge with well-dissected and alluvium-covered tuffs and flows. No doubt some uplift occurred after the lavas were formed. The volcanic rocks of the Davis and Barrilla mountains are generally considered early Tertiary, but diagnostic fossils are absent.

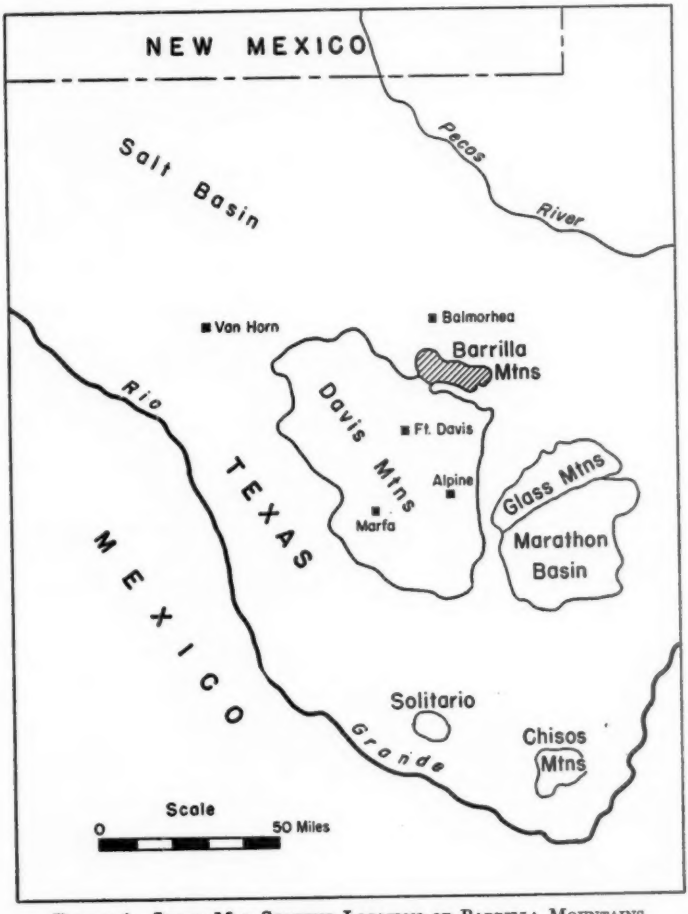

FIGURE 1.—INDEX MAP SHOWING LOCATION OF BARRILLA MOUNTAINS

Field work was conducted during July and August 1947 and June and July 1948 with assistance of Joseph A. Kennedy and Roger S. Plummer. Mrs. Kathryn O. Dickson of the Bureau of Economic Geology, The University of Texas, described the igneous rocks petrographically.

A grant from the Penrose Bequest of The Geological Society of America defrayed expense of part of the field work and cost of aerial photographs and thin sections. This paper is one of a series reporting results of a Trans-Pecos Texas project sponsored by the Bureau of Economic Geology, The University of Texas.

General Stratigraphy

The oldest rocks cropping out in the Barrilla Mountains are Cretaceous, but wells drilled for oil have encountered rocks as old as Permian. Older Paleozoic rocks probably occur at greater depth. A thick Permian section comprises marine limestone, dolomite, subordinate shale, and evaporites near the top. The Leonard, Guadalupe, and Ochoa series have been identified. The Triassic comprises nonmarine red and gray shales and sandstones a few hundred feet thick. The Jurassic is absent. Approximately 1500 feet of marine sandstone, shale, marl, and limestone constitutes the Cretaceous. Although these rocks range from Trinity to Taylor in age, only Washita, Austin, and Taylor strata crop out. The Tertiary comprises thick tuffs and lavas with minor fresh-water limestone and sandstone. Thin gravels and alluvium constitute the Quaternary.

Permian System

In the Humble Oil and Refining Company No. 1 McCutcheon well east of Star Mountain, Skinner (1948, p. 61) identified alternating sandstone, limestone, and dolomite as Capitan (?) in age, the upper part of which possibly is Rustler.

In the Humble Oil and Refining Company No. 2 Flores well northwest of the Barrilla Mountains, Creataceous rocks directly overlie the Permian, of which the Rustler formation, with possibly the Salado and Castile, the Capitan limestone, and the Word were identified. However, some of the beds assigned to the upper part of the Capitan may belong to the Tessey limestone. The identification of many of the formations is not too certain (Skinner, personal communication).

Northeast of the Barrilla Mountains in the Argo Oil Corporation No. 1 Dora Roberts well, Reeves County, W. A. Waldschmidt (personal communication) identified Cretaceous, possibly Triassic, Permian, and Pennsylvanian rocks. The Permian section, approximately 11,500 feet thick, includes well-developed Ochoa, Guadalupe, Leonard, and Wolfcamp series.

From available subsurface data Cretaceous, Triassic, Permian, and Pennsylvanian rocks underlie the Barrilla Mountains area.

Cretaceous System

Comanche Series

Georgetown group.—The oldest Cretaceous strata crop out in the low hills of limestone 2–3 miles east of the U ranch. On the upthrown side of a fault trending northwest, limestone beds, white to light-gray, contain abundant rudistids, some *Toucasia* sp., and one specimen of a large *Neithea*. Fossils could not be broken out. These beds lithologically resemble the Georgetown rudistid facies limestone cropping out along the Fort Stockton-Balmorhea highway to the north. The lack of identifiable fossils precludes a definite correlation, but these beds are tentatively assigned to the Georgetown group.

Gulf Series

Austin group.—Upper Cretaceous marine strata crop out along the periphery of the mountains except to the southwest where covered by Tertiary volcanics along the axis of a syncline (Pl. 1). Good exposures are rare. No section justified measurement and description.

Outcrops are mostly blue green marls weathering ochre yellow, but locally a white to pearl-gray chalky limestone alternates with poorly bedded white indurated marl and marly limestone. These chalky and marly limestones crop out in several ravines about 7½ miles west of the U ranch. They contain fragments of a large *Inoceramus*, probably *Inoceramus undulatoplicatus*, with small cupped oysters attached. Parts of a large rudistid, either *Durania* sp. or *Sauvagesia* sp., are associated with the *Inoceramus*. The exposed section here is only about 20 or 25 feet thick and apparently underlies the yellow-weathering Taylor marls.

In a shallow ravine 6 miles northeast of the Jeff ranch a white chalky limestone, interbedded with cream marl, weathers into small flat chips. A few beds, 1–2 feet thick, resemble the Austin chalk of central Texas. *Gryphaea* sp. and a large *Inoceramus*, possibly *I. undulatoplicatus*, occur in these beds, which apparently underlie Taylor marl. The contact between the chalky limestone and overlying marl is not exposed. Chalky limestone crops out about 7

miles west of the Jeff ranch and about 3 miles southeast.

The chalky and marly limestones probably are Austin chalk. This correlation, however, is based upon the very meager evidence of a few fossils and uncertain field relations with the Taylor marl.

Taylor group.—Taylor marl is exposed along ravines by undercutting and slumping; elsewhere it is covered. It is massive and moderately well consolidated. It weathers ochre yellow and erodes into rounded smooth hills. About midway between the U ranch and Jeff ranch, yellow to brown sandstone concretions occur at an unknown stratigraphic level in the Taylor marl. Approximately 1.1 miles southeast of Star Mountain 85–90 feet of Taylor marl containing abundant *Gryphaea newberryi* (?) underlies Tertiary fluviatile sandstone. The marl is dark gray with interbedded marly limestone and indurated yellow to buff marl. Similar dark, flaky chalky marls and thin beds of limestone crop out on the north slope of a hill west of the Fort Davis-Toyahvale highway 4.74 miles south of Toyahvale close to an igneous intrusion. These dark marls may be stratigraphically higher than the Taylor marl.

Few species of fossils have been found. *Gryphaea newberryi* (?) and *Exogyra ponderosa* are abundant. East of the U ranch the zone of abundant *Exogyra ponderosa* directly overlies the zone of abundant *Gryphaea newberryi* (?). Since no complete section of the Taylor marl was found, these zones of abundance may alternate with each other.

Tertiary System

McCutcheon Volcanic Series

Introduction.—Volcanic rocks aggregating 1500–1700 feet overlie marine Cretaceous rocks. A succession of five lavas alternating with five tuffs, some of which contain sandstones, breccias, and fresh-water limestones, is here named the McCutcheon volcanic series. (Willis McCutcheon ranch 7 miles south of Toyahvale.) The base is the lowest sandstone and conglomerate which here overlie marine Upper Cretaceous. The top, the highest lava, is exposed along the syncline crossed by the Fort Davis-Toyahvale highway north of Star Mountain.

Apparently one unit succeeded another fairly rapidly. Some of the tuffs and lavas may have been slightly eroded, but nowhere is there evidence of channeling or other marked differential erosion. However, a few sandstones and conglomerates with lava fragments interbedded in the series indicate erosion elsewhere in the Davis Mountains area.

Apparently the lavas spread widely over fairly flat surfaces, yet they are silicic and presumably were viscous. Perhaps they erupted from fissures in the Davis Mountains. Each is fairly uniform in thickness and lithologic characteristics.

Age and correlation.—There is very little evidence concerning the exact age of the series. The few fossils are not diagnostic. The series is younger than the Taylor marl and probably is Tertiary. E. W. Berry (1919, p. 4) correlated plants from the lower tuffs of the Barrilla Mountains with those of the Raton and Denver formations (lower Eocene). The tooth of an Oligocene rhinoceros has been reported from the lower tuffs of the volcanic succession of the Davis Mountains about 11 miles west of Balmorhea. Land gastropods and fresh-water algae in the lower tuffs of the Barrilla Mountains near Barrilla Springs can be dated only as Tertiary, possibly early Tertiary. Goldich and Seward (1948, p. 15) assign Eocene, Oligocene, and possibly Miocene age to the volcanic series that overlies eroded Upper Cretaceous rocks in the southeastern part of the Davis Mountains. The tuffs of the Tierra Vieja Mountains, about 60 miles southwest of the Barrilla Mountains, contain vertebrate remains identified by Bryan Patterson as Oligocene (cited by Goldich and Seward, 1948, p. 18). No attempt is made to correlate the tuffs of the Barrilla Mountains with those of the southeastern Davis Mountains or of the Tierra Vieja Mountains.

The series is divided into three formations (from oldest to youngest): Huelster formation, Star Mountain rhyolite, and Seven Springs formation.

Huelster formation.—The Huelster formation forms the lower part of the McCutcheon volcanic series. The type locality is near the head of a deep ravine about 1½ miles south of the ruins of the Huelster ranch house in the northwestern part of the Barrilla Mountains. The

base is the lowest sandstone and conglomerate overlying marine Upper Cretaceous; the top is the highest tuff directly underlying the Star Mountain rhyolite. The formation, almost entirely tuff, contains thin layers of sandstone and conglomerate, lenses of fresh-water limestone, and of trachydoleritic lava. At the type locality it is approximately 400 feet thick, but it thins eastward.

The formation crops out widely about the Barrilla foothills except on the southwest where it dips below the surface in a broad syncline. In the interior parts of the mountains, outcrops occur in deep ravines eroded along major faults. The formation is eroded into low rounded hills. It forms no distinct topographic break with the underlying Cretaceous, but the overlying lava forms high rugged cliffs.

The Jeff conglomerate member, a sandstone and conglomerate unit constituting the lowest beds of the Huelster formation averages 25 feet thick. The type locality is in a tributary ravine on the left bank of Horse Thief Canyon about 3½ miles upstream from its junction with Limpia Creek near the Jeff ranch.

The Jeff conglomerate member lies with slight angularity upon Cretaceous beds, mostly Taylor marl, but also Austin chalk. The contact is sharp and marks the Mesozoic-Cenozoic boundary, but is not well exposed. The member is overlain with apparent conformity by volcanic tuff, although a surface of erosion might separate the two.

The sandstone is moderately well sorted, medium- to coarse-grained, slightly angular, and varies from white to light tan to yellow. The conglomerate is composed mainly of well-sorted pebbles and cobbles, but boulders occur at some localities. Some beds are almost entirely pebbles and cobbles with little sandstone matrix (Pl. 2, fig. 2), and others are mainly sandstone with scattered pebbles and cobbles.

Bedding is poor, but in places indistinct cross-bedding occurs, and at a few exposures the sandstone is distinctly laminated. In general the basal beds are sandstones varying considerably in thickness and in places cross-bedded. Above are conglomerates with abundant pebbles and cobbles in a sparse, sandy matrix. At some localities beds of conglomerate are separated by a thin sandstone or by pudding-stone. Above the conglomerates are sandstones with a few scattered pebbles.

Most of the pebbles, cobbles, and boulders are ellipsoidal to subspherical (Pl. 2, fig. 1), but some are greatly flattened. They are chiefly white to light lemon-yellow structureless quartzite. Others are gray and dark limestone, white, black, pink, and gray chert, chert conglomerate, and quartz. Some pebbles are composed partly of chert and partly of dark limestone. Fragmentary thick shells of *Inoceramus* (?) occur sparingly.

At the base of Santiago Peak about 70 miles south-southeast of Star Mountain the writer (Eifler, 1943, p. 1635) found a similar sandstone and conglomerate overlying eroded Boquillas formation (Upper Cretaceous) and underlying Tertiary volcanic ash. Most of the pebbles in the conglomerate are chert, but some are limestone. South of Alpine Goldich and Seward (1948, p. 13) report a similar conglomerate between the Boquillas formation and the Buck Hill volcanic series (Tertiary). The conglomerate is composed ". . . principally of well-rounded pebbles and cobbles of limestone, with some pebbles of marble, quartzite, chert, and chalcedony in a well-cemented matrix of tuffaceous sandstone" (Goldich and Seward, 1948, p. 18). The conglomerates south of Alpine and at Santiago Peak are probably the same and may be equivalents of the Jeff conglomerate.

The source of the pebbles and cobbles is certainly not the underlying Cretaceous formations. However, fragmentary shells of *Inoceramus* were probably locally derived; they show practically no abrasion. The quartzite pebbles increase in size toward the Van Horn uplift, but no extensive quartzite is known there. The chert, chert conglomerate, and dark limestone resemble some Paleozoic rocks of the Marathon basin. In the northeastern Glass Mountains J. T. Lonsdale (personal communication) found well-rounded quartzite pebbles in a Leonard conglomerate, which might be the source of the Jeff conglomerate.

The Jeff conglomerate member is thought to be continuous throughout the Barrilla Mountains and the northeastern part of the Davis Mountains. It was deposited on a fairly smooth erosion surface either by coalescing streams or by extensive sheetwash. It is too extensive to

be the veneer of a pediment. The thickness is uniform over too great an area for the deposit to be a piedmont alluvial fan, although the sandstone and gravel might have been spread very thin in front of a piedmont fan.

Sandstone, not typical of the Jeff conglomerate member, occurs between Cretaceous rocks and the volcanics at two localities. In a ravine 4½ miles S. 30° E. of the U ranch, sandstone overlies Taylor marl. The basal 6 feet of sandstone, which contains no pebbles, is ochre yellow to brown and is cross-bedded and laminated. The upper contact is not exposed. About 7 miles west of the Jeff ranch, 20 feet of yellow to white sandstone with no pebbles overlies the Austin chalk. The sandstone is cross-bedded and laminated. On the slope above are a few scattered pebbles and tuff beds, which may not be in place. The absence of pebbles and the yellow color of the basal sandstone are thought to be local characters, and the two sections are correlated with the Jeff conglomerate member.

At the type locality the upper contact of the Huelster formation is obscured. Highly generalized section of the lower 294 feet which is exposed is given below.

PARTIAL SECTION OF HUELSTER FORMATION SOUTH OF HUELSTER HOUSE RUINS

Unit	*Description*	*Thickness in feet*
6.	White to cream, fine to coarse tuffs. Petrified tree trunks 2–3 feet across. Upper part ends at top of hill covered by lava debris	104
5.	Flinty-appearing cream tuffs. A few petrified tree trunks	6
4.	Ledges 3–4 feet thick of hard, white to cream tuffs. Brown stains along sharp joints	44
3.	White, buff, and cream tuffs	63
2.	Cream to white tuffs. Yellow-brown stains along joints. Cross-bedded sandstone near top	25
1.	Conglomerate and sandstone. Quartzite and chert pebbles near base; gray marls at top. Underlain by Taylor marl	52
	Total	294

Approximately 100 feet of poorly exposed tuff with an interbedded lens of trachydolerite lies above unit 6 and below the Star Mountain rhyolite.

The Huelster formation varies more in thickness than any other dominantly tuff section of the McCutcheon volcanic series. At a point 3.5 miles north of the Jeff ranch the formation is 136 feet thick, and on the hill 3 miles southeast of the Jeff ranch it is only a few feet thick and locally is missing.

The tuffs are distinctly bedded in layers a few inches to 1 or 2 feet thick. The flatness and continuity of bedding may indicate lacustrine deposition.

At two observed localities, fresh-water limestone is interbedded with tuff near the base of the member. About 1.8 miles south-southeast of the Jeff ranch an unfossiliferous limestone layer 3–4 feet thick lies 50 feet above the Jeff conglomerate member. At the other locality, 1.6 miles north of the Jeff ranch, a 5-foot limestone layer crops out conspicuously along the foot of several low tuff hills. The limestone, light lemon-yellow to light and dark gray and compact, contains many irregular purplish-blue and ochre yellow cherts of secondary origin.

Petrified tree trunks and unidentified low- and high-spired gastropods occur sparingly in the exposed limestone. Concentric, fusiform to ellipsoid organic structures, 4 or 5 inches in longest diameter, compose a large part of the rock. They have been identified as algae by J. Harlan Johnson, whose description follows (personal communication):

Megascopic:

Rounded pellets, with irregularly banded, more or less concentric structure, which make up a large percentage of the limestone sample.

Microscopic:

An algal limestone formed by colonies of an undescribed type of algae, probably belonging among the green algae (Chlorophyta), possibly among the blue-green (Cyanophyta). Shows molds of coarse thread-like filaments which form rounded

PLATE 2.—JEFF CONGLOMERATE SOUTHWEST OF JEFF RANCH

FIGURE 1.—ROUNDED QUARTZITE AND CHERT PEBBLES IN SANDSTONE MATRIX
FIGURE 2.—MASSIVE CONGLOMERATE
Hammer gives scale.

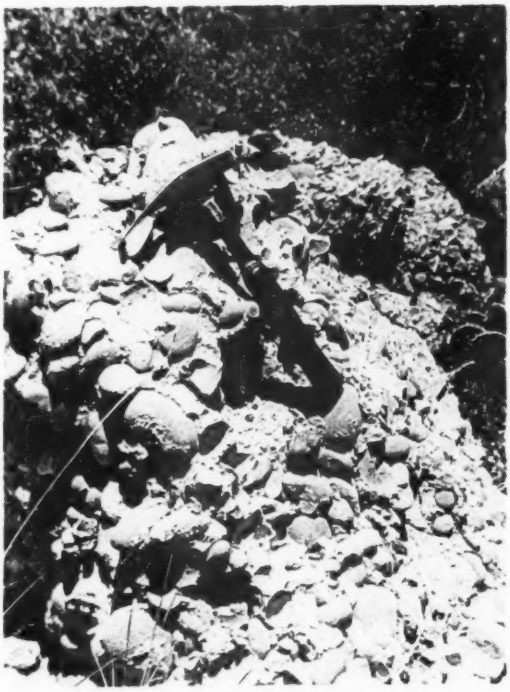

FIGURE 1

FIGURE 2

JEFF CONGLOMERATE SOUTHWEST OF JEFF RANCH

and rosette-shaped colonies (bands and fans in section). Average size of filaments 0.005 mm.
Remarks:
Probably a fresh-water growth.

The algae closely resemble specimens which S. S. Goldich obtained from a fresh-water limestone near the base of the Pruett formation south of Alpine. Goldich and Seward (1948, p. 15) also report an Eocene gastropod, *Goniobasis tenera carterii*. These limestone beds, although not continuous, are probably of the same age.

Thick lenses of a dark igneous rock, probably lava, occur in the upper part of the formation in the western part of the Barrilla Mountains and at Wild Rose Pass in the Davis Mountains. The rock weathers into small brownish-yellow to buff chunks. Megascopically it is a black, fine-grained melaphyre; the microscope reveals a porphyritic, slightly ophitic texture. The rock can be called a porphyritic olivine trachydolerite.

Star Mountain rhyolite.—The thick rhyolitic lavas overlying the Huelster formation are named the Star Mountain rhyolite after Star Mountain. The base is the lowest lava above the Huelster formation and the top is the highest lava below the tuffs of the Seven Springs formation. The number of individual flows cannot be ascertained. In the high vertical cliff on the east side of Star Mountain there appears to be at least six distinct flows, but possibly there are more. At the type locality the formation is 496 feet thick, but it thins to the northeast. About 3.5 miles north of the Jeff ranch it is 262 feet thick. The rock is typically black to brownish black, but some parts, particularly the lower, are green, greenish gray, and purplish lavender.

Owing to its great thickness and resistance to erosion the Star Mountain rhyolite crops out widely throughout the area. The lava is exposed in vertical cliffs east of Star Mountain, along parts of Limpia Creek, and near the summit and northeastern part of the Barrilla Mountains. The formation is commonly surmounted by a distinct bench where the overlying tuff has been eroded.

The flows commonly exhibit Palisade structure, and columnar jointing is less commonly developed. Many joints, which essentially parallel the Palisade structure, extend through several flows and must therefore be of tectonic origin. Flow structure is commonly developed. Some flows are highly vesicular at the top and poorly vesicular at the bottom. Blue to gray chalcedony fills many of the vesicles.

The rock is porphyritic with conspicuous phenocrysts in an aphanitic groundmass and is a riebeckite soda rhyolite porphyry.

Seven Springs formation.—The Seven Springs formation includes the lavas, tuffs, and interbedded sediments between the Star Mountain rhyolite and the top of the McCutcheon volcanic series. The formation is named for Seven Springs near the Willis McCutcheon ranch house 7 miles south of Toyahvale. A composite section near the type locality is 682 feet thick. The formation is completely exposed in the syncline north of Star Mountain. Elsewhere the upper beds are eroded. Where horizontal or with low dip the formation erodes into distinct benches.

The formation is divided into four lava members and four tuff members, which alternate with one another.

Tuff member No. 1, at the base of the formaion, includes the tuffs and interbedded sediments between the top of the Star Mountain rhyolite and the base of the overlying lava member No. 1. It is 102 feet thick on the lower northeast slopes of Star Mountain but is considerably thinner in the Barrilla Mountains.

The tuff is evenly bedded in layers up to 2 feet thick. The beds are white, gray, blue green, and lemon yellow. At the west end of Kunz Mesa, tuff is interbedded with a well-cemented conglomerate which contains igneous boulders up to 2 feet in diameter. Similar conglomerates and breccias with igneous fragments are widespread but do not occur throughout the Barrilla Mountains. Associated with them, but not present everywhere, is a blue green, highly vesicular lava.

Lava member No. 1, which includes all lavas above tuff member No. 1 and below tuff member No. 2, consists of a thin, inconspicuous vitrophyre below and a thicker, prominent granophyre above, each representing a single flow.

The average thickness of the vitrophyre is 4–8 feet, but it is at least 30–40 feet thick about

1 mile southeast of Seven Springs. Although very thin, the vitrophyre must have spread over the entire region.

Typically the rock is black, grading in places into light greenish yellow phases. It is notably devoid of vesicles and columnar jointing. Large phenocrysts are included in a glassy groundmass with perlitic structure. Some parts may be fragmental. It is classed as a soda rhyolitic vitrophyre.

The granophyre is persistently 30–40 feet thick with excellent columnar jointing and Palisade structure. The rock is purplish red, maroon, and reddish brown. At the top and bottom the flow is distinctly vesicular. The base is a conglomeratelike mass of pieces apparently derived from the granophyre while flowing. The rock can be called a spherulitic riebeckite soda granophyre.

Tuff member No. 2 includes all tuffs and sediments between the top of lava member No. 1 and the base of the overlying lava member No. 2. At Star Mountain the member is 105 feet thick, on top of the Barrilla Mountains east of the McCutcheon ranch it is 114 feet thick, on Kunz Mesa it is 90 feet thick, but in the eastern and northeastern part of the Barrilla Mountains the interval is much thinner. The tuffs are commonly white to gray and are well bedded in 1- to 2-foot layers. In places the tuff contains conglomerate and cross-bedded sandstone.

Lava member No. 2 includes all lavas above tuff member No. 2 and below tuff member No. 3. It ranges in thickness from 10 feet to 77 feet and forms no distinct topographic bench.

The base is a red lava (possibly a well-consolidated tuff) up to 2 feet thick, overlain at one locality by a 20-foot interval of tuff, but elsewhere by lava. The lava consists of three basaltic phases: a chocolate-brown with flow layers and blue chalcedonic amygdules, a blue-black, scoriaceous, conglomeratelike rock with chalcedonic amygdules; and a compact and specular phase. These phases are similar lithologically and can be called glassy basalt or trachybasalt porphyry.

Tuff member No. 3 includes all tuffs and sediments above lava member No. 2 and below the overlying lava member No. 3. It is 138 feet thick at Star Mountain, 227 feet on the mesas on top of the Barrilla Mountains east of the McCutcheon ranch, 185 feet on Kunz Mesa, but it thins rapidly to the east and on Beard Mountain is only 25–30 feet thick.

The interval is mainly white to gray tuff and contains very little sediments.

Lava member No. 3 includes all lavas above tuff member No. 3 and below the tuff member No. 4. It forms the caprock of Star Mountain, of the two mesas on top of the Barrilla Mountains east of the McCutcheon ranch, and of Kunz Mesa. It is 42–65 feet thick.

The lavas have moderately well defined palisade structure and abundant platy flow layers. The rock is prevailingly gray, but also red and black. The rock can be classified as granophyric rhyolite porphyry.

Tuff member No. 4 includes all tuffs, sediments, and interbedded lava above lava member No. 3 and below lava member No. 4. It is approximately 200 feet thick in the syncline between Star Mountain and the Barrilla Mountains. A single lava flow near the top is 5½ feet thick. This lava, a vitric rhyolite porphyry, is brown at the base and lavender to light purple at the top.

Lava member No. 4 includes all lavas above tuff member No. 4 and the top of the McCutcheon volcanic series. At the type locality of the series a thin tuff may overlie this lava member, but if so it is covered by alluvium. The lava crops out continuously along the flatirons north of Star Mountain. A few scattered outcrops occur in the extensive alluvial flat northnortheast of the junction of the Jeff ranch road with the Fort Davis-Balmorhea highway. The lava member is at least 41 feet thick. The rock is gray and is stratiform in intervals 4–6 inches thick; it is a granophyric rhyolite porphyry.

Possible Intrusions

Igneous rocks of unknown relations crop out at two localities along the Fort Davis-Balmorhea highway, 4 and 5 miles south of Toyahvale. The northern occurrence, apparently a tabular body intrusive into the Taylor marl, is probably a dike. The southern body crops out more widely, underlying two hills west of the highway. Contact with the surrounding Taylor marl is not exposed, and it is impossible to tell whether the rock is intrusive or extrusive. Some

marl close to the igneous rock is darkened, perhaps by heat. This igneous body might be a sill whose roof has been removed by erosion, but more likely it is a dike. The rocks of the two occurrences are soda trachyte porphyries.

Structural Features

Introduction

There is only slight angularity between the Cretaceous rocks and the overlying McCutcheon volcanic series. The structural features of the volcanic series are probably quite similar to those of the Cretaceous rocks, but Cretaceous formations were slightly warped and faulted before the Jeff conglomerate was deposited. Because Paleozoic rocks do not crop out in the area and subsurface data are scarce, no attempt is made to interpret their structural relations with the Cretaceous or the volcanic rocks.

Folds

Broad folds trend northwestward in the region, the most conspicuous of which is a syncline separating the Barrilla Mountains from the Davis Mountains. The southwest limb with a dip of 18°–20° has a structural relief of approximately 2500 feet and the northeast limb about 2000 feet. A few miles northwest of Seven Springs the syncline is mostly covered by the alluvium of Toyah Creek. About 2 miles north-northeast of the Jeff ranch road junction with the Fort Davis-Balmorhea highway a structural basin is superimposed on the northeast limb. The areal extent and structural relief of the basin is not determined because of alluvium. Near the Jeff ranch the northeast limb is almost horizontal, but the southwest limb dips steeply. Below the alluvium of Limpia Creek there is either the continuation of the syncline greatly narrowed or a fault upthrown to the northeast.

An anticline trends northwestward through Star Mountain, from which the volcanic beds dip steeply northeastward into the syncline, and southwestward at angles of 1°–2°. This structural feature is probably a continuation of the Hovey anticline (King, 1937, p. 141). Another anticlinal uplift trends northwestward through the crest of the Barrilla Mountains. The greatest structural height along this uplift is in the western part of the mountains.

Folding occurred after the outpouring of lava member No. 4 of the Seven Springs formation and is not related to the Laramide movements. The exact date is not yet determined.

Faults

Longitudinal high-angle faults cut the rocks of the McCutcheon volcanic series into long narrow blocks. These faults are fairly abundant in the Barrilla Mountains but do not occur in the syncline or in the adjoining part of the Davis Mountains. The crest of the Barrilla Mountains east of the McCutcheon ranch is a grabenlike block (Pl. 1). The fault bounding the block on the southwest dropped tuff member No. 3 of the Seven Springs formation against the Star Mountain rhyolite and has a throw of approximately 490 feet. The fault on the northeast has less throw but extends for two-thirds the length of the Barrilla Mountains. It is a rotary fault, and the rocks forming the graben become upthrown as they extend southeastward. The northeast slopes of the Barrilla Mountains may contain many small faults downthrown to the northeast, but the thick mantle of igneous debris prevents an interpretation of the structural relations. The lava-topped mesas at the northeast margin of the Barrilla Mountains are bounded on the southwest by faults downthrown to the northeast. This line of faults continues southeastward between Beard Mountain and the main body of the Barrilla Mountains. Narrow fault blocks on the northeastern slope of Beard Mountain have apparently resulted from landslide faulting. They are downthrown to the northeast and are tilted at steep angles to the southwest. A fault 2 miles east of the U ranch separates the Georgetown and Huelster formations. The upthrown side of this fault is probably part of an uplift paralleling the anticline along the crest of the Barrilla Mountains.

The structural relations are not clear in the foothills of the Barrilla Mountains north and east of the Kunz ranch. Here the Star Mountain rhyolite is apparently faulted against Taylor marl. The fault, if present, trends northwestward at the southwest foot of Kunz Mesa and

turns at 90° down the ravine for a short distance and then, making another 90-degree turn, resumes its northwestward trend. It is possible that the Huelster formation here is not faulted out but that the Star Mountain rhyolite rests directly on Taylor marl.

The faults displace beds as young as the tuffs and lavas of the Seven Springs formation, but whether the movement preceded or followed the folding is not clear. Faulting probably followed folding. If the faults are genetically related to folding, they would likely have formed along the anticlinal uplift through Star Mountain and be as abundant in the northeastern part of the Davis Mountains as they are in the Barrilla Mountains. Furthermore, if the faults formed in response to the anticlinal uplifts, then the fault block 3 miles east of the McCutcheon ranch would likely have been a horst instead of a graben.

Geomorphology

The Barrilla Mountains have not been extensively eroded. The highest parts essentially coincide with the greatest uplift. A cross section (Pl. 1) northeast from Star Mountain shows that topographic relief is not much less than structural relief. Nevertheless erosion has been sufficient to form several low fault-line scarps where the Star Mountain rhyolite was faulted against the less resistant Taylor marl and Huelster formation. This relation is well shown 2 miles north of the Jeff ranch and on the southwest side of the mesas which border the mountains on the northeast. The lavas are the most resistant rocks; they top the mesas and form the flat part of benches and scarps. The Star Mountain rhyolite, owing mainly to its great thickness, forms high vertical cliffs where undermined by the erosion of the Huelster formation and the Taylor marl.

Economic Geology

Subsurface water is the most important natural resource in the Barrilla Mountains. Small gravity springs are fairly abundant in the western part of the mountains. Practically all of them occur at the contact between the permeable Jeff conglomerate and the impermeable Taylor marl. Where sufficiently large the springs are dammed, and the water is piped and used for watering stock, but each of these springs flows very little water and is fairly sensitive to fluctuations in rainfall.

The vitrophyre at the base of lava member No. 1 of the Seven Springs formation was found unsuitable as a lightweight aggregate because of the phenocrysts. Further exploration, however, might reveal a phase of the vitrophyre without phenocrysts.

Oil has not been produced commercially in the Barrilla Mountains, but the thick sequence of Permian rocks offers excellent opportunity for oil exploration. If structural relations between these rocks and the Tertiary lava flows can be established, perhaps the structural features of the lavas will aid in the discovery of structural oil traps in the Permian rocks.

Petrography

By Kathryn O. Dickson

General Statement

The igneous rocks of the Barrilla Mountains belong to the same Tertiary alkalic province as those of the Terlingua-Solitario, Big Bend, and southern Davis Mountains regions of Brewster and Presidio counties, Texas (Lonsdale, 1940; Goldich and Elms, 1949). Anorthoclase is the typical alkali feldspar. Plagioclase is negligible in the felsic members, and analcime is sometimes present in the mafic members. In the main, the lava flows are porphyritic quartz-poor soda rhyolites which grade to quartz trachytes. These lavas are characterized by soda pyriboles and granophyric, trachytic, or glassy groundmasses. The mafic types are more limited in occurrence. Aside from one extensive basaltic flow, they appear as local lenses which have diabasic texture and are composed principally of titaniferous augite, olivine, labradorite, and magnetite. The important rock types of the area are discussed, and rocks from specific localities are shown in Table 1. The percentages represented are estimates because of the highly altered state of most of the mafic minerals and the fine-grained groundmasses. Where volume percentages were practicable and informative, Rosiwal analyses were made.

Probably the major portion of the groundmasses is anorthoclase. However, as the data are not critical, all alkali feldspar is included in the table under one heading with a notation when anorthoclase phenocrysts are present.

Riebeckite Soda Rhyolite Porphyry

Lava flows of the Star Mountain rhyolite with very few exceptions are composed of this rock. It is fine-grained light gray to reddish with abundant feldspar phenocrysts 1–5 mm. in size and small grains of dark minerals visible in hand specimen. The groundmass is trachytic to micrographic with alkali feldspar laths 0.01–0.3 mm. in length, averaging 0.04 mm. Quartz occurs interstitially or in intergrowth. A basal flow (Table 1, No. 6) contains no quartz and is a trachyte. Occasionally a trace of riebeckite or other soda amphibole is present, but most of the original soda amphibole sponges have been altered to an opaque black mineral and hematite. There are discrete grains of iddingsite (?), a trace of fluorite, and a few prisms of apatite as accessories. Chalcedony and calcite appear in vesicles with hematite.

Spherulitic Riebeckite Soda Granophyre

This rhyolite makes the top of lava member No. 1 of the Seven Springs formation. Specimens are dull gray to brick red with distinct flow lines and a few minute vesicles. Some specimens have a fragmental appearance both in hand specimen and under magnification. Recognizable megascopically are anorthoclase phenocrysts 3–8 mm. in length oriented along flow lines. A few phenocrysts are feldspar and quartz intergrown micropegmatitically. The groundmass appears aphanitic in hand specimen but in several slides consists largely of spherulitic intergrowths of quartz and alkali feldspar averaging 0.2–0.3 mm. in diameter. Rarely riebeckite is found in needles in the spherulites. Rare fine aegirite grains and a few grains of iddingsite about 0.5 mm. in diameter are present in the groundmass. Opal and chalcedony are abundant in amygdules together with hematite and limonite. In the reddish fragmental type, there are spherulites but to a rather limited extent. The cryptocrystalline groundmass encloses euhedral feldspar phenocrysts, some of which are much embayed. Patches and stringers of hematite are common. The spherulitic fragments as well as those of micrographic or trachytic texture apparently are inclusions incorporated in the rock during flow.

Granophyric Rhyolite Porphyry

The lava members No. 3 and No. 4 of the Seven Springs formation and one bed in the base of the Star Mountain rhyolite section fall under this heading. The rhyolite is purple- to red gray, with a spotty appearance because of numerous light-colored feldspar phenocrysts and amygdules. Some flows or facies of flows are highly vesicular; others are dense and glassy. The groundmass ranges from granophyric quartz and alkali feldspar containing altered poikilitic ferromagnesian sponges to glass densely packed with felty (−0.05 mm.) feldspar laths and opaque ferromagnesian dust. The anorthoclase phenocrysts are stubby in habit, averaging about 4 mm. in length. The mafic phenocrysts, as well as the mafics in the groundmass, are altogether altered, but the phenocrysts have the general habit of a pyroxene and average 1 mm. in greatest dimension. One slide has in addition microlites of a green ferromagnesian, probably aegirite-augite, and a trace of biotite bordering the discrete ore grains. Hematite and limonite are present as alteration products, and zircon, apatite, and fluorite were found in trace quantities. Opal, chalcedony, calcite, and secondary quartz are common amygdules with cristobalite spherulites prominent in the vesicular rocks.

Soda Rhyolitic Vitrophyre

This glass occurs at the base of lava member No. 1 of the Seven Springs formation; it is a black and gray banded glass containing shining feldspar phenocrysts, 1–5 mm. in length, and fragments of basalt and rhyolite. Some samples are easily crumbled due to perlitic structure in the glass. The resinous black glass is pale brown in section; $n = 1.517, \pm 0.002$, which indicates an SiO_2 content of about 65 per cent. The glass has a lower silica content than the phenocrysts indicate, these latter being anorthoclase, quartz, graphically intergrown quartz and feldspar, augite, and aegirite-

TABLE 1.—PETROGRAPHY OF IGNEOUS ROCKS, BARRILLA MOUNTAINS

Sample No.	Analcime	Quartz	Alkali feldspar	Labradorite	Glass and opal	Augite	Soda pyribole	Microlites and/or alter. prod. of olivine and pyroxene undifferentiated	Biotite	Olivine	Magnetite and/or ilmenite	Apatite	Fluorite	Zircon
1	—	—	9	66	—	9	—	—	1	8	7	Tr	—	—
2	—	—	Mo	Ch	—	Mo	—	—	Li	Li	Mo	Tr	—	—
3	Tr?	—	Li	Ch	—	Mo	—	—	—	Mo	Mo	Tr	—	—
4	Li	—	Mo	Ch	—	Mo	—	—	—	Mo	Mo	Tr	—	—
5	—	Mo	Ch*	—	Tr	—	Li	—	—	—	Li	—	Tr	—
6	—	—	Ch*	—	Li	—	Tr	—	—	—	Tr	—	Tr	—
7	—	Mo	Ch*	—	Tr	—	Mo	—	—	—	Li	—	Tr	—
8	—	Mo	Ch*	—	Tr	—	Li	—	—	—	Li	—	Tr	—
9	—	Li	Ch*	—	Tr	—	Mo	—	—	—	Li	Tr	Tr	—
10	—	Li	Ch*	—	Tr	—	Mo	—	—	—	Li	Tr	Tr	—
11	—	11	74*	—	3	—	9	—	—	—	3	—	—	—
12	—	Mo	Ch*	—	Tr	—	Mo	—	—	—	Mo	Tr	Tr	—
13	—	—	Mu*	—	Mu	—	—	—	Tr	—	Mo	—	—	—
14	—	—	Mo	Ch	Li	Li	—	—	—	Mo	Mo	?	—	—
15	—	Mo	Ch*	—	Li	—	Li	—	—	—	Mo	—	—	—
16	—	Li	Mu*	—	Ch	—	Li	—	—	—	Mo	—	—	—
17	—	Mo	Mu*	—	Ch	—	Li	—	—	—	Mo	—	—	—
18	—	—	Mo	Ch	Li	Mo	—	Mo	—	Mo	Mu	Tr	—	—
19	—	—	—	Ch	Mu	Mo	—	Mo	—	Mo	Mu	—	—	—
20	—	—	—	Ch	Mu	Li	—	Li	—	—	Mu	—	—	—
21	—	—	Mo	Ch	Li	Mo	—	Mu	—	Mo	Mu	—	—	—
22	—	—	Mo	Ch	Li	Mo	—	Mu	—	Mo	Mu	—	—	—
23	—	—	Mu	Ch	Li	Mo	—	Mu	—	Mo	Mu	—	—	—
24	—	—	6	70	Tr	—	—	20	—	—	4	—	—	—
25	—	Mu	Ch*	—	Li	—	Mo	—	—	—	Li	—	—	Tr
26	—	Mo	Ch*	—	Mo	—	Mo	—	—	—	Li	—	—	Tr
27	—	Mo	Ch*	—	Mo	—	Mo	—	—	—	Mo	—	—	Tr
28	—	?	Ch*	—	Mo	—	Mo	—	—	—	Mo	—	—	Tr
29	—	Mo	Ch*	—	Mo	—	Mo	—	—	—	Mo	—	—	Tr
30	—	Mo	Ch*	—	Mo	—	Mo	—	—	—	Mo	—	—	Tr
31	—	Mo	Ch*	—	Li	—	Mo	—	—	—	Li	Tr	—	Tr
32	—	Mo	Ch*	—	Mo	—	Mo	—	Tr	—	Mo	—	—	Tr
33	—	Tr	Ch*	—	Tr	—	Li	—	Tr	—	Li	Tr	—	—
34	—	Li	Ch*	—	Li	—	Mo	—	—	—	Li	Tr	—	—
35	—	Li	Ch*	—	Li	—	Mo	—	—	—	Li	Tr	—	—
36	—	—	Ch*	—	Mu	—	Mo	—	—	—	Li	Tr	—	—
37	—	—	Ch*	—	Mu	—	Mo	—	—	—	Li	Tr	—	—

Tr = trace; Li = little; Mo = moderate; Mu = much; Ch = chief.

* Includes anorthoclase phenocrysts.

Lenses in the upper Huelster formation:

1. Porphyritic olivine trachydolerite in tuffs of the Huelster formation, road cut in Wild Rose Pass.
2. Porphyritic olivine trachydolerite in tuffs of the Huelster formation, Wild Rose Pass.
3. Olivine trachydolerite in tuffs of the Huelster formation, western Barrilla Mountains.
4. Porphyritic olivine trachydolerite in tuffs of the Huelster formation, western Barrilla Mountains.

Star Mountain rhyolite:

5. Riebeckite soda rhyolite porphyry from Star Mountain.
6. Riebeckite soda trachyte porphyry, lower contact from basal lava in road cut between Fort Davis and Toyahvale north of Seven Springs.

7. Hornblende (?) soda rhyolite porphyry, gray-green flow.
8. Soda rhyolite porphyry, Hill P-1, base of Kunz Mesa.
9. Hornblende (?) soda rhyolite porphyry, southwest side of Kunz Mesa.
10. Soda rhyolite porphyry, base of formation on CCC road south of Toyahvale.
11. Soda rhyolite porphyry, igneous hill ½ mile west of Kunz ranch.
12. Hornblende soda rhyolite porphyry, outlier west of U ranch.
13. Granophyric soda rhyolite porphyry, basal lava of Star Mountain rhyolite at contact with lower ash southwest of Jeff ranch.
14. Olivine trachydolerite, basal lava directly overlying "flinty" lava above Huelster tuffs south of Seven Springs.

Seven Springs formation:

15. Spherulitic riebeckite soda granophyre, Kunz Mesa.
16. Spherulitic riebeckite soda granophyre, Kunz Mesa.
17. Spherulitic riebeckite soda granophyre, Kunz Mesa.

Lava member No. 2:

18. Basalt porphyry, north slope of Star Mountain.
19. Basalt "conglomerate" lava, north slope of Star Mountain.
20. Basalt "conglomerate" lava, Beard Mountain.
21. Porphyritic olivine trachybasalt, Kunz Meas.
22. Olivine trachybasalt porphyry, Kunz Mesa.
23. Olivine trachybasalt porphyry, north of Fort Davis-Toyahvale highway at entrance to McCutcheon ranch.
24. Olivine trachydolerite, north of Fort Davis-Toyahvale highway at entrance to McCutcheon ranch.

Lava member No. 3:

25. Granophyric soda rhyolite porphyry, east end of Barrilla Mountains.
26. Granophyric soda rhyolite porphyry, top of Kunz Mesa.
27. Soda rhyolite porphyry, road cut at Seven Springs.
28. Soda rhyolite porphyry, road cut at Seven Springs.

Lava member No. 4:

29. Granophyric soda rhyolite porphyry, north slope of Star Mountain.
30. Granophyric soda rhyolite porphyry along Limpia Creek, isolated hill just east of Jeff ranch turnoff from Fort Davis-Toyahvale highway.
31. Granophyric soda rhyolite porphyry, near McCutcheon ranch entrance.
32. Granophyric soda rhyolite porphyry, highway cut near McCutcheon ranch entrance.

Intrusives:

33. Soda trachyte porphyry, $\frac{1}{10}$ mile toward Toyahvale from fork of old and new Fort Davis-Toyahvale highways.
34. Soda trachyte porphyry; same as No. 33.
35. Quartz soda trachyte porphyry, dike (?) in Cretaceous on Fort Davis-Toyahvale highway, south of locality for No. 33.
36. Aegirite-augite soda trachyte porphyry; same as No. 33.
37. Aegirite-augite soda trachyte porphyry; same as No. 33.

augite. Fragments of basalt, granophyric riebeckite soda rhyolite, and plagioclase are also present. The glass is devitrified in places bordering amygdules and cracks, and some otherwise euhedral crystals are deeply embayed. One specimen contains large amygdules of chalcedony 1–5 cm. long. Under the microscope this type shows a groundmass of spherulitic glass and numerous tiny amygdules (averaging 0.1 mm. greatest dimension) of chalcedony. No perlitic cracks are present.

Soda Trachyte Porphyry

There are two intrusives of trachyte. The rock is a light-gray quartz soda trachyte porphyry, with small (1–3 mm.) feldspar phenocrysts and narrow plates of reddish biotite and hematite. Brown concentric rings ¼–¾ inch across result from weathering. The phenocrysts are anorthoclase. The groundmass is trachytic with alkali feldspar laths 0.04–0.2 mm. in length and a small amount of interstitial quartz

varying from a trace to 2 or 3 per cent. A sodic amphibole, riebeckite (?), occurs in the groundmass in sponges and shreds and is largely altered to an opaque black mineral. Some samples contain minute grains of a sodic pyroxene, probably aegirite-augite. Magnetite is present in discrete grains. Iddingsite (?), hematite, and reddish-brown biotite (?) are alteration products after mafics, and apatite is an accessory mineral. A facies of aegirite-augite soda trachyte porphyry occurs in the intrusives. This type is distinctive under the microscope but megascopically is similar to the weathered specimens of the main rock. This peculiarity makes the relations of the two kinds somewhat equivocal. In hand specimen it is a dark gray-green to black fragmental-appearing rock with darker-green fragments up to an inch in diameter seemingly imbedded in the lighter-colored matrix. In some specimens the darker material is apparently in bands which are separated from the light matrix by sharp boundaries. The groundmasses are glass filled with alkali feldspar laths and ferromagnesian microlites, and a greater concentration of the latter imparts the darker green color. The feldspar laths of the matrix are 0.01–0.2 mm. in length. The anorthoclase phenocrysts average 1 mm. in length. Veinlets of chalcedony 0.04–0.2 mm. wide cut through the rock, and augite and aegirite-augite occur in fine grains in the groundmass and in phenocrysts up to 1 mm. in greatest dimension. A yellow mineral has completely replaced some of the smaller grains and has formed an alteration rim around some of the larger pieces of the pyroxene. This mineral is pleochroic in yellow, 2V about 70°–80° (−), $n_\beta = 1.68$, $n_\gamma - n_\alpha = 0.025$, with a prominent cleavage, length slow, extinction about 7°–9° from the cleavage. It is tentatively identified as an amphibole. Small ore grains and apatite are accessories.

Porphyritic Olivine Trachydolerite

This is the principal rock occurring in lenses of lava in the upper Huelster formation; it ranges in some places to a labradorite microsyenite. Trachydolerite also makes one lens at the base of the Star Mountain rhyolite south of Seven Springs (Table 1, No. 14). It is a fine-grained black rock with a finely crystalline groundmass and small phenocrysts which are rare in one occurrence (Table 1, Nos. 3 and 4). A few grains of mafic mineral are distinguishable megascopically. The phenocrysts are narrow, dark, shiny laths of plagioclase (An_{62}) commonly having an armor of anorthoclase. Labradorite is, for the most part, the dominant feldspar, but in some cases the alkali feldspar forms the bulk of the matrix as well as heavily armoring the phenocrysts. The groundmass feldspar grains are 0.02–0.3 mm. across, and the texture is hypautomorphic granular to trachytic with augite ophitic to the feldspar. The augite is pale gray to lavender with optically continuous patches measuring up to 2 mm. in greatest dimension. Olivine, largely serpentinized, is present between the feldspar laths in grains averaging 0.2 mm. in size. Magnetite is prominent, and some slides show brown biotite formed on the peripheries of a few grains. Apatite is a common accessory, and traces of calcite and analcime are present interstitially.

Basalt and Trachybasalt Porphyry

This is the type found in the flows of lava member No. 2 of the Seven Springs formation. It is dark gray to dull purple brown; some hand specimens are amygdaloidal, and a few show narrow plagioclase phenocrysts. Flow structure is prominent, and vesicles and amygdules are numerous. The groundmass ranges from glass containing barely visible plagioclase laths to plagioclase laths 0.01–0.3 mm. long, generally prominently armored by alkali feldspar. One specimen (Table 1, No. 24) is sufficiently coarse-grained to be considered a trachydolerite. The groundmass plagioclase is slightly less calcic than the labradorite (An_{58-60}) phenocrysts. Alkali feldspar also occurs in the interstices between groundmass laths and along cracks in phenocrysts. The texture is ophitic. Abundant microlites of augite and ore make the glassy matrix opaque to pasty. Iddingsite grains after olivine, abundant in the matrix, are rare as phenocrysts. Apatite is present in fine needles, and chalcedony, calcite, and serpentine (?) fill opal-lined amygdules.

Vitric Rhyolite Porphyry or Vitrolithic Tuff

Several lavas are partially vitric or vitrolithic tuff. These include a lava in the top of tuff member No. 1, the red lava at the base of lava member No. 2 (or top of tuff member No. 2), and a lava in tuff member No. 4, all of the Seven Springs formation. They are brick-red to purple-brown dense flinty rocks with notable glassy feldspar phenocrysts (usually anorthoclase) or fragments visible in hand specimen. The groundmasses are usually glassy, n < canada balsam, with perlitic structure, or finely crystalline with prominent flow structure. The matrices enclose euhedral and corroded phenocrysts of alkali feldspar and quartz, and a few pieces of aegirite-augite, biotite, and magnetite along with inclusions of rhyolite and basalt. Broken fragments of alkali and plagioclase feldspar and quartz are common as are amygdules and stringers of calcite, chalcedony, or hematite. Hematite is also prominent in the groundmasses. The tuffaceous parts are similar in composition, except the major constituent is glass in the form of shards which occasionally exhibit a somewhat welded character.

References Cited

Berry, E. W. (1919) *An Eocene flora from Trans-Pecos Texas*, U. S. Geol. Survey, Prof. Paper 125, p. 1–9.

Eifler, G. K., Jr. (1943) *The geology of the Santiago Peak quadrangle, Texas*, Geol. Soc. Am., Bull., vol. 54, p. 1613–1644.

Goldich, S. S., and Elms, M. A. (1949) *Stratigraphy and petrology of the Buck Hill quadrangle, Texas*, Geol. Soc. Am., Bull., vol. 60, p. 1133-1182.

——Seward, Clay (1948) *Green Valley-Paradise Valley trip*, West Texas Geol. Soc., Guidebook Fall Field Trip, p. 11–36.

King, P. B. (1937) *The geology of the Marathon region, Texas*, U. S. Geol. Survey, Prof. Paper 187, 148 pages.

Lonsdale, J. T. (1940) *Igneous rocks of the Terlingua-Solitario region, Texas*, Geol. Soc. Am., Bull., vol. 51, p. 1539–1626.

Skinner, John W. (1948) *Geologic section of the Humble Oil and Refining Company's McCutcheon No. 1*, West Texas Geol. Soc., Guidebook Fall Field Trip, p. 61.

The University of Texas, Department of Geology, Austin, Texas.

Manuscript Received by the Secretary of the Society, October 24, 1949

Project Grant 500-46-S47.

Published with Permission of the Director of the Bureau of Economic Geology, The University of Texas.

BULLETIN OF THE GEOLOGICAL SOCIETY OF AMERICA
VOL. 62, PP. 355-372, 16 FIGS., 2 PLS. APRIL, 1951

MECHANICAL BASIS FOR CERTAIN FAMILIAR GEOLOGIC STRUCTURES

By M. King Hubbert

Abstract

A simple experiment with loose sand shows that this material exhibits faulting under deformational stresses in a manner remarkably similar to rocks. Moreover, the sand experiment is amenable to theoretical analysis with good agreement between predicted and observed behavior. The same theoretical treatment, with slight modification, is alsoa pplicable to the behavior of rocks, and appears to afford a basis of understanding for a variety of empirically well-known geologic structures.

CONTENTS

	Page
Introduction	355
Experimental faulting in sand	356
Experimental apparatus	356
Average dip of normal faults	356
Average dip of reverse faults	357
Comparison of results with geological faults	357
Mechanical basis for the faulting	358
Nature of stresses produced	358
Stress on arbitrary plane	358
Mohr's stress circle	359
Properties of the material	360
Fracture lines on Mohr diagram	361
Analysis of reverse faulting	362
Analysis of normal faulting	362
Application to cohesive materials and to geologic structures	363
Coulomb equation	363
Data upon angle ϕ for rocks	364
Tension in normal faulting	367
Problem of asymmetrically folded and faulted belts	367
One-sided thrust hypothesis	367
Application of the Newtonian laws of motion	368
Interior stress distribution	369
Surfaces of potential faulting	370
Conclusion	371
References cited	371

ILLUSTRATIONS

Figure	Page
1. Initial states of stress	358
2. States of stress when partition is moved to the right	358
3. Stresses across a surface making angle α with axis of least principal stress	359
4. Mohr's stress circle	360
5. Test box for measuring τ/σ ratio at which slippage occurs	361
6. Normal and shear stresses acting upon surface layer at angle of repose	362
7. Regions of stable and of unstable stresses on the $\sigma\tau$ plane	362
8. Reverse-fault conditions	363
9. Normal-fault conditions	364
10. Position of the fracture lines on $\sigma\tau$ diagram for cohesive materials	365
11. Stress conditions for faulting in cohesive materials	366
12. Conditions for zero horizontal stress in normal faulting	366
13. Compressive stresses on ends of section of asymmetrically folded and faulted sediments	368
14. Complete system of two-dimensional stresses acting upon boundaries of block	369
15. Directions of shear stresses in various quadrants defined by principal stresses	370
16. Trajectories of principal stresses, and of potential reverse-fault surfaces compatible with the boundary stresses of Figure 14	370

Plate	Facing page
1. Experimental faulting in sand	356
2. Experimental faulting in sand—reverse faults	357

Tables	Page
1. Angles of dip of normal faults	357
2. Angle of dip of reverse faults in sand	357

Introduction

During the last century and a half, a large volume of empirical data on the mechanical behavior of rocks in response to tectonic stresses has been accumulated in the course of geologic mapping over all parts of the earth. In addition geologists have given considerable attention to the relation between various well-defined classes of geologic structures and the associated forces or stresses. This has included both small-scale structures such as slaty and fracture cleavage and joints, and large-scale structures such as faulting and folding. During the same period in the fields of physics and engineering, a great deal of exact knowledge has been acquired concerning the properties of stress in extended media and the response of matter to

various stress situations, but only a beginning has been made toward an amalgamation of this knowledge with geologically well-known situations.

The present paper will examine some of the more common types of large-scale geologic structures in the light of physical relations which have to be satisfied, to see whether a better understanding of these structures may thus be acquired. Historically, the paper is based upon a series of lectures in structural geology delivered at Columbia University during the period 1931–1940. For his original interest in the geological aspects of the problem, the author is indebted to Professors J Harlen Bretz and Rollin T. Chamberlin; for the experiment to be described and the applicable theory, he is principally indebted to the writings of, and personal conferences with, Dr. A. Nádai (1928, 1931*a*, 1931*b*).

The essential theory appears to have first been established by W. J. M. Rankine in 1857 in a study of the conditions of stability of loose earth. This was elaborated in a series of papers by Otto Mohr (1871; 1872; 1882; 1900) who, in addition to developing simple graphical methods of stress analysis, also enquired into the conditions of failure. Within recent decades, these principles have been extensively employed in the newly developed subject of soil mechanics. In geological literature it was noted by Chamberlin and Shepard (1923, p. 511–512), in some model experiments on geologic structures, that loose sand exhibited reverse faulting, with dip angles ranging from 20° to 35°. W. J. Mead (1925) reported further upon this property as related to dilatancy, but without analysis otherwise. Recently E. M. Anderson (1942) has reverted to the original work and methods of Rankine and has reached by a somewhat different route conclusions in essential agreement with those presented here.

Experimental Faulting in Sand

Experimental Apparatus

Plate 1, Figure 1 shows a box with a plate-glass front which is divided into two compartments by a rigid partition. The partition is attached to a longitudinal screw which can be turned by a crank. When the screw is rotated, the partition is moved by translation to the right or the left, parallel to the long axis of the box.

The box is filled to a depth of about 2½ inches with a fine-grained, loose, dry sand obtained from the beach at Galveston. Embedded in the sand next to the plate glass are three horizontal white lines composed of dry powdered plaster of Paris placed on the sand when the box was being filled; except as visible markers, they are without significance.

The sand in the box will stand at a maximum angle of repose of about 30° on a free slope.

When the partition is moved from left to right the left-hand compartment is lengthened, the right-hand compartment is shortened by the same amount and since the behavior of the sand in one is independent of that in the other, two separate experiments are performed simultaneously.

The first thing that happens (Pl. 1, fig. 2) is the development in the left-hand compartment of a distinct normal fault whose measured angle of dip is 63°. In the meantime, nothing other than a slight bulging is observable in the right-hand compartment. As the partition is cranked farther to the right, reverse faults (Pl. 2 figs. 1, 2) with a measured angle of dip of about 28° develop. These extend from the bottom of the box near the foot of the partition to the surface of the sand where clearly visible escarpments are produced. This experiment has been repeated a number of times and the results are presented in Tables 1 and 2.

Average Dip of Normal Faults

In the case of the normal faults, the frictional drag of the sand on the glass plate invariably produced a steeper angle at the plate than in the interior of the box. Since the fault plane extends from the scarp on the surface to the foot of the partition its angle in the interior can be determined approximately by the equation,

---

Plate 1. EXPERIMENTAL FAULTING IN SAND

Figure 1. Experimental Apparatus
Box is filled with loose, dry sand. Markers are powdered plaster of Paris.
Figure 2. Oblique View of Normal Fault Showing Escarpment

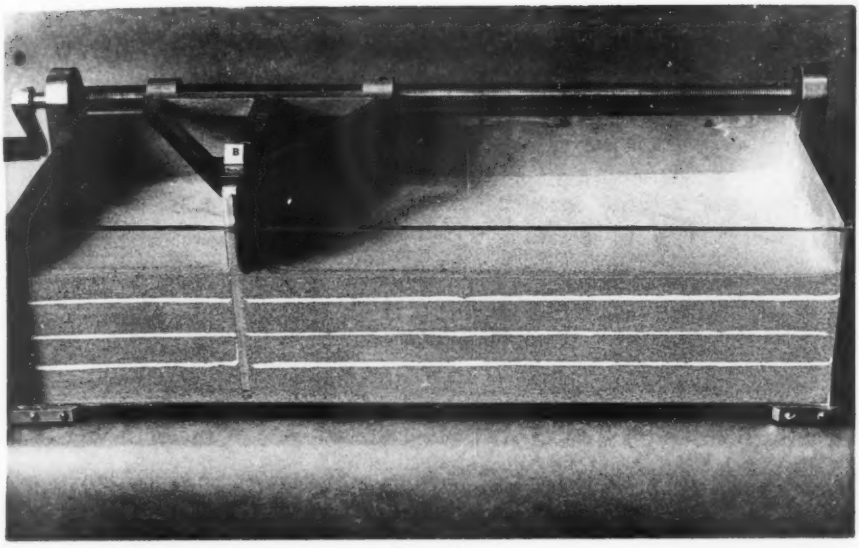

FIGURE 1

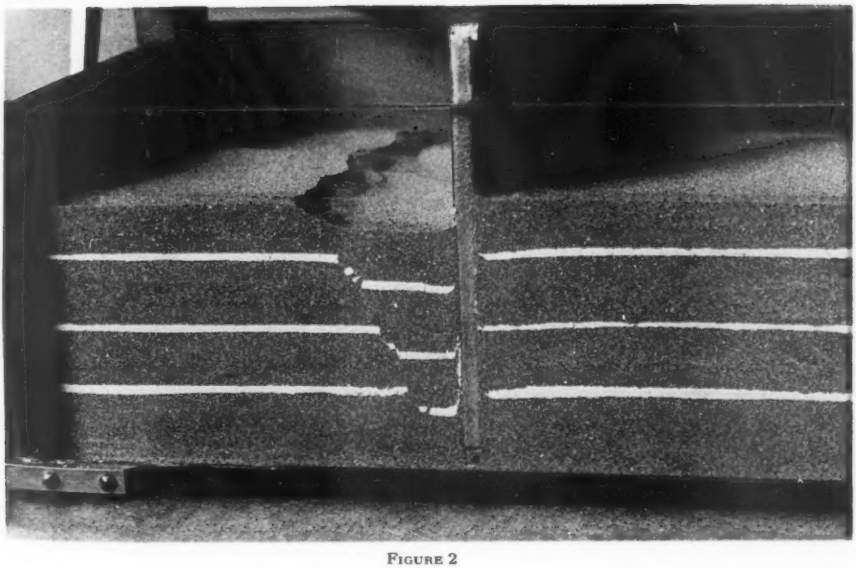

FIGURE 2

EXPERIMENTAL FAULTING IN SAND

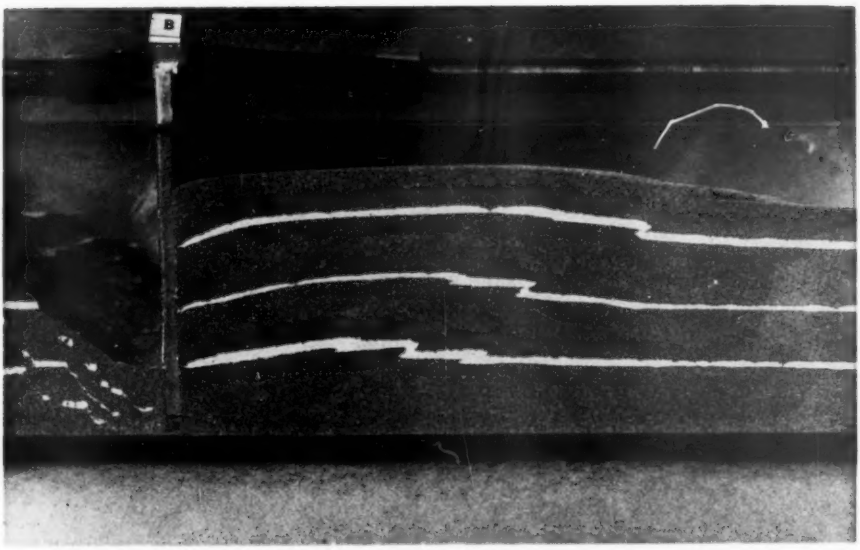

FIGURE 1

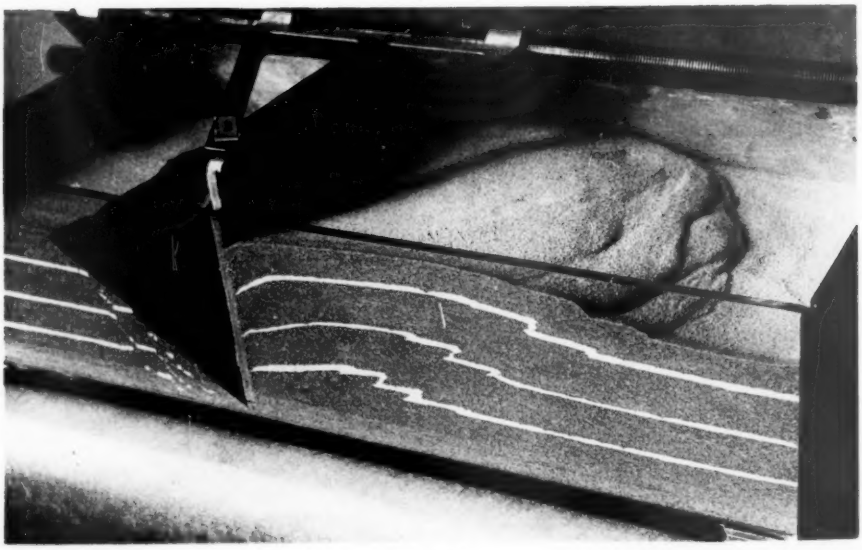

FIGURE 2

EXPERIMENTAL FAULTING IN SAND—REVERSE FAULTS

$$\alpha = \tan^{-1} z/x \quad (1)$$

where x is the distance of the escarpment from the partition in the interior of the box and z the depth of the sand.

TABLE 1.—ANGLES OF DIP OF NORMAL FAULTS

Experiment No.	Depth z of sand (inches)	Distance x of fault scrap from partition (inches)	Angle of Dip	
			Interior of sand	At glass surface
1	2.56	1.4	61.3°	64°
2	2.7	1.4	62.6	63
3	2.65	1.3	63.9	67
4	2.8	1.5	61.8	63
5	2.65	1.6	58.9	60
6	2.65	1.6	58.9	60
7	2.6	1.4	61.7	62.5
8	2.75	1.4	63.1	64.5
9	2.65	1.35	63.0	62.5
10	2.7	1.45	61.8	62
11	2.6	1.5	60.0	60
12	2.7	1.7	57.8	59
13	2.5	1.4	60.8	64
Average			61.2°	63.2°

Four of the measurements for normal faults were made with loosely packed sand; the remainder were made after the sand had been shaken to a closer packing. The angles for loosely packed sand were somewhat less steep than those for the closely packed sand, and the fault planes were less sharply defined.

Average Dip of Reverse Faults

It was not possible to compute the angle of dip of the reverse faults in the interior, because the fault planes did not originate at the bottom edge of the partition, but at a variable distance in front. Angles of dip of the reverse faults as observed against the glass plate appear to be somewhat steeper than the angles in the interior of the box. This is indicated by the arcuate shape of the fault scarp which is convex in the direction of the thrusting. The difference, however, is probably not more than a degree or two.

COMPARISON OF RESULTS WITH GEOLOGICAL FAULTS

No field geologist can observe this experiment without being impressed by the remarkable similarity between the faults produced in the sand and those which occur in rocks in the field. Although statistical evidence on the observed angles of dip of faults is sparse, it is a matter of common geological observation that in areas of medium topographical relief and mild tectonic deformation (where the deformation is insufficient to seriously change the initial angle of dip of faults) normal faults occur with dips consistently greater than 45°—rarely less—and reverse faults have dips consistently less than 45°.

TABLE 2.—ANGLES OF DIP OF REVERSE FAULTS IN SAND

Experiment No.	Angle of Dip
1	23°
2	22
3	28
4	23
5	25
6	28
7	27
8	26.5
9	26.5
10	29.5
11	24.5
12	22
13	26
14	21.5 27.5
15	24.5 20.5
16	27
Average	25.2°

This generalization is confirmed strikingly by a recent study by Sax (1946, p. 42–46) of faulting in the coal measures in the Netherlands. In this study, measurements were made underground of the angles of dip of 2102 separate faults. Of these, 1651 (79 per cent) were

PLATE 2. EXPERIMENTAL FAULTING IN SAND—REVERSE FAULTS

FIGURE 1. DEVELOPMENT OF REVERSE FAULTS
FIGURE 2. OBLIQUE VIEW OF REVERSE FAULTS

normal and 451 (21 per cent) were reverse faults (thrusts and overthrusts). Frequency curves in 5°—interval groups were also plotted. The curve for each class of fault showed a well-defined peak, that for normal faults at 63° and that for reverse faults at 22°.

In 1913, C. K. Leith (p. 55) reported on the same object as follows:

> "The dip of a thrust fault is usually low, that of a normal fault, high. An average from the United States Geological Survey Folios gives a dip of 36° for reverse fault planes and 78° for normal fault planes."

These figures are of only qualitative significance since without doubt many faults where placed on the cross sections for which accurate dip measurements were unobtainable.

Many normal faults are known from subsurface work in the Texas and Louisiana Gulf Coast region. In most of these, dips steeper than 45° are reported, though some have dips as low as 35°. In this region, the faulting in most cases has occurred in incompletely compacted sediments which subsequently have become compacted by amounts up to as much as 50 per cent of their initial thickness. Hence, an initial dip of 60° could be reduced to as little as 41°, or an initial dip of 50° to 31°.

Billings (1946, p. 206) shows a line drawing of a graben structure made by Hans Cloos with soft mud as his experimental material. The principal normal fault even in this "incompetent" material has a dip of 50°.

Thus, not only is there a qualitative resemblance between the faults in the sand box and those in rocks, but the angles of dip in the two cases are in reasonable agreement. This strongly suggests that the mechanical basis for the phenomena in both cases is essentially the same.

Mechanical Basis for the Faulting

Nature of Stresses Produced

Consider the state of stress at a point in the interior of the sand in the right-hand compartment of the box (Fig. 1). In the undisturbed state, the vertical and horizontal normal stresses will be approximately equal, and the stress state will be hydrostatic with the normal stress σ on any surface equal approximately to the pressure of the overburden, or

$$\sigma = p = \rho g z \qquad (2)$$

where ρ is the bulk density of the sand, g the acceleration of gravity, and z the depth beneath the surface of the sand.

As the partition is advanced to the right

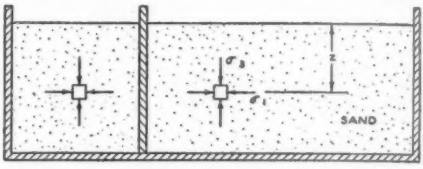

$\sigma_1 = \sigma_3 = \rho g z$

FIGURE 1.—INITIAL STATES OF STRESS

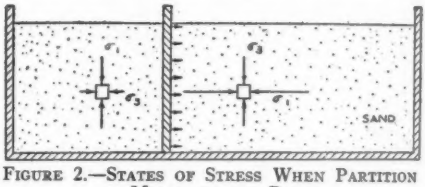

FIGURE 2.—STATES OF STRESS WHEN PARTITION IS MOVED TO THE RIGHT

(Fig. 2), the vertical stress σ_z remains constant but the horizontal stress σ_x is gradually increased. From the geometry of the deformation, these two stresses will also be, respectively, approximately the minimum and the maximum stresses acting, so we may regard them as the minimum and maximum principal stresses σ_3 (minimum) and σ_1 (maximum). An intermediate principal stress, σ_2, will exist at right angles to these two, but in a two-dimensional problem it does not require consideration.

Starting with the maximum and minimum principal stresses σ_1 and σ_3, let us first enquire as to the nature and the magnitude of the stresses acting across a plane which is obliquely oriented with respect to the axes of greatest and least principal stresses. Let such a plane be parallel to the axis of the intermediate principal stress, and let it make an angle α with the axis of the least principal stress σ_3.

Stress on Arbitrary Plane

Figure 3 is a section in the plane of the greatest and least principal stresses. Let this section be of unit thickness and let the line MN be the trace of the plane across which the stresses are to be determined. Let ABC be a

small right-triangular prism whose sides are respectively perpendicular to the axes of the stresses σ_1 and σ_3. Let dS be the area of its hypotenuse, and let σ and τ be respectively the normal and shear stresses which act upon this surface.

We take the prism small enough that its weight is negligible as compared with the surface forces which act upon it. It will be accordingly in equilibrium, under the influence of the surface forces due to the stresses σ_1, σ_3, σ, and τ. Resolving these forces into horizontal and vertical components, the sum of the vertical components must be zero, and also the sum of the horizontal components.

The forces acting upon the prism are the products of the stresses and the areas acted upon. The areas of three sides are:

$$\left.\begin{aligned} &\text{side } AB = dS, \\ &\text{side } BC = dS \sin\alpha, \\ &\text{side } CA = dS \cos\alpha. \end{aligned}\right\} \quad (3)$$

The sums of the horizontal and vertical components are respectively:

$$\left.\begin{aligned} &\sigma_1 dS\cos\alpha - \sigma\cos\alpha\, dS - \tau\sin\alpha\, dS = 0; \\ &\sigma_3 dS\sin\alpha - \sigma\sin\alpha\, dS + \tau\cos\alpha\, dS = 0. \end{aligned}\right\} \quad (4)$$

If we eliminate dS and solve equations (4) for the two unknowns τ and σ, we obtain

$$\left.\begin{aligned} \sigma &= \sigma_1\cos^2\alpha + \sigma_3\sin^2\alpha, \\ \tau &= (\sigma_1 - \sigma_3)\sin\alpha\cos\alpha. \end{aligned}\right\} \quad (5)$$

From trigonometry:

$$\cos^2\alpha = \frac{1 + \cos 2\alpha}{2},$$

$$\sin^2\alpha = \frac{1 - \cos 2\alpha}{2},$$

$$\sin\alpha\cos\alpha = \frac{\sin 2\alpha}{2}.$$

When these values are substituted into equations (5), those reduce to the simpler forms:

$$\left.\begin{aligned} \sigma &= \frac{\sigma_1 + \sigma_3}{2} + \frac{\sigma_1 - \sigma_3}{2}\cos 2\alpha, \\ \tau &= \frac{\sigma_1 - \sigma_3}{2}\sin 2\alpha, \end{aligned}\right\} \quad (6)$$

wherein τ and σ are expressed as simple functions of σ_1 and σ_3 and the angle 2α.

Mohr's Stress Circle

These equations are capable of a very simple geometrical representation if we choose coordinates with τ as the axis of ordinates and σ as the axis of abscissas. In such a system, σ_1

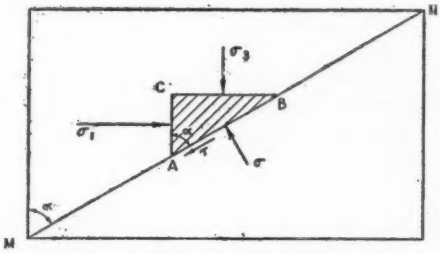

FIGURE 3.—STRESSES ACROSS A SURFACE MAKING ANGLE α WITH AXIS OF LEAST PRINCIPAL STRESS

and σ_3 (Fig. 4) will be points on the σ-axis. The quantity $(\sigma_1 + \sigma_3)/2$ will be a point midway between σ_1 and σ_3, and $(\sigma_1 - \sigma_3)/2$ will be a length equal to half the distance between σ_1 and σ_3.

Now if we let the point $(\sigma_1 + \sigma_3)/2$ be an origin for a radius vector which makes an angle 2α with the positive σ-axis, and if we let $(\sigma_1 - \sigma_3)/2$ be the length of this radius vector, we shall find that for every value of the angle α the coordinates of the terminus of this vector satisfy equations (6) and hence give the values of σ and τ for the plane which makes an angle α with the axis of least stress. Also, since $(\sigma_1 - \sigma_3)/2$ is constant, as α is changed the radius vector describes a circle which is the locus of all of the values σ and τ for all possible orientations of the reference plane.

This construction (Fig. 4), originally described by the German engineer Otto Mohr (1882) and known as Mohr's circle, enables one to determine by inspection the magnitudes of both the normal and the shear stresses upon a plane of arbitrary orientation α through a given point when the principal stresses σ_1 and σ_3 at that point are known. For example, when α is zero, $\sigma = \sigma_1$, and $\tau = 0$; upon a surface perpendicular to the greatest principal stress, the normal stress is equal to the greatest principal stress and the shear stress is zero. Likewise, when the surface is perpendicular to

the least principal stress ($\alpha = 90°$, $2\alpha = 180°$) $\sigma = \sigma_3, \tau = 0$. We can also see that the shear stress is a maximum at $2\alpha = \pm 90°$, or $\alpha = \pm 45°$, and that magnitude of the maximum shear stress is

$$\tau_{max} = \frac{\sigma_1 - \sigma_3}{2}. \tag{7}$$

Another interesting observation pertains to the shear stresses upon any two mutually perpendicular surfaces α and $\alpha + 90°$. The points on Mohr's circle for these two planes will be at 2α and $2\alpha + 180°$ and so will be diametrically opposite one another Consequently

$$\tau_\alpha = -\tau_{90+\alpha}, \tag{8}$$

which indicates that the two shear stresses will be of equal magnitudes but of opposite sense.

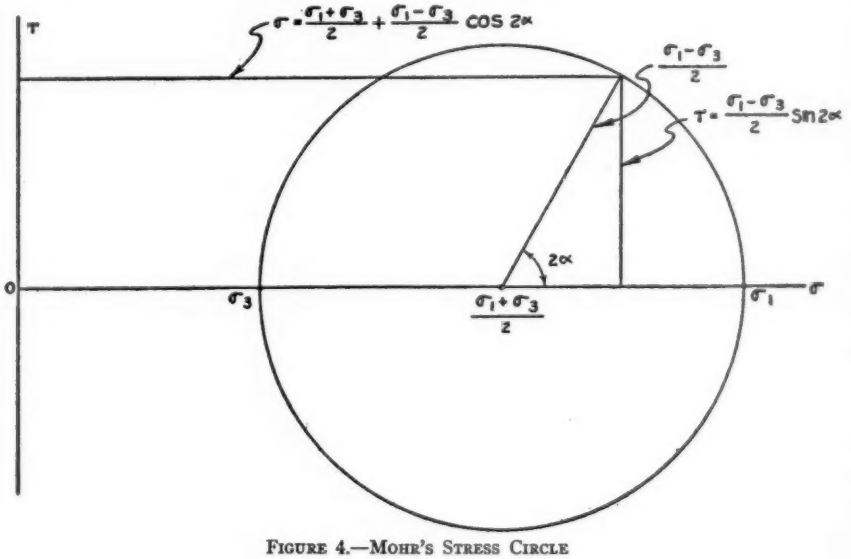

FIGURE 4.—MOHR'S STRESS CIRCLE

Properties of the Material

We now require some additional knowledge of the physical properties of the material. We have observed that the material (sand) fails by slippage along discrete surfaces; it will be of interest, therefore, to consider under what conditions of tangential and normal stress upon a given surface slippage will occur. We can get this information by a separate investigation. If we place the sand in a box (Fig. 5) whose upper half can be skidded with respect to the lower half, thereby producing slippage in the sand along the plane of shear, we can vary the normal stress σ by increasing the load N pressing upon the sand. For a given value of σ, we can increase the shear stress τ by increasing the force T until slippage occurs.

This experiment upon sand has been performed many times by the students of soil mechanics. It is found, to a first approximation, that failure occurs when

$$\frac{T}{N} \text{ or } \frac{\tau}{\sigma} \cong \text{const.} \tag{9}$$

This experiment is closely analogous to that for determining the friction between two solids. In the latter case a block of one solid is rested upon the horizontal surface of another and loaded by various amounts. For each load, the force required to slide the block is determined. In this case, too, it has been found that for given materials

$$\frac{T}{N} \text{ or } \frac{\tau}{\sigma} \cong \text{const.}$$

The forces T and N or the stresses τ and σ

at failure can be thought of as being the two components of a force or a stress, respectively, acting across the surface of contact at an angle ϕ to the surface normal which is a constant of the material. Hence

$$\frac{T}{N} \text{ or } \frac{\tau}{\sigma} = \tan \phi. \tag{10}$$

In ordinary friction, ϕ is said to be the angle of friction between the given materials; in continuous materials, such as the sand here discussed, ϕ is said to be the *angle of internal friction* of the material. Extensive tests (Krynine, 1941, p. 179) have shown that for sand the angle ϕ is not strictly constant but ranges from about 30° to 35°. The angle of 30° is characteristic of loose sand, whereas the higher angles occur when the sand is in a state of close packing.

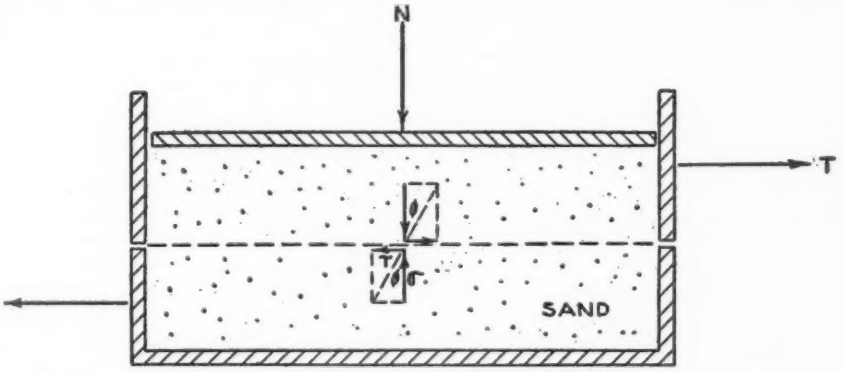

FIGURE 5.—TEST BOX FOR MEASURING τ/σ RATIO AT WHICH SLIPPAGE OCCURS

The lower angle of 30° is also the approximate angle of repose of loose sand. That this should be so can be seen by noting that upon a slope of inclination β, the normal and tangential stresses across the bottom of a surface lamina of sand will be respectively

$$\begin{aligned} \sigma &= w \cos \beta, \\ \tau &= w \sin \beta, \end{aligned} \tag{11}$$

or

$$\frac{\tau}{\sigma} = \tan \beta. \tag{12}$$

Hence, when the slope is tilted until $\beta = \phi$, slippage will occur. Since in this case ϕ is about 30°, it follows that this is the steepest angle at which the slope is stable (Fig. 6).

Fracture Lines on Mohr Diagram

Let us now combine our knowledge of the property of the material as expressed by equation (10) with the general properties of stress as expressed by Mohr's diagram. Upon the $\tau\sigma$-plane of Mohr's diagram (Fig. 7), equation (10) represents a straight line of slope ϕ passing through the origin. From symmetry there will be two such lines, one with a slope of $+\phi$ and the other with a slope of $-\phi$. These lines mark the boundaries between regions of stable and unstable states of stress for the sand. The state of stress corresponding to any point in the region between these lines and the σ-axis has a value

$$\frac{\tau}{\sigma} < \tan \phi,$$

and hence is a condition of stability; for any point outside the lines

$$\frac{\tau}{\sigma} > \tan \phi,$$

so that fracture will occur before this state can be reached. These lines may also be regarded as *fracture lines*, since when the stresses upon any surface reach the values represented by points on either of the two lines, fracture will occur.

Analysis of Reverse Faulting

Combining now the fracture lines of Figure 7 with Mohr's diagram, we can anticipate what

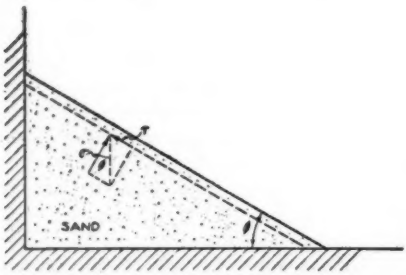

FIGURE 6.—NORMAL AND SHEAR STRESSES ACTING UPON SURFACE LAYER AT ANGLE OF REPOSE

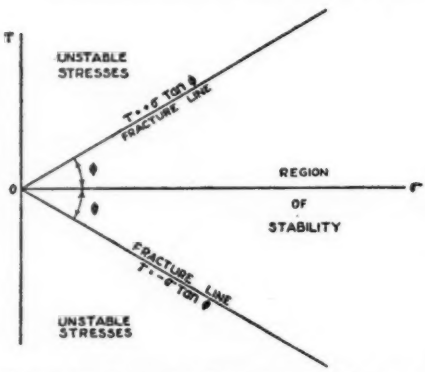

FIGURE 7.—REGIONS OF STABLE AND OF UNSTABLE STRESSES ON THE $\sigma\tau$ PLANE

should happen in the sandbox experiment (Fig. 8). In the initial stage

$$\sigma_1 \cong \sigma_3 = \rho g h.$$

As the partition is pushed forward, the vertical stress σ_3 remains constant while the horizontal stress σ_1 is gradually increased. For each value of σ_1 a particular Mohr's circle will correspond, of which σ_3 and σ_1 will lie at opposite ends of the horizontal diameter. As σ_1 is increased, the Mohr's circle will get larger until finally it will become tangential to the two lines of fracture. At this point, fracture will occur upon one or more of those planes in the body whose trangential and normal stresses have reached the critical ratio. These will be the planes whose angles α correspond to the points of tangency of the Mohr's circle with lines of fracture. From the diagram the points of tangency occur at

$$\left.\begin{aligned} 2\,\alpha &= \pm\,(90^\circ + \phi) \\ \text{or} \\ \alpha &= \pm\left(45^\circ + \frac{\phi}{2}\right). \end{aligned}\right\} \qquad (13)$$

Since, as we have noted, ϕ for sand ranges from 30° to 35°, fracture should occur along one or both planes, making an angle of about 60° to 62.5° to the least principal stress, which is vertical, or 27.5° to 30° to the horizontal. This is in fair agreement with the dip of the reverse faults shown in the photographs. It is a few degrees higher than the average dips observed for the reverse faults—a discrepancy to which we shall return later.

Analysis of Normal Faulting

Let us now consider what happens in the compartment where the normal faults occur. Here, as in the reverse-fault compartment, the initial state of stress at a point inside the sand is given approximately by

$$\sigma_1 = \sigma_3 = \rho g z.$$

In this case, however, as the partition begins to recede, the horizontal stress, which now becomes the least stress σ_3, begins to diminish, while the vertical stress, which is now the greatest stress σ_1, remains stationary, as before.

On Mohr's diagram (Fig. 9) we have, in this case, a fixed maximum stress and a diminishing minimum stress, with again a Mohr's circle of increasing radius. Ultimately, as σ_3 is further decreased, the circle will again become tangential to the fracture lines $\tau = \sigma \tan \phi$, and fracture will occur. As before, the angles α of the planes along which fracture will occur will be given by

$$\left.\begin{aligned} 2\,\alpha &= \pm(90^\circ + \phi), \\ \text{or} \\ \alpha &= \pm\left(45^\circ + \frac{\phi}{2}\right) \end{aligned}\right\} \qquad (14)$$

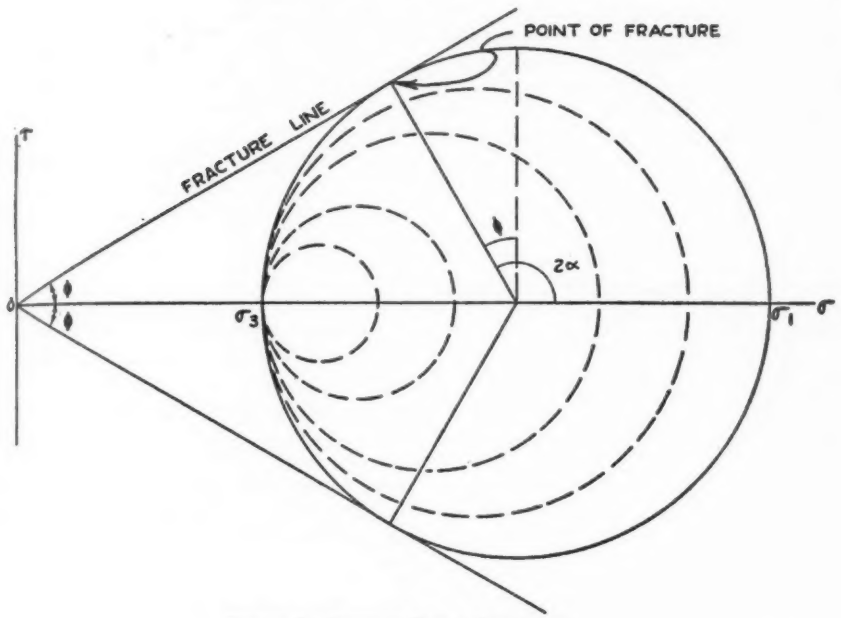

FIGURE 8.—REVERSE-FAULT CONDITIONS

Stress σ_1 increases until Mohr's circle reaches fracture lines. Fracture occurs at angle $\alpha = 45° + \frac{\phi}{2}$.

so that in this case also the fracture should be at an angle of about 60° to 62.5° to the least principal stress. In this instance, the least principal stress is horizontal, so the fracture plane should dip about 60° to 62.5°.

The average dip for normal faults in Table 1 was 61.2°, which is a very satisfactory agreement.

The normal-fault case is instructive in still another respect. Geometrically, normal faults correspond to a horizontal elongation of the section in which the faulting occurs. These faults accordingly have commonly been attributed to tensile stress and are often referred to as "tension faults." Loose, dry sand has zero tensile strength and is incapable of sustaining a tensile stress. We observe, however, that normal faults occur in it as readily as in solid rocks, and entirely as the result of compresive stresses. In fact, in both cases the fracture occurs along planes making an angle of 45°—$\phi/2$ to the greatest principal stress. In the reverse-fault case this stress is horizontal; in the normal-fault case it is vertical.

APPLICATION TO COHESIVE MATERIALS AND TO GEOLOGIC STRUCTURES

Coulomb Equation

So far our theory has been restricted to a noncohesive material; rocks, however, are cohesive materials, so it remains to be seen how we may modify the theory to include these also. Since Mohr's circle represents a general property of stress and needs no modification, we need only modify equation (10) which describes the behavior of the material. This modification consists only in adding a cohesive shear stress τ_0 to the stress τ of equation (10) to overcome the cohesion or initial shear strength of the material. The equation then reads

$$\left.\begin{aligned} &\frac{\tau - \tau_0}{\sigma} = \tan\phi, \\ &\text{or} \\ &\tau = \tau_0 + \sigma \tan\phi. \end{aligned}\right\} \qquad (15)$$

This equation appears to have been first proposed by the French physicist Coulomb (1776), and, while it may not be rigorously correct, it serves as an excellent first approximation to the behavior of cohesive solids,

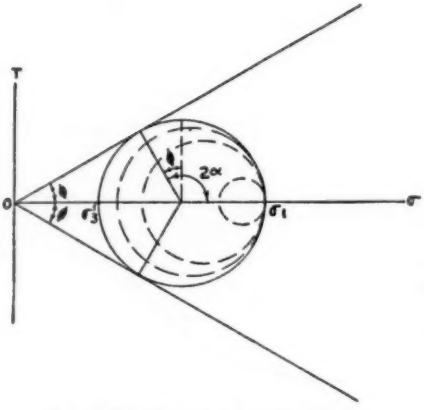

FIGURE 9.—NORMAL-FAULT CONDITIONS
Minimum stress σ_3 decreases until Mohr's circle reaches fracture lines.

including rocks. When plotted upon the $\sigma\tau$-diagram (Fig. 10), equation (15) represents a pair of straight lines with slopes $+\phi$ and $-\phi$ intersecting on the σ-axis at a point $\sigma = \tau_0/\tan\phi$.

The geometrical relations (Fig. 11) of the stresses at the time of fracture in this case are the same as in the noncohesive case. Fracture occurs when the Mohr's circle becomes tangential to the lines of fracture on the $\sigma\tau$-diagram, and, as before, the planes of fracture make an angle of $45° + \phi/2$ to the axis of least stress, or of $45° - \phi/2$ to the axis of greatest stress.

Data upon Angle ϕ for Rocks

Two methods are available for determining the angle of internal friction, ϕ, for rocks. One consists in computing ϕ from the observed angle between the surfaces of slip and the axes of principal stress when the latter are known; the second is by means of tests of rock specimens under known conditions of triaxial stress.

Prandtl and Rinne (Nádai, 1931a, p. 109–110) carried out a series of tests on polished cylindrical specimens of rock by compressing them axially to incipient failure. On the cylindrical surfaces, two families of helical lines of fracture were observed intersecting at an angle 2θ bisected by the axis of greatest stress. The angle θ is then complementary to the angle α, and from the Mohr diagram (Fig. 11)

$$\phi = 2\alpha - 90 = 90 - 2\theta.$$

On two photographs of marble specimens (shown by Nádai) the angle 2θ was 41° and 45°, respectively. The corresponding values of ϕ would therefore be 49° and 45°.

The same principal may be used in connection with the dip angles of simple normal and reverse faults. When faulting occurs at or near the surface of the ground in nearly level topography, the principal stresses must be respectively nearly vertical and horizontal. Here also

$$\phi = 90 - 2\theta$$

where θ is the angle of dip of reverse faults, or the angle of hade of normal faults.

Thus from fault data, with the angles of dip of simple reverse faults, or the hades of normal faults lying between the limits 20° and 40°, the angle of internal friction would lie between 10° and 50°. For the peak frequency in the angle of hade for normal faults of 27°, as reported by Sax, the peak frequency for the angle ϕ would be 36°.

The second method, that of testing specimens under known conditions of triaxial stress, consists in testing a cylinder under simultaneous radial and axial stress. The radial stress is supplied by a fluid pressure and the axial stress by a piston. The fluid is set at a chosen pressure $p = \sigma_2 = \sigma_3$ (or $p = \sigma_1 = \sigma_2$) and the axial stress, σ_1, is increased (or decreased if the axial stress is σ_3) until failure occurs. The Mohr's circle for the values of σ_1 and σ_3 at which failure occurs is constructed. This procedure is repeated with additional specimens of the *same* material until a family of over-lapping circles of increasing radii is obtained. The envelopes of these circles obviously represent the empirically determined loci of the fracture curves of the diagram. The angle of slope of the curves

with respect to the σ-axis is the angle of internal friction for the given material.

Tests of this kind appear first to have been made on rocks by von Kármán (1912); he ran a series of tests on marble which was found to behave as a brittle material at lower radial pressures but to flow plastically at higher pressures. The envelopes of the Mohr's circles thus obtained were convex outward with ϕ varying from an initial value of about 40° (corresponding to $\theta = 25°$) to a final value of near zero. Also conjugate slip surfaces on the slightly deformed specimens show an acute angle $2\theta \cong 50°$.

Triaxial tests on concrete were reported by Ros and Eichinger (1928). The angle θ as observed directly varied from 22° to 33°, which would correspond to values from 24° to 46° for the angle ϕ.

The U. S. Bureau of Reclamation at Denver has recently installed a large triaxial testing machine for testing cores of rock and concrete in connection with the construction of large dams (Blanks and McHenry, 1945), and a few results on rock and concrete have now been published (Jones, 1946; Balmer, 1946; McHenry, 1948). On rock cores from Boulder Dam (rock type not specified), the results of 16 tests gave for ϕ the value of 35°, which would correspond to $\theta = 27.5°$. Tests on concrete by both Jones and McHenry have given values of $\phi \cong 45°$, or of $\theta \cong 22.5°$.

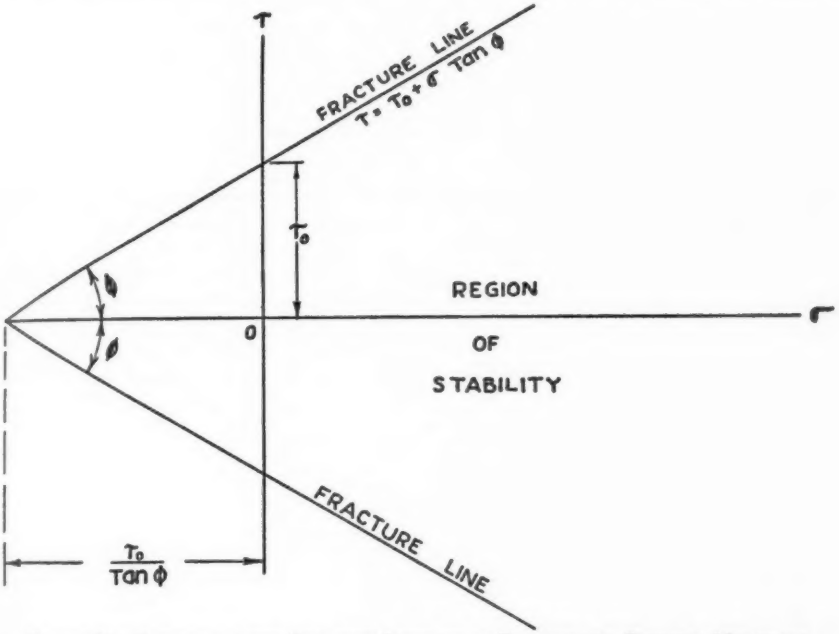

FIGURE 10.—POSITION OF THE FRACTURE LINES ON $\sigma\tau$ DIAGRAM FOR COHESIVE MATERIALS

It is interesting to compare these results with tests on asphalt aggregates for road building recently reported by Nijboer (1942). Triaxial tests were made upon dozens of different mixes under a wide range of conditions. In most cases the envelopes of the Mohr circles were straight lines though occasionally one with a small outward convexity was observed.

The angles ϕ found by these tests ranged between the extremes of 19° and 38°. The most frequently observed value, however, was 28°, and, for more than 95 per cent of all the measurements made, the observed values lay within the range $28° \pm 4°$. For rocks, this would correspond to normal faults with hades, or reverse faults with dips, of $31° \pm 2°$. Kry-

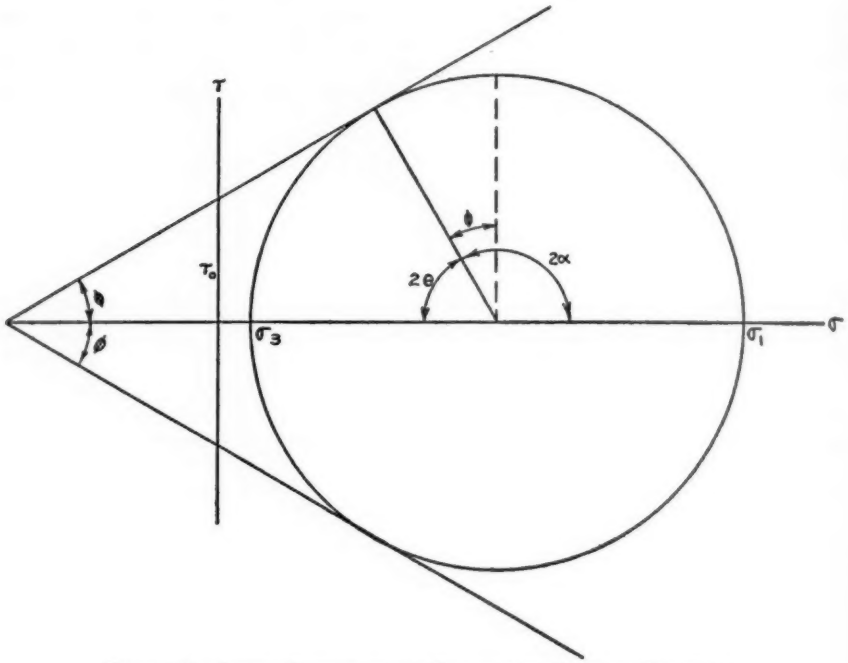

FIGURE 11.—STRESS CONDITIONS FOR FAULTING IN COHESIVE MATERIALS
Faults occur at angle $\alpha = 45° + \frac{\phi}{2}$ to the axis of least stress.

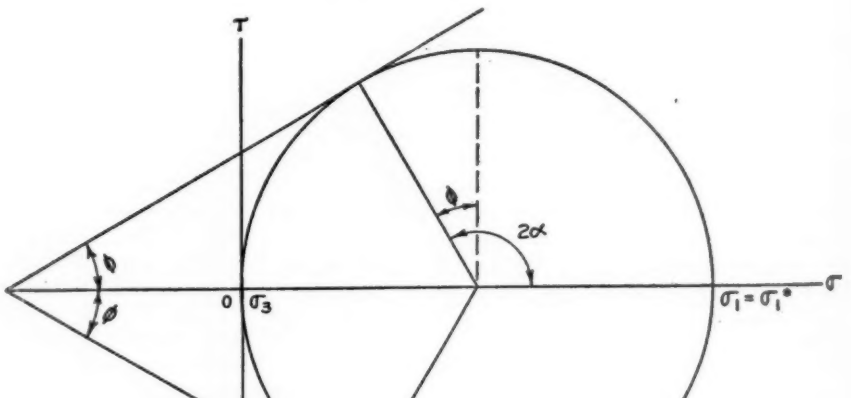

FIGURE 12.—CONDITIONS FOR ZERO HORIZONTAL STRESS IN NORMAL FAULTING

nine (1941, p. 172) reports that, for wet clay, ϕ ranges from a few degrees to 15° or 20°. This would correspond to normal-fault dips between 45° and 55°.

Thus, although data upon the angle of internal friction for rocks are as yet sparse, the computed angles of faulting are in good agreement with field observations.

Tension in Normal Faulting

We have already seen that, in the case of cohesionless materials, normal faults are produced only under compression. For cohesive materials (Fig. 12), it will be seen that, for any given material, there must exist at the time of faulting a certain critical value of σ_1, say σ_1^* for which σ_3 will be zero. Then, for all values of $\sigma_1 > \sigma_1^*$, the horizontal stress σ_3 in normal faulting will be compressive, and for all values of $\sigma_1 < \sigma_1^*$ the horizontal stress σ_3 will be one of tension.

Since, in the case of normal faulting, the vertical stress at a given depth is equal to the pressure of the overburden, there will be some critical depth for a given material below which the horizontal stress producing normal faults will be compressive and the existence of a tensile stress will be impossible. At less than this depth, the horizontal stress will be one of tension.

The approximate depth at which this transition will occur can be obtained from crushing-strength data of rocks. The conditions

$$\sigma_3 = O,$$

$$\sigma_1 = \sigma_1^*,$$

are those which are satisfied approximately in the crushing-strength tests for rocks at atmospheric pressure. Consequently, for a given rock the critical stress σ_1^* is equal approximately to its crushing strength. For dry rocks the depth at which this vertical stress occurs would be

$$z^* = \sigma_1^*/\rho g$$

where ρ is the bulk density of the material. In the earth, however, the rocks ordinarily are saturated with ground water, which exerts an upward force of buoyancy. In this case, the effective stress is that transmitted by the solid system. Hence this effective stress $\bar{\sigma}_1$ at a given depth is

$$\bar{\sigma}_1 = (\rho_s - \rho_w)\, g\, (1 - \epsilon)\, z,$$

or for the critical depth

$$z^* = \bar{\sigma}_1^*/[(\rho_s - \rho_w)\, g\, (1 - \epsilon)], \qquad (16)$$

where ρ_s is the grain or mineral density ρ_w the density of water, and ϵ the porosity of the rock.

The crushing strengths of rocks range from values near zero, for recent sediments, to as high as 3×10^9 dynes/cm² for granites. Such tests, however, are made upon nearly flawless specimens, so that, for large volumes of rock broken by numerous joints, the effective values will no doubt be considerably smaller. The Beaumont clay underlying Houston for example has a bearing strength of only about 10^6 dynes/cm². Recorded crushing strengths of sedimentary rocks are commonly of the order of $5—15 \times 10^8$ dynes/cm².

Introducing these values of σ_1^* into equation (16) and solving for z^*, we find the maximum depths at which tension can exist in rocks of various types. In the Gulf Coast sediments, for example, this depth is found to be of the order of 10^3 cm., or 10 meters (about 30 feet). In the more consolidated sediments, it may increase to a few hundred meters; and, in the strongest crystalline rocks, it may reach values of several kilometers.

Yet the Gulf Coast sediments are cut by numerous normal faults extending from the surface to depths of thousands of meters. It is clear, therefore, that aside from a surface veneer, these sediments have been broken by a series of normal faults in response exclusively to compressive stresses.

Problem of Asymmetrically Folded and Faulted Belts

One-sided Thrust Hypothesis

With this background, let us consider an equally familiar but more complex problem. One of the commoner types of orogenic structure is the belt of asymmetrically folded and faulted sediments as exemplified in North America by the Appalachian Mountains, the Ouachitas, the foothills of the Rocky Moun-

tains, and some of the West Coast ranges, and in Europe by the Alps, the Juras, and the Scottish Highlands. In these cases, the folds are unidirectionally overturned and accompanied by reverse faulting, with the direction of thrusting —that is, the direction of the relative displacement of the upper block with respect to the lower—in the same sense as the overturning of the folds. Moreover, where data are available, as in the foothills region of Alberta where seismic surveys have been made and numerous oil wells drilled, the fault surfaces have been found to be concave upward, the dip decreasing with depth.

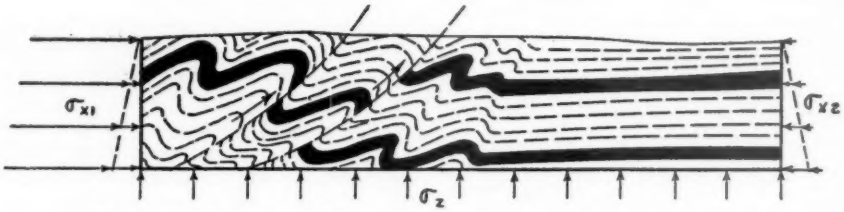

FIGURE 13.—COMPRESSIVE STRESSES ON ENDS OF SECTION OF ASYMETRICALLY FOLDED AND FAULTED SEDIMENTS

Considerable attention has been given to the causes of these structures, and the hypothesis most often favored has been that formulated by J. D. Dana (1847a; 1847b)—that such structures are formed by a one-sided "active thrust" from the direction opposite to that of the overturning. Thus, the Appalachian Mountains would have been formed by an active thrust from the southeast, which presumably died out with distance toward the northwest. An auxiliary question often considered is how far rocks of a given strength are capable of transmitting such a thrust.

The state of stress thus postulated and its associated orogeny is illustrated in Figure 13, where a large "active thrust" σ_{z_1} acts on the left-hand end of the section and dies out to the much smaller stress σ_{z_2} on the right-hand end. Not only does this appeal to the intuition, but it is supported by the deformational evidence as well. Since the rocks on the left are intensely deformed whereas those on the right are undistorted, the inference is justified that σ_{z_1} is very much greater than σ_{z_2}.

Application of the Newtonian Laws of Motion

That this picture is somehow deficient becomes evident when considered in the light of the Newtonian laws of motion, according to which the sum of all the forces acting upon the block in a given direction must equal the product of the mass of the block and the component of its acceleration in that direction. Taking the x-axis as horizontal, this requires that in the x-direction

$$\Sigma F_x = \int_0^{z_1} (\sigma_{x1} - \sigma_{x2})dz = ma_x \qquad (17)$$

As an order of magnitude, $(\sigma_{z_1} - \sigma_{z_2})$ may be taken to be about 10^{+9} dynes/cm^2. Then if the block of Figure 13 is assumed to be 100 kilometers wide, 10 kilometers deep, and 1 centimeter thick, ΣF_x will be about 10^{15} dynes.

For the ma-term, the mass of the block will be about 3×10^{13} grams. Velocities in known orogenies are rarely more than a few centimeters per year, so that secular accelerations much greater than a centimeter per year per year or about 10^{-13} cm/sec^2 are unlikely. Hence, the ma-term would have a magnitude only of the order of 10^{-2} gm cm/sec^2, which is infinitesimal as compared with the forces acting, and the sum of all forces must effectively be zero throughout the orogenic process.

Since, with the stress distribution postulated in Figure 13, the sum of the horizontal forces acting upon the block is manifestly not zero, some essential element must be lacking. Since body forces are ineffective horizontally, the only remaining possibility is shear stresses upon the vertical faces parallel to the plane of

the drawing and along the bottom of the block. In arcuate structures, shear stresses on the vertical faces normal to the strike exist, but they vanish as the curvature approaches zero and the structure becomes rectilinear.

Assuming the structure to be rectilinear, we are then left only with the bottom shear stress τ_{zz}, whose magnitude at any given distance x along the bottom must just be sufficient to balance the force due to the stress difference $d\sigma_z$ in the horizontal distance dx. Thus, at distance x

$$\tau_{zz}dx = + \int_0^{z_1} \left[\left(\sigma_z + \frac{\partial \sigma_z}{\partial x} dx \right) - \sigma_z \right] dz$$

or

$$\tau_{zz} = + \int_0^{z_1} \frac{\partial \sigma_z}{\partial x} dz ; \qquad (18)$$

that is the shear stress on the bottom of the block at a given point is proportional to the gradient of the normal stress in that direction. The gradient of the normal stress would be approximately the same as the gradient of the intensity of the deformation. Hence, in Figure 13 the shear stress would have a maximum value near the lower left-hand corner of the block and would decline to near zero at the lower right-hand corner. The complete equation of forces in the x-direction must therefore be

$$\Sigma F_x = \int_0^{z_1} (\sigma_{x_1} - \sigma_{x_2}) dz - \int_{x_1}^{x_2} \tau_{zz} dx = 0. \qquad (19)$$

As noted, the components of shear stress parallel to a plane normal to both are the same on any two mutually perpendicular planes, but of opposite rotational senses. Hence there must also be a downward-directed shear stress on the left-hand vertical face of the block equal in magnitude at the bottom corner to the stress on the bottom, and approaching zero toward the top. A similar shear stress, but of magnitude near zero and directed upward, must exist on the right-hand end.

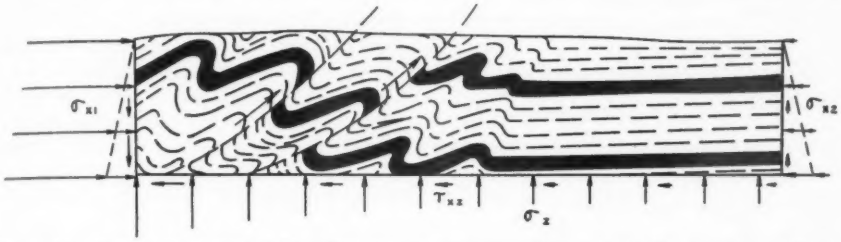

FIGURE 14.—COMPLETE SYSTEM OF TWO-DIMENSIONAL STRESSES ACTING UPON BOUNDARIES OF BLOCK

In addition, all surface forces and body forces must be so related that all turning moments acting on the block are zero. When these several conditions are satisfied the approximate set of boundary stresses shown in Figure 14 is obtained as being necessary to produce the generalized type of orogeny shown.

Interior Stress Distribution

From the boundary stresses shown in Figure 14, the approximate pattern of the stress distribution in the interior of the block can be inferred.[1] Trajectories of principal stress are curves which at every point are tangent to a given principal stress. Since the principal stresses are mutually perpendicular, then three perpendicular stress trajectories, one each for σ_1, σ_2, and σ_3, must pass through each point. In a two-dimensional stress system on a plane parallel to σ_1 and σ_3, two families of orthogonal stress trajectories, one everywhere parallel to σ_1 and the other to σ_3, will exist.

Recalling that, when the principal stresses are unequal, shear stresses exist upon all sur-

[1] The reasoning here is intentionally only qualitative, the objective being to convey an intuitive sense of the principles involved. A more formal quantitative analysis is given in a companion paper by the author's colleague, W. Hafner (1951).

faces except those perpendicular to the stress trajectories, the approximate pattern of the stress trajectories in the interior of the block may be determined from the combination of normal and shear stresses on its boundaries.

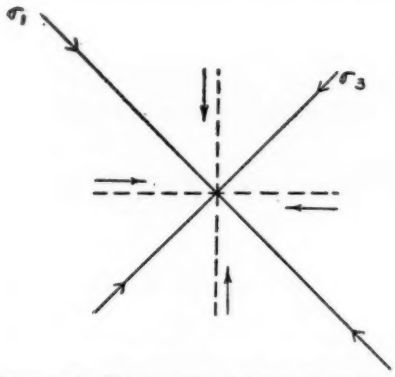

FIGURE 15.—DIRECTIONS OF SHEAR STRESSES IN VARIOUS QUADRANTS DEFINED BY PRINCIPAL STRESSES

can be definitely known. Across any plane on which a compressive normal stress σ and shear stress τ exists, the axis of greatest principal stress, σ_1, will lie in the quadrant between the plane normal and the direction *from* which the shear stress occurs (Fig. 15).

The boundary stresses of Figure 14 will produce the approximate pattern of principal-stress trajectories in the interior shown by the solid curves of Figure 16. The family of greatest-stress trajectories, σ_1, is tangential to the upper surface of the block, plunging downward and divergent to the right, and convex upward. The family of least-stress trajectories, σ_3, is orthogonal with this.

Surfaces of Potential Faulting

If we now assume that faulting is most likely to occur along surfaces tangent to the intermediate stress, σ_2, and at an angle of about $45°-\frac{\phi}{2}$ to the greatest stress, where ϕ

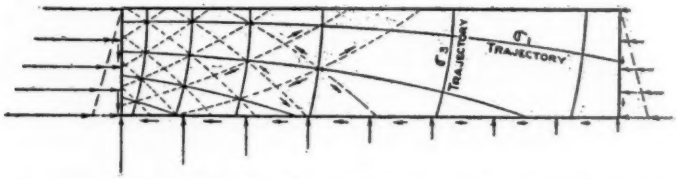

FIGURE 16.—TRAJECTORIES OF PRINCIPAL STRESSES (SOLID LINES), AND OF POTENTIAL REVERSE-FAULT SURFACES (BROKEN LINES) COMPATIBLE WITH THE BOUNDARY STRESSES OF FIGURE 14

Arrows indicate directions of potential slip

On the upper surface of the block, the normal stress is the atmospheric pressure and the shear stresses are zero. Therefore, at any point upon this surface, one of the stress trajectories must terminate perpendicularly, and the other must be tangential to the surface.

Across the left-hand end of the block, and the bottom, the stress trajectories must cross obliquely, with the angle of obliquity approaching zero near the upper surface, and increasing downward. Without knowing the actual magnitudes of both the normal and shear-stress components, the angles of incidence of the stress trajectories can be determined only qualitatively, but the quadrant in which each falls

may be taken to be about 30°, we are able to sketch in on Figure 16 the traces of the surfaces of potential faults, and indicate their directions of relative displacement. These comprise two families of curves (shown by dashed lines) which everywhere intersect the σ_1-trajectories at an angle of about 30°. In virtue of the divergence and curvature of the stress trajectories, these surfaces are also curved, one set convex and the other concave upward.

At any given point, the stresses on each of these conjugate surfaces are the same; so that if they are at the critical value for fracturing on one surface, the same is true for the other. However, slippage along a finite surface in-

volves an integral of conditions along the entire surface. Whatever this integral should be, in homogeneous materials with symmetrical stress distributions, its value over each of a pair of conjugate surfaces of potential slippage will be the same, so that equal slip should occur on each family of surfaces.

In asymmetrical cases, the integral of any stress quantity over one surface or family of surfaces will in general be different from that over the conjugate surface or family. Because of this inequality, slippage should occur on one set before on the other, or on only one of the two sets. In the asymmetrical geological system here considered, faulting develops almost exclusively on the concave-upward set of surfaces. The same was true for the reverse faulting in the sandbox experiment.

In experiments with symmetrical systems, slippage on both sets of surfaces is observed.

Returning to the sandbox experiment, it will be recalled that the average angle of hade for the normal faults was about 29°, and of dip for the reverse faults was 25°, whereas our theory indicated that the two should be the same. Perhaps we can now explain this discrepancy. We assumed the principal-stress trajectories to be strictly horizontal and vertical. However, in the reverse-fault case, the sand was pushed along the bottom which exerted a frictional reaction in the form of a bottom shear stress. The effect of this would be to deflect the horizontal stress trajectories downward and thus to lower the dip angle of the reverse faults.

Other shear stresses along the vertical faces of the partition must also have existed which would likewise tend to produce some deviation in observed angles from the idealized conditions assumed.

Conclusion

It thus appears that some of the more common large-scale geological structures are in satisfactory agreement with theoretical deductions based upon the stress patterns inferred from the observed deformation and Newton's laws of motion, and the empirically determined properties of rocks under known stress conditions.

References Cited

Anderson, E. M. (1942) *Dynamics of faulting and dyke formation*, Oliver and Boyd, Edinburgh and London, p. 191.

Balmer, Glenn G. (1946) *A revised method of interpretation of triaxial compression tests for the determination of shearing strength*, U. S. Bur. Reclamation Basic Structural Lab. Rep. No. SP-9.

Billings, Marland P. (1946) *Structural geology*, Prentice-Hall, Inc., New York, p. 206.

Blanks, R. F., and McHenry, Douglas (1945) *Large triaxial testing machine built by Bureau of Reclamation*, Eng. News-Record, vol. 135, p. 171–173.

Chamberlin, R. T., and Shepard, F. P. (1923) *Some experiments in folding*, Jour. Geol., vol. 31, p. 490–512.

Coulomb, C. A. (1776) *Essai sur une application des regles des maximis et minimis à quelques problèmes de statique relatifs a l'architecture*, Acad. Sci., Paris, Mem. pres. divers savants, vol. 7.

Dana, J. D. (1847a) *Geological results of the earth's contraction*, Am. Jour. Sci. (2), vol. 3, p. 176–188; vol. 4, p. 88–92.

—— (1847b) *On the origin of continents*, Am. Jour. Sci. (2), vol. 3, p. 381–398.

Hafner, W. (1951) *Stress distributions and faulting*, Geol. Soc. Am., Bull., vol. 62, p. 373-398.

Jones, Valens (1946) *Tensile and triaxial compression tests of rock cores from the passageway to penstock tunnel N-4 at Boulder Dam*, U. S. Bur. Reclamation, Basic Structural Res. Rept. No. SP-6.

von Kármán, Th. (1912) *Festigkeits Versuche unter allseitigen Druck*, Mitteilungen über Forschungzarbeiten auf dem Gebiete des Ingenieurswesens, H. 118, V.d.I.

Krynine, D. P. (1941) *Soil mechanics*, McGraw-Hill, Inc., New York, p. 451.

Leith, C. K. (1913) *Structural geology*, 1st Ed., Henry Holt & Co., p. 55.

McHenry, Douglas (1948) *The effect of uplift pressure on the shearing strength of concrete*, International Congress on Large Dams, June 1948.

Mead, W. J. (1925) *Geologic role of dilatancy*, Jour. Geol., vol. 33, p. 685–698.

Mohr, Otto (1871; 1872) *Beiträge zur Theorie des Erddrucks*, Zeitschr. Architekten und Ingenieur —Ver. Hannover, vol. 17, p. 344; vol. 18, p. 67 and 245.

—— (1882) *Über die Darstellung des Spannungzustandes eines Körpelementes*, Zivil Ingenieure, p. 113.

—— (1900) *Welche Umstände bedingen die Elastizitätsgrenze und den Bruch eines Materials*, Zeitschr. Vereins deutsches Ing., p. 1524.

Nádai, A. (1928) *Plasticität und Erddruck*, Handbuch der Physik, VI, J. Springer, Berlin, p. 428–500.

—— (1931a) *Plasticity*, McGraw-Hill, Inc., New York, p. 349.

—— (1931b) *Phenomenon of slip in plastic materials*, Edgar Marburg Lecture, Am. Soc. Test. Mat., Pr., vol 31, pt. II, p. 11–46.

Nijboer, L. W. (1942) *Onderzoek naar den weerstand*

van bitumen-mineraalaggregaat mengsels tegen plastische deformatie, N. V. Noord-Hollandsche Uitgevers Maatschappij, Amsterdam, p. 232.

Rankine, W. J. M. (1857) *On the stability of loose earth*, Royal Soc. London, Philos. Tr., vol. 147.

Sax, H. G. J. (1946) *De tectoniek van het Carboon in het Zuid-Limburgsche mijngebied*, Mededeelingen van de Geologische Stichting, Ser. C-I-I no. 3, p. 1–77.

Ros, H. C. M., and Eichinger, A. (1928) *Experimental attempt to solve the problem of failure in materials—nonmetallic materials*, Federal Mat. Testing Lab., E. T. H., Zürich, Rept. No. 28. Translation by F. Stenger, U. S. Bur. Reclamation, Denver.

SHELL OIL CO., 3737 BELLAIRE BLVD. HOUSTON 5, TEXAS.

MANUSCRIPT RECEIVED BY THE SECRETARY OF THE SOCIETY OF AMERICA, SEPTEMBER 23, 1949.

BULLETIN OF THE GEOLOGICAL SOCIETY OF AMERICA
VOL. 62, PP. 373-398, 9 FIGS., 1 PL. APRIL 1951

STRESS DISTRIBUTIONS AND FAULTING

BY W. HAFNER

ABSTRACT

Tectonic deformations result from a condition of internal stress caused, in turn, by primary and secondary forces. In the geological literature, a great deal of discussion is based on a direct connection between forces and deformation, completely by-passing the concept of stress. This paper is a contribution in the intermediate field of stress relations. It presents the complete solutions of certain stress systems caused by various forms of boundary forces. Furthermore, the location and attitude of the fault surfaces likely to be associated with them is determined.

The basic concept of stress is briefly reviewed and some of the fundamental differences between the force-vector and the stress-tensor are pointed out. The fallacy of applying the familiar methods of vector-addition of forces to problems in stress is demonstrated.

For certain systems of external boundary forces acting on a portion of the earth's crust, the internal stress distribution can be calculated by means of the familiar equations of elasticity. Appropriate calculation methods for two-dimensional cases are shown and the basic equations applicable to a series of important boundary conditions are derived. The examples here presented include: (1) superposed horizontal compression with constant lateral and vertical gradients; (2) horizontal compression with exponential attenuation; and (3) sinusoidal vertical and shearing forces acting on the bottom of a block. The latter equations provide solutions for differential vertical uplift and for the important case of drag exerted on the bottom of the crust by convection currents in the substratum. Diagrams show configuration of the stress trajectories and distribution of the maximum shearing stress for the resulting stress systems.

A parallel series of diagrams shows the disposition between the relatively stable and unstable segments of the blocks and the probable attitude of the fault surfaces likely to be associated with the individual stress systems. The construction of the fault surfaces is based on the original stress distributions alone, the influence of local stress alterations due to the occurrence of fracture being disregarded. The full effect of this inter-action is not known, due to the extreme complexity of the problem. The fault patterns shown are strictly applicable only to the initial stages of fracture, but may also represent fair approximations during the more advanced stages, since the original stress remains the dominating influence and stress-alterations due to faulting diminish rapidly with distance.

CONTENTS

	Page
Introduction	374
Acknowledgments	374
Stress and force	374
Method of calculating stress systems	377
The standard state	380
Faulting associated with stress distribution	381
Examples of two-dimensional stress systems	384
Introduction	384
Supplementary horizontal stress without superposed vertical stress	384
Supplementary horizontal stress decreasing exponentially in the horizontal direction	389
Variable vertical and shearing stress acting on the bottom of a block	391
Convection currents	396
Conclusions	397
References cited	398

ILLUSTRATIONS

Figure	Page
1. Limited definition of stress	375
2. Complete expressions of stress tensor	376
3. Two-dimensional stress components and stress ellipse	376
4. Composition of stresses and forces	377
5. Determination of boundaries of stable portions of block	383
6. Supplementary stress system consisting of	

Figure Page
superimposed horizontal pressure constant with depth and with constant lateral gradient 385
7. Supplementary stress system consisting of superimposed horizontal pressure with constant lateral and vertical gradients... 386
8. Superposed horizontal stress decreasing exponentially in horizontal direction..... 387
9. Convection currents and boundary stresses at bottom of crust..... 397

Plate Facing page
1. Supplementary stress systems..... 384

Introduction

The earth's crust is unceasingly undergoing deformations because of the interplay of forces acting upon it. The primary forces are sufficiently powerful to produce disturbances of enormous magnitude, such as mountain chains or the crustal down-buckling deduced from gravity observations; the secondary ones tend to bring about partial or complete restoration of equilibrium.

Many hypotheses have been advanced regarding the origin and nature of the deformative forces but, as yet, all these theories are speculative in varying degree and a wide divergence of viewpoint exists. Knowledge of the results of these processes is much more advanced, at least with respect to the uppermost portion of the crust. A vast and ever-growing body of observational data on the nature of the deformations is becoming available. In fact, the validity of the various hypotheses on the origin of the deformations rests largely upon the degree of agreement with this accumulated store of data, aside, of course, from the inherent soundness of the principles employed.

In all quantitative studies on the relationship between the original forces and the resulting deformations, an intermediate field of investigation enters, the condition of stress in the earth's crust. The original forces—whether primary or secondary, whether internal body or external boundary forces—set up a state of stress in the earth's crust which, in turn, produces the observed distortions. In the geological literature, we quite often find arguments attempting to explain the deformations *directly* in terms of the original forces. While this approach may be justified in certain simple qualitative considerations, it is an inherently fallacious procedure and more often than not leads to confusion, rather than elucidation, of the problem discussed. It is especially inappropriate in quantitative analysis.

This paper offers the results of some studies in the intermediate field of stress relations. It presents the complete solutions of the stress distributions produced by certain systems of external boundary stresses. The nature of the faulting most likely to be associated with them is analyzed, although certain complications for which no complete solutions are available have to be disregarded in this phase of the investigation. The stress distributions here analyzed were selected with the view of covering some of the geologically more important groups of boundary stresses acting on portions of the earth's crust, such as lateral compression, differential vertical uplift, and drag exerted on the bottom due to viscous currents in the substratum. No attempt is made to enter the more speculative field of the origin of these forces. However, the author believes that any advance made in our understanding of the relation between the observed tectonic phenomena and the causal stress systems will indirectly promote progress in the more important, but much more illusive, field of the ultimate causes of the earth's deformations.

Acknowledgments

The writer wishes to thank Shell Oil Company, Incorporated, for permission to publish this paper. He further wishes to express his appreciation to Dr. M. King Hubbert for his stimulating influence concerning the quantitative approach to geological problems in general, for a critical reading of the manuscript, and for helpful suggestions during discussions of the fault problem. Thanks are also due to Miss B. J. King for assistance in the numerical calculations, and to C. B. Metcalfe for the drafting of the diagrams.

Stress and Force

In the geologic literature we encounter not infrequently a misunderstanding of the concept

of stress. Many authors use the terms "force" and "stress" synonymously, in the sense of dynamical forces, and are not aware of the fundamental differences between the two concepts. In view of this fact, it appears advisable to review briefly the general properties of the

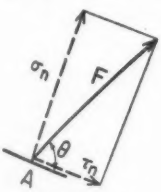

$$S = \lim \frac{\delta F}{\delta A}$$

FIGURE 1.—LIMITED DEFINITION OF STRESS

state of stress and its relation to forces. Such considerations, though of elementary character, may be helpful to readers not thoroughly familiar with these concepts.

Stress is force per unit area. A more precise definition (Timoshenko, 1934, p. 3) states that it represents the limiting value of the ratio of a surface force divided by the area upon which it acts (Fig. 1); in formula:

$$S = \lim \frac{\delta F}{\delta A}$$

This force may be resolved into a normal component σ_n, and a tangential component τ_n. Depending upon whether σ_n is directed outward or inward, it represents a tension or a pressure, respectively. The tangential component τ_n, which is acting parallel to the surface element, is a shearing stress.

This definition brings out one of the differences between stress and force: that the two quantities are dimensionally at variance. The dimensions of force are (m, l, t^{-2}); those of stress are (m, l^{-1}, t^{-2}). Hence, the statement that stress *is* force, as found in a well-known textbook on structural geology, is incorrect. However, the difference between stress and force goes much deeper. If we are dealing with dynamical forces only, it would always be possible by the process of resolution of forces to determine the normal and tangential components with respect to *any* direction of the surface element δA passing through the point. When dealing with stress, on the other hand, we know nothing whatever of the magnitude of stress after rotation of the element into a different direction. To solve this simple problem, we need an expression for the state of stress which defines this quantity for *every* surface element leading through a given point, irrespective of direction. Mathematically, this more comprehensive expression is a tensor quantity and, more specifically, a symmetric tensor of second degree. This is in marked contrast to force, which is a vector quantity. A tensor requires for its description more than three components and is therefore a more complicated concept than a vector. The relation is thus similar to that between a vector and a scalar. It is as misleading to think of stress in terms of a vector as it would be to treat a problem involving force in terms of a scalar function. The specific properties of the stress tensor can be adequately described without recourse to the general theory of tensors. The most important fact is that a total of six quantities is needed for a complete determination of the state of stress at any one point in a solid. In contrast, force, being a vector, requires only three quantities for specification. This explains why the above simple problem is indeterminate if only the three parameters of a force-vector are given.

There are two convenient ways to describe the six parameters of the stress tensor (Fig. 2): (1) State the stress components acting on the surface of a cubic element whose faces are parallel to the coordinate axes or (2) Use the well-known stress ellipsoid. The stress ellipsoid is defined by three mutually perpendicular directions, called the principal directions, and the intensities of the stresses in these directions, called the principal stresses. Each method requires six independent quantities; if known at each point, the condition of stress throughout the body is completely determined. The stress systems analyzed in the present paper will be restricted to two-dimensional cases of plane deformations. These are characterized by the fact that variable displacements occur only in parallel planes, namely those planes which are oriented perpendicular to the axes of the structures. Elongation in the third, or longitudinal, direction may or may not take place; if it does, it is constant over the entire cross-section. In such systems, two of the independent

shear stress components are automatically zero, and the normal stresses parallel to the longitudinal axes do not vary in this direction. The solution of stress problems is then reduced to the determination of three components instead simultaneously at a point, the resultant force may be obtained by the well-known method of vector addition. Not infrequently we find this method applied to stresses too, sometimes quite specifically, more often in rather vaguely

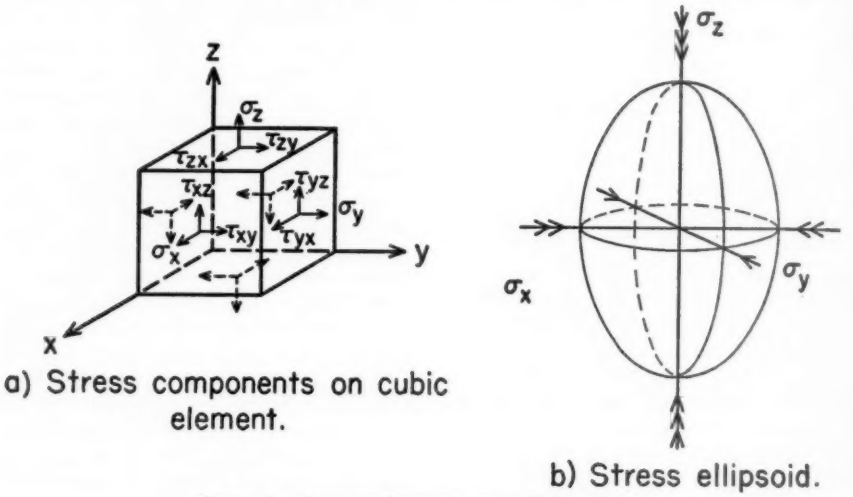

FIGURE 2. COMPLETE EXPRESSIONS OF STRESS TENSOR

of six, as in the general three-dimensional case. Taking the x-axis as the horizontal direction *in* the cross-section, the y-axis vertically downward (the z-coordinate being in the longitudinal direction), the three components then are σ_x, σ_y, and τ_{xy}, and the stress ellipsoid is reduced to a stress ellipse in the xy-plane (Fig. 3).

The stress ellipse provides a simple and convenient means of illustrating some of the fundamental differences between the stress-tensor and the force-vector. Two of them concern the methods of resolution and composition of forces and stresses. To illustrate the first case, assume a surface force acting in the direction of σ_x (Fig. 3). Its vector component at right angle, in the y-direction, is zero, whereas the corresponding stress component σ_y may be of any magnitude. This again shows that the process of resolution of forces for the purpose of determining the stress components acting upon a surface in any direction other than that specified in the limited definition of stress is inapplicable. A similar situation exists with respect to the composition of forces and stresses. When several forces act

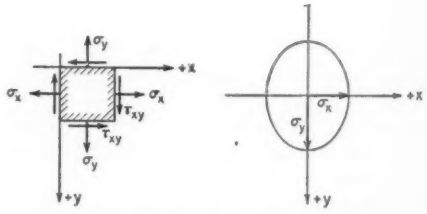

FIGURE 3.—TWO-DIMENSIONAL STRESS COMPONENTS AND STRESS ELLIPSE

phrased statements. Such deductions are basically wrong and lead often to complete confusion in the process of reasoning. When a solid is subjected to several simultaneous stresses, they can, of course, also be combined into a single stress system, but the procedure is quite different from the method of vector addition. The same is true for the respective results. The combination of stresses is based on the principle of superposition. It states that addition—in the form of linear functions—of the stress components from two, or several, valid stress systems, produces a new one which is likewise valid, provided the resulting defor-

mation is still within the elastic limit. An important example of this principle will be given later. Again the stress ellipse is useful to illustrate the difference between the methods of combining stresses and forces. Let us assume a uniform and uniformly directed pressure σ_x acting in the direction of the x-axis and a second similar pressure σ_y acting in the y-direction. Each of these systems satisfies the required equations and, hence, represents a permissible stress system. The method of superposition yields a two-dimensional stress system characterized by the stress ellipse shown in Figure 4. Its principal directions coincide with the co-ordinate axes, and the intensity of the stress acting on any surface element at right angles to the xy-plane is represented by one of the radius vectors of the stress ellipse. It is to be noted, however, that the direction of the normal to the surface element and that of the corresponding radius vector are not identical (except for the principal planes); the exact relation between these directions is somewhat complicated but need not be considered here. If, on the other hand, we should apply the method of vector-addition to forces of equal intensity as σ_x and σ_y, the result would be totally different. Compare Figures 4*a* and 4*b*. The vector sum of f_x and f_y yields a force f_s which is substantially in excess of any radius vector in Figure 4*a*, regardless of direction. Hence this procedure cannot be applied to stress relations. It is, nevertheless, frequently employed in discussions on structural problems, and leads to serious errors, both in the quantitative results as well as the more general qualitative deductions.

A further difference between stress and force concerns statements of direction. One may speak of a force as acting in a certain direction, say towards the north. When applied to internal stresses, such statements have no sense. A stress component acting upon one side of a surface element exists only in co-ordination with a component of equal intensity but opposite direction, acting on the other side. This is true for normal, as well as shear stresses. Hence a pressure or a tension may exist in a north-south direction, but not towards the north or towards the south.

The co-existence of stress and counter-stress on opposite sides of a surface element is a general property existing on any imaginary internal surface of a body, as well as on all its boundary surfaces. One very important implication of this condition concerns its application to the surface of the earth. Since the air is incapable of sustaining a shearing stress, τ_{xy} must be zero everywhere along this surface. Furthermore, the vertical pressure is reduced to the normal atmospheric pressure and cannot exceed it. This pressure is a very small quantity when compared to the internal stresses in the crust in which we are here interested; hence, it can safely be neglected. These considerations impose two specific boundary conditions which *must* be satisfied by every stress distribution applicable to geological problems: that σ_y and τ_{xy} vanish for every point along the free surface of the earth.

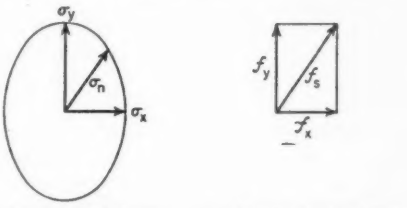

FIGURE 4.—COMPOSITION OF STRESSES AND FORCES

METHOD OF CALCULATING STRESS SYSTEMS

The methods applied to derive complete solutions of geologically significant stress distributions will be briefly outlined. Only two-dimensional cases will be treated. This simplification is fully justified for numerous structural problems but is not applicable, of course, to those of essentially three-dimensional character. A further assumption is that the stressed medium is homogeneous. This second restriction is geologically much more undesirable; however, the mathematical treatment of non-homogeneous cases would be extremely complicated.

The internal state of stress in a block of the earth's crust is adequately portrayed by the following sets of curves:

(1) *The stress trajectories*, defined by the property that the directions of the principal stresses are the tangents to these curves at all points. One set determines the direction of the maximum principal stress and a second one that of the minimum principal stress. The two sets are orthogonal everywhere.

(2) *Lines of equal maximum shearing stress*, consisting of a series of lines each of which connects all points of equal magnitude of this quantity.

The intensities of the two principal stresses can be illustrated by similar curves; however, they are less important for our purposes and are omitted from the illustrations to avoid overcrowding. Conversely, the external forces, or boundary stresses, form an integral part of each analysis and are, therefore, plainly marked on the diagrams.

The method here employed for the calculation of the internal stress distributions is based on the use of the Airy stress function, which offers an especially convenient approach for two-dimensional cases. It can be shown that for plane stress distributions—as well as for plane deformations—all three stress components can be expressed as second partial derivatives of a single function Φ which is a scalar function of x and y. Thus its role is somewhat similar to the potential function as applied to gravity, magnetism or other force fields. As is well known, the three force-components of such fields can likewise be expressed as partial derivatives of a single scalar function—the potential function—which greatly facilitates the mathematical treatment of the respective fields. However, the vector-components of the force fields are the *first* partial derivatives of the potential function, whereas the three components of the stress-tensor are the *second* partial derivatives of the stress function.

Now the theory of elasticity shows that the equations of static equilibrium are automatically satisfied if we define the stress components by the expressions

$$\sigma_x = \frac{\partial^2\Phi}{\partial y^2}; \quad \sigma_y = \frac{\partial^2\Phi}{\partial x^2}; \quad \tau_{xy} = -\frac{\partial^2\Phi}{\partial x \partial y}; \qquad (1)$$

when body forces are absent, and by the expressions

$$\sigma_x = \frac{\partial^2\Phi}{\partial y^2}; \quad \sigma_y = \frac{\partial^2\Phi}{\partial x^2} - \rho g y; \quad \tau_{xy} = -\frac{\partial^2\Phi}{\partial x \partial y}; \qquad (1)'$$

when gravity represents the only body force. Here ρ is the density of the material, assumed to be constant, and g is the constant of gravitational acceleration. (When applied to engineering problems, expressions (1)′ are usually stated in a different form, the term $-\rho g y$ here added to σ_y being replaced by a term $-\rho g x$, attached to τ_{xy}. (See Timoshenko, 1934, p. 25). The variation here adopted likewise satisfies the equilibrium equations and is preferable for geological investigations because the physical interpretation of the gravity term is more directly apparent. The resulting loss of symmetry is of no consequence.)

In order to yield a valid stress system, another requirement must be fulfilled. This arises from the fact that the stress components are connected by Hooke's law with the strain components (elongations), which, in turn, are defined as functions of the displacements. In two-dimensional problems, there are three stress and three corresponding strain components but only two displacements; hence, the former are not independent but must be connected by an equation establishing a condition of internal consistency of the displacements. This equation is called the compatibility equation. When applied to the stress function, it can be shown that a necessary—but also sufficient—requirement is that this function satisfy the equation:

$$\frac{\partial^4\Phi}{\partial x^4} + 2\frac{\partial^4\Phi}{\partial x^2 \partial y^2} + \frac{\partial^4\Phi}{\partial y^4} = 0 \qquad (2)$$

If this requirement is fulfilled, the stress function provides a method for the direct determination of the three stress components, making it unnecessary to first determine the displacements. The method then consists in finding suitable functions Φ which satisfy equation (2) and simultaneously yield a system of boundary stresses which are of interest to geological investigations.

Having found a suitable function of this type, the solution of the complete stress system is simple and straightforward. The three stress components are given directly by differentiation of Φ, according to formulae (1). The remaining significant stress quantities are then

obtained by the well-known equations of elasticity. The maximum shearing stress at any point is:

$$\tau_{max} = \pm \left\{ \left(\frac{\sigma_x - \sigma_y}{2} \right)^2 \tau_{xy}^2 \right\}^{\frac{1}{2}} \qquad (3)$$

The intensities of the two principal stresses are:

$$\sigma_1 \text{ or } \sigma_2 = \tfrac{1}{2} (\sigma_x + \sigma_y) \pm \tau_{max}, \qquad (4)$$

and the directions of the stress trajectories are given by:

$$\tan 2\beta = \frac{2\tau_{xy}}{\sigma_x - \sigma_y}, \qquad (5)$$

where β represents the angle between the outward-directed normal of the surface element and the positive x-axis, in the direction from the latter towards the positive y-axis. In the following calculations, the two normal stress components σ_x and σ_y are taken positive if they represent tensile stresses, negative if they are compressive stresses.

The relation between the internal stress distribution of a body of limited extent and the forces causing it need some further explanation. The stress components defined by equations (1)′ include the effect of gravity, whereas those of equations (1) are due only to the surface forces acting upon the boundaries of a block. In contrast to many engineering problems where gravity is a negligible factor, it constitutes one of the primary forces in geological systems and hence requires special consideration. This will be discussed in more detail in the next section. First we will focus our attention on the surface forces. The stress systems to be analyzed are defined by analytical functions which, in most cases, extend to infinity. In geological problems, on the other hand, we wish to investigate finite portions of the earth's crust which are exposed to the action of surface forces along their boundaries. Since such blocks are essentially stationary, the surface forces cannot be chosen arbitrarily but only such combinations are admissible which, on the whole, satisfy the equations of static equilibrium. Now the relation between the internal stress distribution defined by equations (1) and the boundary forces responsible for it is directly given by a fundamental principle. It states that any imaginary surface inside a stressed medium can be made a boundary surface without causing a disturbance in the internal stress distribution, provided a system of surface forces equivalent to the former internal stress components is applied to this boundary. By this process we can arbitrarily select any desired location and limits of a block within the confines of an analytically defined stress distribution and can also immediately state the system of surface forces which produces it. This principle will be used extensively in the later treatment of specific examples.

The method of determining stress systems here outlined is, in some respects, an indirect approach. The stress distribution is defined first and the causal boundary forces are then fixed automatically. This is obviously not an altogether ideal procedure. Yet it has decided advantages and in reality is much more flexible than one might expect it to be. First the system of boundary forces thus derived automatically satisfies the requirement of static equilibrium. This imposition might constitute a tedious complication in all but the simplest cases if the direct approach of starting with arbitrarily selected boundary conditions were used. Second, numerous boundary systems representing some of the geologically most interesting cases can easily be obtained by suitable choices in the selection of the Airy stress function. Another important factor greatly enhances the flexibility of this method. As seen from equation (2), the stress function Φ is obtained by a solution of a fourth order differential equation. Hence it contains four independent integration constants which will also enter the expressions for the stress components (1). Now, as previously pointed out, any stress distribution applicable to our problems *must* satisfy the boundary conditions at the surface of the earth. Due to this restriction, two of the four integration constants must be expended for this purpose. The remaining two, however, are unassigned by general theoretical requirements and, therefore, can be used for the modification of the boundary stresses. It will be seen later that this freedom provides the means for a considerable degree of variability in the selection of geologically interesting cases.

The Standard State

E. M. Anderson (1942) has introduced the term "standard state," defined (p. 137) as

"a condition of pressure which is the same in all directions at any point, and equal to that which would be caused by the weight of the superincumbent material, across a horizontal plane, at the particular level in the rock. It is assumed in this definition that the surface is flat, and that the strata are of uniform specific gravity."

It will be shown that the standard state—according to this definition—represents a stress system composed of two parts: (1) the effect of gravity, and (2) a superposed horizontal stress which is constant in any horizontal plane but increasing uniformly with depth. The manner in which gravity affects our investigations must be clearly understood, since it represents one of the major causes of stress. Being a body force, it plays a somewhat different role in the analytical treatment than do the surface forces. For this reason—and also to illustrate the discussed calculation methods—the standard state is briefly derived as follows:

We select the Airy stress function in the form of a polynomial of third degree

$$\Phi = k_1x^3 + k_2x^2 + k_3xy^2y + k_4y^3,$$

which satisfies equation (2). The stress components (1)′ then are:

$$\sigma_x = \frac{\partial^2\phi}{\partial y^2} = 2k_3x + 6k_4y;$$

$$\sigma_y = \frac{\partial^2\phi}{\partial x^2} - \rho gy = 6k_1x + 2k_3y - \rho gy;$$

$$\tau_{xy} = \frac{\partial^2\phi}{\partial x \partial y} = -2k_3x - 2k_1y.$$

In view of the boundary conditions at the surface, k_1 and k_2 must be set zero; k_3 and k_4 can be chosen arbitrarily. We select $k_3 = 0$; $k_4 = -\frac{1}{2}\rho g$ and obtain:

$$\begin{aligned} \sigma_x &= \sigma_y = -\rho gy; \\ \tau_{xy} &= 0 \end{aligned} \qquad (6)$$

These are the stress components for the standard state. The normal stresses are equal in all directions and for all points on a horizontal plane (y = constant) and the shear stress is zero throughout the body. This stress system is, therefore, equivalent to the hydrostatic pressure in a liquid. Its physical significance for solid bodies is apparent from the following consideration. In a homogeneous solid body of infinite horizontal extent, uniform lateral extension is prevented by lack of space. Therefore, if the weight of the body is the only source of stress, the strain components (elongations) in the horizontal directions are zero. From this the relation

$$\sigma_{hor} = \sigma_{vert}\frac{\nu}{1-\nu}$$

is derived, where σ_{hor} and σ_{vert} represent the horizontal and vertical stress components, respectively, and ν is Poisson's ratio. It is seen that $\sigma_{hor} = \sigma_{vert}$ only if $\nu = 0.5$. Hence, the hydrostatic state is produced by gravity alone only in liquids. In solid bodies the horizontal stress components due to weight are substantially smaller than the vertical component; they are only a third of the latter if Poisson's ratio is taken to be 0.25, which is a good approximation in most cases. The term $6k_4y$ in the above derivation of the standard state thus includes two effects: roughly a third of it is due to gravity, while the remaining portion represents a superposed horizontal stress, constant in any horizontal plane, but directly proportional to depth.

The important result derived from these considerations is that the effect of gravity can be incorporated into a stress system which is essentially hydrostatic in character. This is a consequence of the fact that a stress system of the form:

$$\sigma_x = ky; \qquad \sigma_y = \tau_{xy} = 0$$

is likewise a valid one—as shown by the above derivation—and thus can be combined with the weight of the body to produce a hydrostatic system. It does not matter whether the complementary horizontal stress ky actually exists in any particular case; the standard state represents an idealization which is probably only seldom realized in nature. Its principal usefulness—aside from offering a convenient "standard of reference—"arises from an application of the already discussed principle of superposition of stresses, which can now be

formulated more precisely. Let Φ_1 and Φ_2 be two stress functions, each of which represents a correct solution. Then the sum of the two is

$$\Phi = \Phi_1 + \Phi_2 \qquad (7)$$

also a valid solution. Now let Φ_1 be the standard state which includes the effect of gravity. Since no other body force is involved, equation (7) states that we may superimpose upon it any other valid stress system Φ_2 caused by surface forces alone. Anderson has named such systems "supplementary stresses." Their mathematical treatment is now divorced from the effects of gravity, and the stress components are given by the simpler expressions of equations (1). The physical implication of this procedure is, of course, merely a statement of the fact that the standard state contributes nothing to the shearing stress and has no influence on the configuration of the stress trajectories. Conversely, it forms a major component of the total stress and, therefore, must be taken into account in phenomena depending upon the magnitude of the confining pressure. One of these phenomena is faulting.

Faulting Associated with Stress Distribution

While the determination of the stress properties is amenable to exact mathematical analysis, the occurrence of faulting presents an intricate problem for which no complete theory has yet been worked out. It is, therefore, important to discuss its critical aspects and to point out the shortcomings of the present treatment.

The principal object of the fault analysis is two-fold: (1) to know the attitude of the fault surfaces and their variations in the calculated stress systems, and (2) to determine the location of faulting in the stressed medium, i.e., the distribution of the stable and unstable portions.

The first problem is readily solved if we accept a widely held theory on the relation between the fault surfaces and the directions of the principal stresses. It states that fracture occurs along two planes which have a specific angle θ with the direction of the maximum principal pressure. This angle is a material constant and, therefore, variable. It is, however, always less than 45°, and for most types of rock falls between 20° and 40°. A value of 30° appears to form a good overall approximation. In three-dimensional stress systems the direction of the two fault surfaces is parallel to that of the intermediate principal stress, the angles θ being measured in the plane containing the maximum and least principal stresses. In the two-dimensional cases here analyzed, we shall presume that this is the plane containing the variable stress components—that the third dimension is parallel to the intermediate principal stress. Then the attitude of the fault surfaces is obtained by drawing two sets of curves having everywhere a selected constant angle with the direction of maximum principal pressure. This is evidently a simple procedure, once the configuration of the stress trajectories has been completely determined. While the choice of θ is arbitrary within certain limits, a value in the neighborhood of 30° appears most appropriate. Corresponding to the plus and minus sign of θ, the method always yields two sets of potential fault surfaces, which intersect each other at an oblique angle. While there is no theoretical basis for a discrimination between the two systems in a homogeneous medium, geological observations indicate that in most areas only one of them has been utilized, or that it strongly predominates. Nevertheless, examples of the co-existence of both sets within the same structural belt are known for all classes of faults.

The validity of the above theory on the attitude of the fault surfaces has been questioned by some authors (Jeffreys, 1936), but it finds much support both from the results of experiments and from geological observations. It is based on the assumption that fracture in a stressed medium takes place along that plane which offers the least resistance to it. To produce faulting, the available energy represented by the condition of strain has to overcome not only the strength of the material but also the internal friction opposing the motion. The latter is proportional to the normal pressure across the fault surface. The shear stress is always greatest in a direction at 45° to those of the maximum and minimum principal stresses. Now if we rotate a plane from

this position towards the axis of maximum principal pressure, both the shear stress—which tends to produce faulting—and the normal pressure—which opposes motion—become smaller. Depending upon the specific properties of the material, there will be one particular angle for which the combined effect of the two opposing factors becomes most favorable for the occurrence of faulting; this is the angle θ above referred to. A detailed mathematical formulation of this principle is found in Anderson (1942, p. 9–10).

The second problem of faulting accorded attention here deals with the determination of the boundaries between the stable and unstable portions of the stress systems. We will first examine the problem solely upon the basis of the statical theory as applied to the original stress distribution.

The basic principle is easily stated: faulting occurs where the shearing stress exceeds the strength of the material. The magnitude of strength depends, first, upon the material, falling in the range of approximately 500–3000 kg/cm^2 under atmospheric pressure for the most common rock types. Second, it varies widely for a given material as a function of other factors, such as the confining pressure, temperature, presence or absence of solutions, and even the time of application of the shearing stress. Only the first of these has been adequately investigated in laboratory experiments. It was generally found that the breaking pressure increases with the confining pressure and that in many cases the rate of increase is nearly linear over a wide pressure range. Since little information is available on the influence of the other factors, the boundary equation for the separation of the stable and unstable portions adopted in the present paper is:

$$\sigma_{min} \leqq n\sigma_{max} + \sigma_0 \tag{8}$$

where:

σ_{min} = maximum compressive stress (compressive stresses being given the negative sign, the maximum compressive stress is, algebraically, the smallest),
σ_{max} = minimum compressive stress,
σ_0 = breaking strength under atmospheric confining pressure,
n = material constant.

As pointed out, while the standard state contributes nothing to the shearing stress in a homogeneous medium, it adds a vital component to the total confining pressure; hence σ_{min} and σ_{max} in (8) represent total principal stress, including that due to the standard state. They are obtained by adding to the components from equation (4) the hydrostatic pressure defined by (6):

$$\left.\begin{aligned}\sigma_{min} &= \tfrac{1}{2}(\sigma_x + \sigma_y) - \tau_{max} - \rho gy\\ \sigma_{max} &= \tfrac{1}{2}(\sigma_x + \sigma_y) + \tau_{max} - \rho gy\end{aligned}\right\} \tag{9}$$

For the calculation of numerical examples it will be necessary to assign the constants ρg, σ_0 and n specific values. The selections for the present paper are:

ρg = 250 kg/cm^2 per kilometer or 400 kg/cm^2 per mile,
σ_0 = 1000 kg/cm^2,
n = 4.

While in nature each of these quantities is variable, the figures chosen represent the right order of magnitude. The value for n is based mostly on geological evidence, but it is also substantially in agreement with the results of experimental data.

In the practical application, a simple method was used for the solution of equation (8) which is illustrated in Figure 5. The curve σ_{11} represents the standard state, to which the principal supplementary stresses derived from equation (4) are added algebraically (compressive components being negative). Then the curve: $(n\sigma_{max} + \sigma_0)$ is drawn (dashed line). Faulting occurs where the latter is to the left of σ_{min}. The intersections between the two curves mark the boundaries between the areas of stability and those in which the shear stress exceeds the strength. In the specific examples, the boundary lines were determined for not only one, but several, values of the significant constants appearing in the formulae for the external boundary stresses.

In the preceding discussion, the distribution and mode of faulting were examined solely in relation to the original stress system. With the first occurrence of faulting, an entirely new problem arises. The process of fracturing causes an instantaneous and drastic alteration in the pre-existing stress system, accompanied by the

introduction of a new internal boundary surface. It is thus evident that any subsequent faulting must take place in accordance with the changed conditions, and the value of the original stress system as a guide to further deformation may rightfully be questioned. This interaction between repeated changes in the stress distribution and the successive occurrences of faulting introduces a complication which presents great difficulties to an adequate mathematical analysis. No attempt is made here to deal with this problem. However, some qualitative arguments are advanced which may shed some light on the degree of control which the original stress distribution still exercises during the more advanced stages of faulting.

A mathematical solution of the alteration of stress due to the occurrence of a fault is given by Anderson for a simple case (1942, p. 144–156); this is the only example known to the writer. The results demonstrate that pronounced changes in both direction and intensity of the stresses occur in the immediate neighborhood of the fault surface, but that they diminish rapidly with distance. This is especially true in a direction at right angle to the fault where the alterations soon become insignificant. Near the central portion of the fracture the shear stress is greatly reduced, which has the effect of preventing further faulting in this vicinity. Conversely, there is a substantial increase in stress at both ends of the fracture, indicating a tendency for lateral extension, once the process has been initiated. While the solution applies to a specific case only, it is probable that the basic results are similar in other, more complicated situations.

In the light of these data we may visualize the following sequence of events. Under the action of external forces, a condition of stress is produced in a block of the earth's crust. As long as the shearing stress is everywhere below the strength of the material, the stress distribution is static and can be determined by means of the discussed methods. The various examples given below are rigorously correct during this stage only. With further intensification of the stresses, a point is reached where the strength is exceeded at some particular place, and faulting will occur there. The general location of this place is determinable from the initial conditions. How far the fracture extends itself laterally into regions where the original shear stress is still well below the strength is an unsolved problem. Theoretical results suggest the possibility of

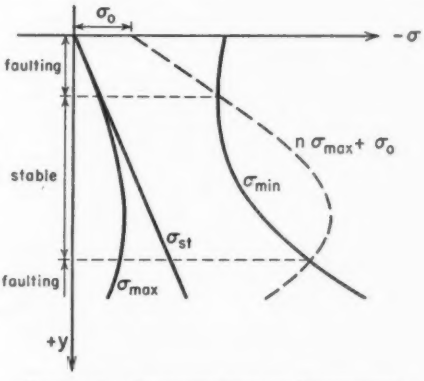

FIGURE 5.—DETERMINATION OF BOUNDARIES OF STABLE PORTIONS OF BLOCK

pronounced extension, whereas geological observations demonstrate that the majority of faults are of rather limited extent. Regardless of this apparent conflict, the principal result will be a drastic diminution of stress in the neighborhood of the origin of the fracture, while farther away the initial stress distribution remains substantially unaltered. The first fault thus provides local relief in the most intensively stressed portion of the block. After its occurrence, the further building-up of the stress system is presumed to go on, and additional portions of the block will gradually reach and exceed the strength limit. Renewed faulting then occurs some distance away from the first fracture, at a place where the stress-relief is of negligible amount. Hence, while no longer exactly the same, the conditions producing the new fracture should still conform closely to the original stresses. A further implication of this process of reasoning is the probability that the later faulting belongs to the same set as the initial one, since a secondary fracture utilizing the alternative complementary direction would lead straight into the protective zone of the preceding one. This, perhaps, is the

explanation of the relative scarcity of complementary faults.

In this manner the process may continue until the maximum development of the system has been reached. At this stage the extent of the unstable areas has likewise reached its maximum expansion which, depending upon the ultimate intensities of the causal forces, will include a smaller or greater portion of the entire block. Due to the limited extent of the influence of previous fractures in adjacent areas, it appears probable that the initial faulting in each portion of the unstable segments is primarily controlled by the original stresses. The local relief of stress provided by the existing fractures will then gradually disappear again due to the tendency of the original stress system to re-establish itself. This can lead to renewed faulting in already fractured segments. The process thus becomes more and more complicated, on account of the introduction of a new internal boundary surface along each additional fault and the adjacent zone of pronounced stress alterations. In extreme cases, the stress system may be substantially changed during the final stages of deformation and the further course of events is then beyond the scope of theoretical analysis.

From this line of reasoning it appears justified to assume that the original stress system constitutes the controlling influence on the location and type of faulting at least during the initial stages of deformation in each faulted segment. The author, therefore, believes that illustrations showing the attitude of fault surfaces and the boundaries between stable and unstable segments based purely on the original stress system serve a useful purpose in studies of this nature.

Examples of Two-Dimensional Stress Systems

Introduction

Using the methods outlined in the preceding sections, we will now present a series of examples of two-dimensional stress systems. One or several numerical examples for each group are illustrated graphically in Figures 6–8 and on Plate 1. In each figure, the upper diagram shows the complete solution of the internal stress distribution in the form of stress trajectories and lines of equal maximum shearing stress; the lower diagram shows the attitude of the fault surfaces and the distribution of the stable and unstable portions of the block. All graphs show the respective systems of boundary stresses.

Supplementary Horizontal Stress without Superposed Vertical Stress

In the first group to be analyzed, we assume the presence of a supplementary horizontal stress but absence of an associated vertical stress component, i.e., there is no pressure or tension across any horizontal plane in the body in addition to the normal hydrostatic component. Mathematically this is expressed by:

$$\sigma_y = \frac{\partial^2 \Phi}{\partial x^2} = 0 \quad \text{for all values of } y.$$

Integrating we obtain the stress function:

$$\Phi = cf(y)x + ax + bf_2(y) + d.$$

To satisfy equation (2)

$$\frac{\partial^4 \Phi}{\partial x^4} + 2\frac{\partial^4 \Phi}{\partial x^2 \partial y^2} + \frac{\partial^4 \Phi}{\partial y^4} = cxf_1^{IV}(y) + bf_2^{IV}(y) = 0$$

the fourth order derivatives of f_1 and f_2 must be zero. Hence the second order derivatives may be either linear functions of y, constants, or zero. The stress components then are (equations (1))

$$\left.\begin{aligned} \sigma_x &= \frac{\partial^2 \Phi}{\partial y^2} = cf_1^{II}(y)x + bf_2^{II}(y); \\ \sigma_y &= \frac{\partial^2 \Phi}{\partial x^2} = 0; \\ \tau_{xy} &= -\frac{\partial^2 \Phi}{\partial x \partial y} = -cf_1^{I}(y). \end{aligned}\right\} \tag{10}$$

The boundary conditions at the surface require that $f_1^I(y) = 0$ for $y = 0$. Keeping within the limits of the above restrictions we can set up the following three subgroups:

a)
$$\left.\begin{aligned} f_1^I(y) &= 0; \quad f_2^{II}(y) = y + d \\ \sigma_x &= by + d; \\ \sigma_y &= 0; \\ \tau_{xy} &= 0. \end{aligned}\right\} \tag{10a}$$

b)
$$\left.\begin{aligned} f_1^I(y) &= y; \quad f_2^{II}(y) = 0 \\ \sigma_x &= cx; \\ \sigma_y &= 0; \\ \tau_{xy} &= -cy. \end{aligned}\right\} \tag{10b}$$

c)
$$\left.\begin{aligned} f_1^I(y) &= \tfrac{1}{2}y^2; \quad f_2^{II}(y) = 0 \\ \sigma_x &= cxy; \\ \sigma_y &= 0; \\ \tau_{xy} &= -\frac{c}{2}y^2. \end{aligned}\right\} \tag{10c}$$

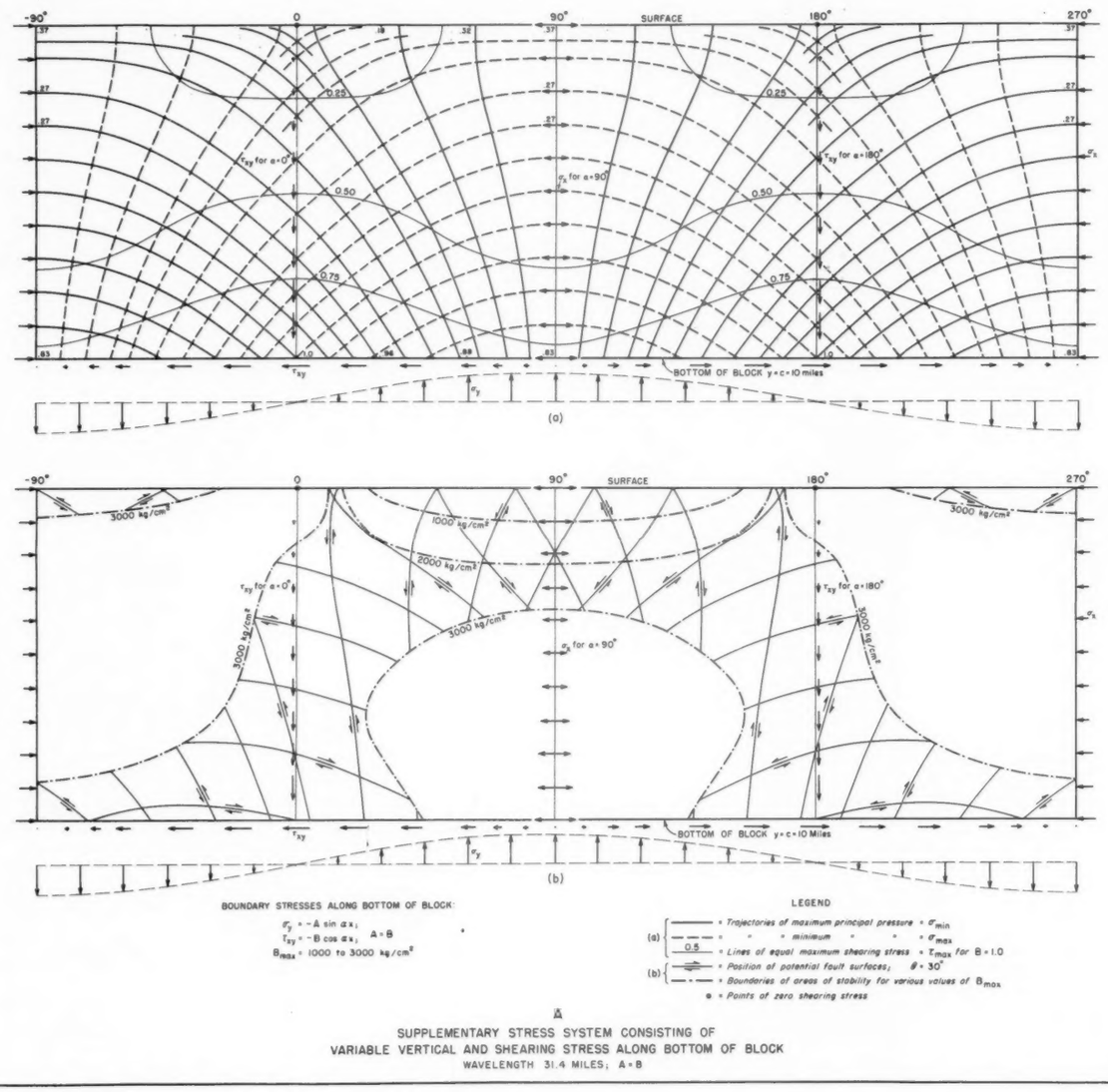

A

SUPPLEMENTARY STRESS SYSTEM CONSISTING OF
VARIABLE VERTICAL AND SHEARING STRESS ALONG BOTTOM OF BLOCK
WAVELENGTH 31.4 MILES; A=B

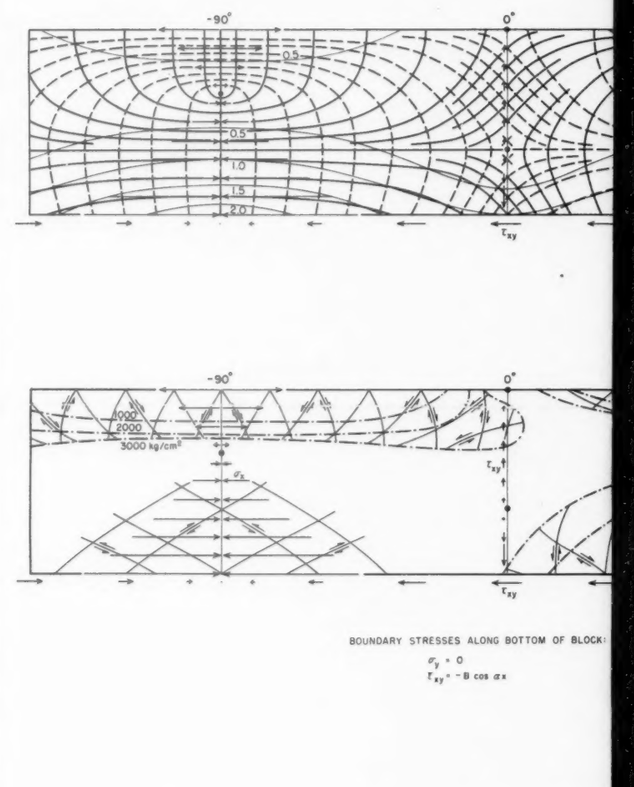

BOUNDARY STRESSES ALONG BOTTOM OF BLOCK:
$\sigma_y = 0$
$\tau_{xy} = -B \cos \alpha x$

VA

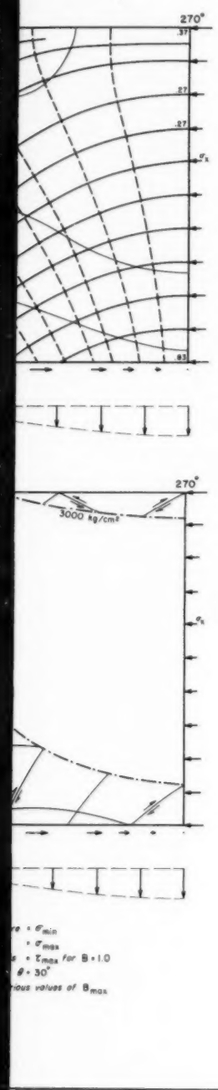

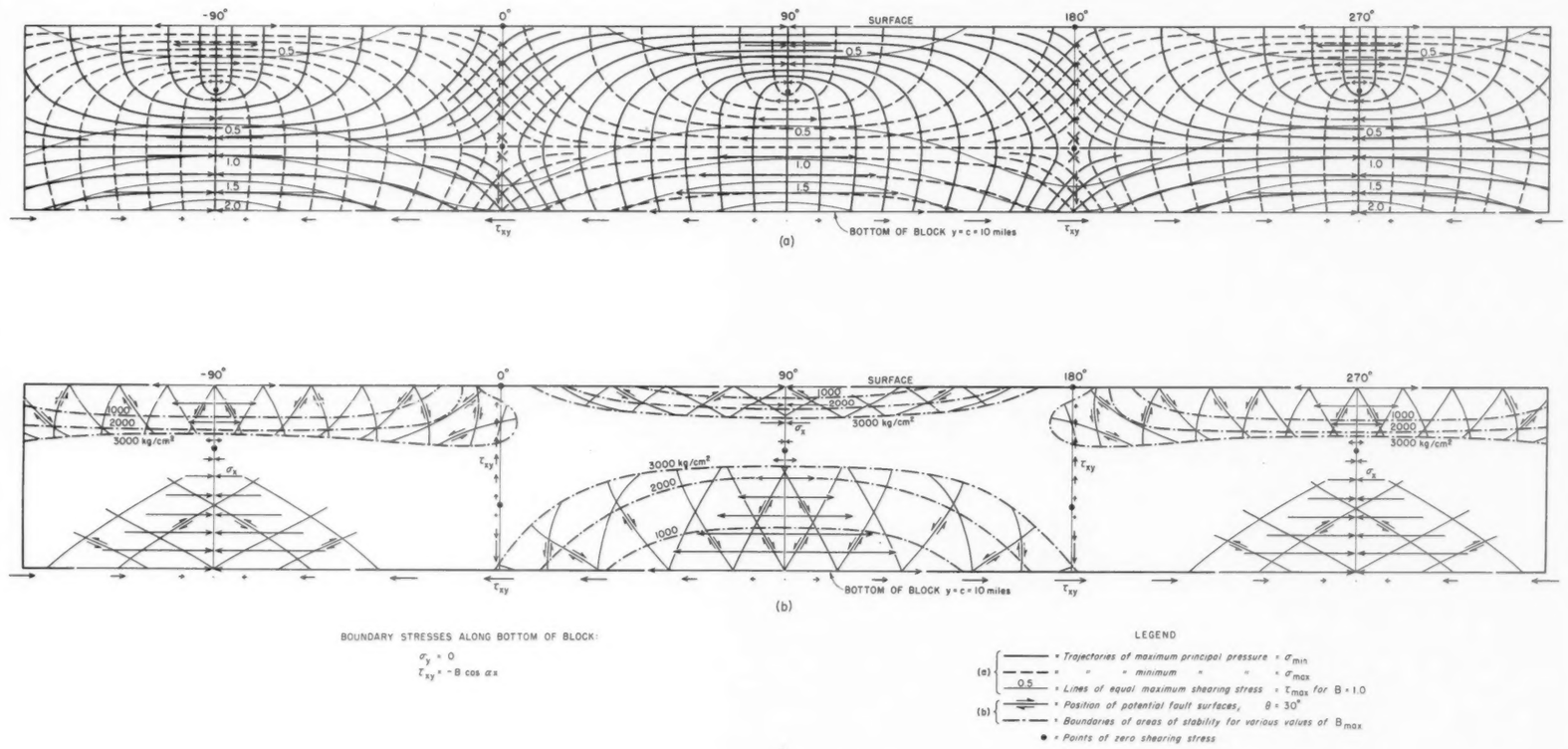

BOUNDARY STRESSES ALONG BOTTOM OF BLOCK:

$\sigma_y = 0$

$\tau_{xy} = -B \cos \alpha x$

LEGEND

(a) — = Trajectories of maximum principal pressure = σ_{min}

– – = " " " minimum " " = σ_{max}

0.5 = Lines of equal maximum shearing stress = τ_{max} for B = 1.0

(b) ⇌ = Position of potential fault surfaces, θ = 30°

–·– = Boundaries of areas of stability for various values of B_{max}

● = Points of zero shearing stress

B

SUPPLEMENTARY STRESS SYSTEM CONSISTING OF
VARIABLE SHEARING STRESS ALONG BOTTOM OF BLOCK
WAVELENGTH 62.8 MILES; A = 0

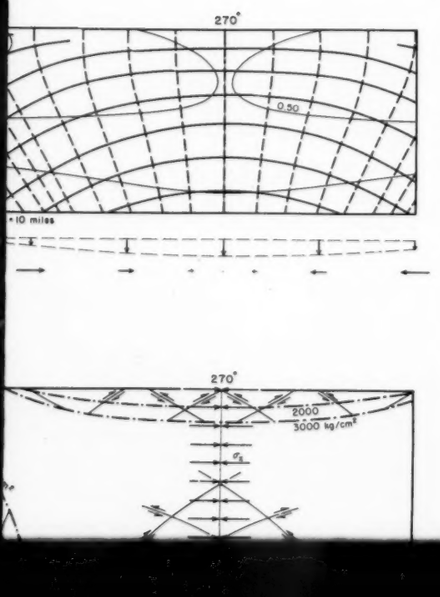

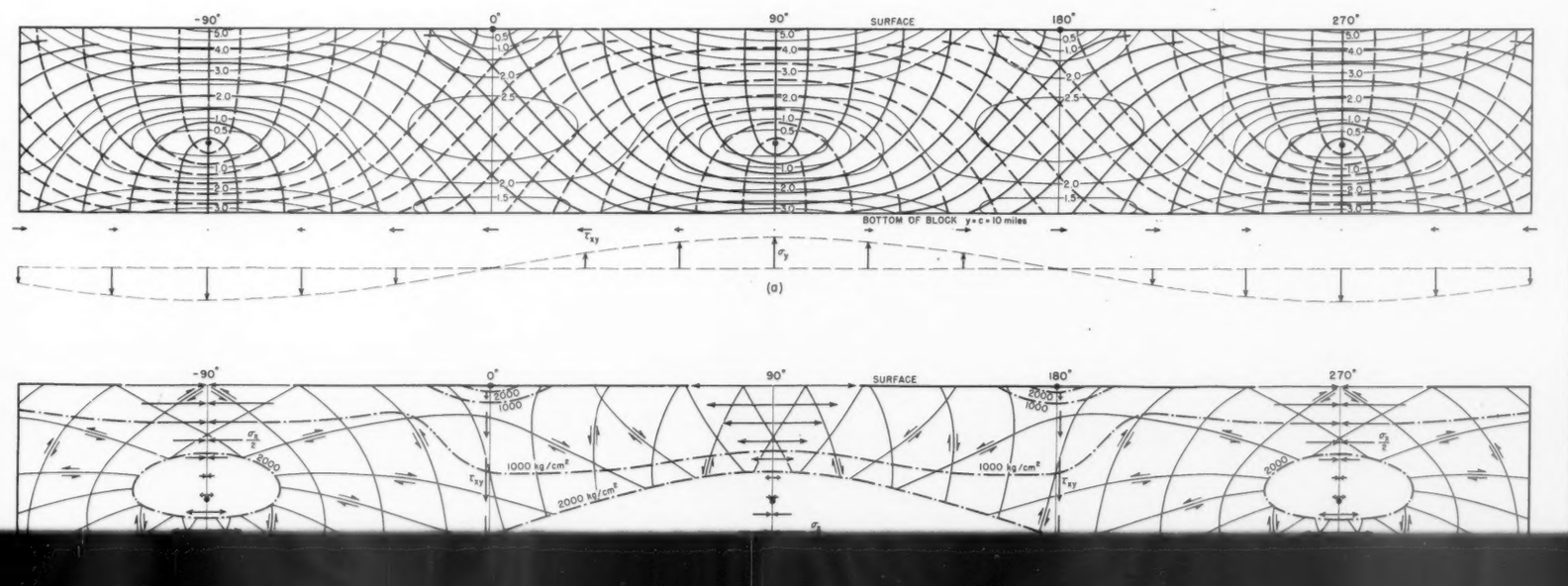

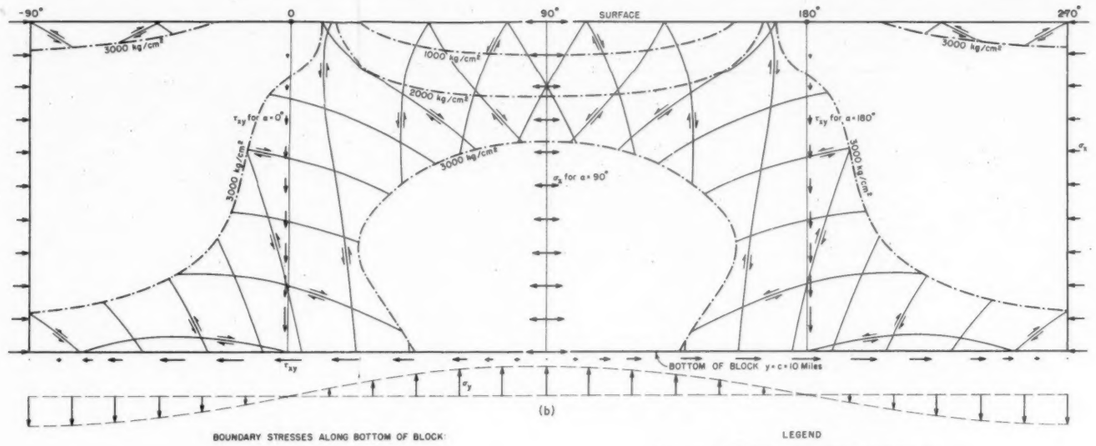

BOUNDARY STRESSES ALONG BOTTOM OF BLOCK:

$\sigma_y = -A \sin \alpha x$;
$\tau_{xy} = -B \cos \alpha x$; $A = B$
B_{max} = 1000 to 3000 kg/cm²

LEGEND

(a) —— = Trajectories of maximum principal pressure = σ_{min}
(a) – – = " " minimum " = σ_{max}
0.5 = Lines of equal maximum shearing stress = τ_{max} for B = 1.0
(b) ⇌ = Position of potential fault surfaces; $\theta = 30°$
(b) —·— = Boundaries of areas of stability for various values of B_{max}
● = Points of zero shearing stress

A

SUPPLEMENTARY STRESS SYSTEM CONSISTING OF
VARIABLE VERTICAL AND SHEARING STRESS ALONG BOTTOM OF BLOCK
WAVELENGTH 31.4 MILES; A = B

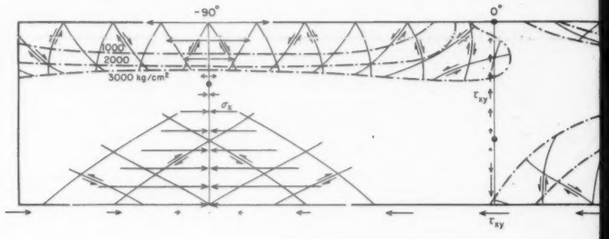

BOUNDARY STRESSES ALONG BOTTOM OF BLOCK:

$\sigma_y = 0$
$\tau_{xy} = -B \cos \alpha x$

VA

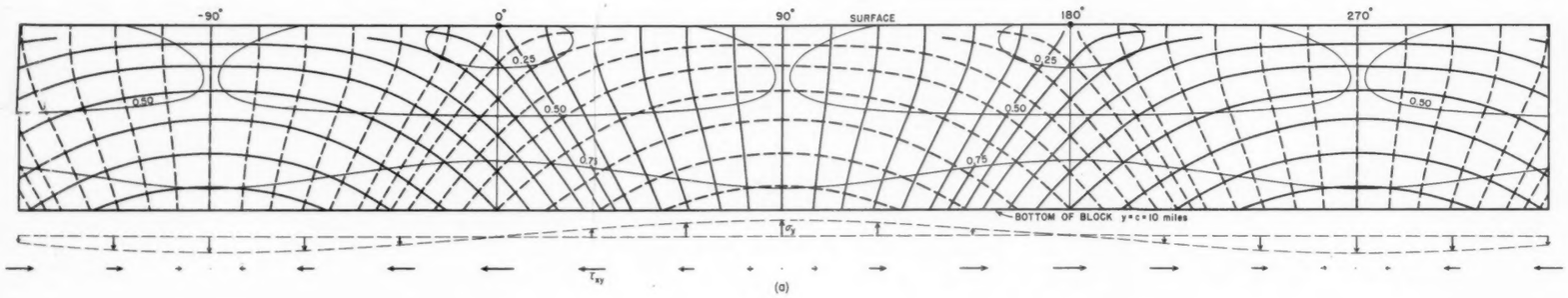

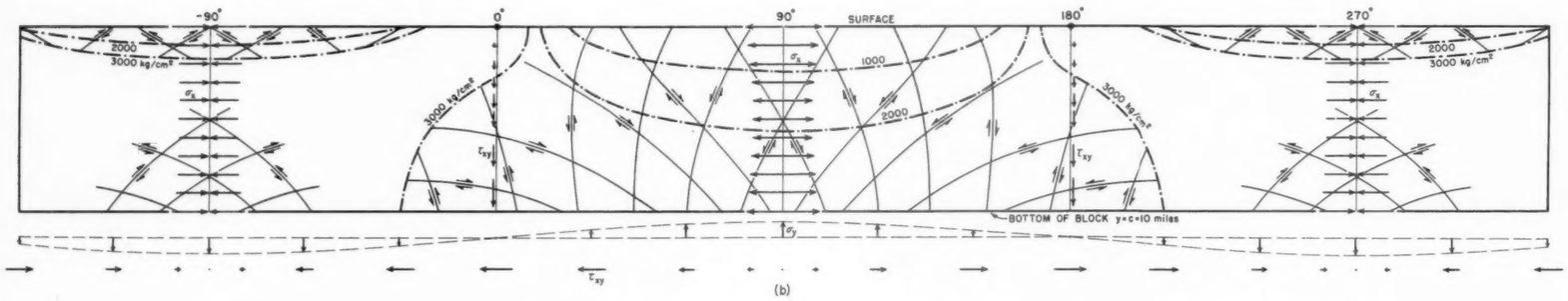

BOUNDARY STRESSES ALONG BOTTOM OF BLOCK:

$\sigma_y = -A \sin \alpha x$;
$\tau_{xy} = -B \cos \alpha x$; $A = \frac{1}{2}B$
B_{max} = 1000 to 3000 kg/cm²

LEGEND

(a) —— = Trajectories of maximum principal pressure = σ_{min}
(a) – – = " " minimum " = σ_{max}
0.5 = Lines of equal maximum shearing stress = τ_{max} for B = 1.0
(b) ⇌ = Position of potential fault surfaces; $\theta = 30°$
(b) —·— = Boundaries of areas of stability for various values of B_{max}
● = Points of zero shearing stress

C

SUPPLEMENTARY STRESS SYSTEM CONSISTING OF
VARIABLE VERTICAL AND SHEARING STRESS ALONG BOTTOM OF BLOCK
WAVELENGTH 62.8 MILES; $A = \frac{1}{2}B$

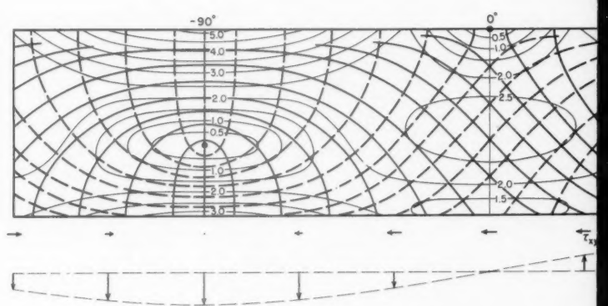

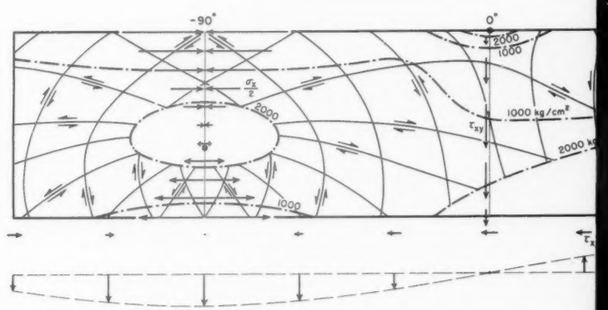

BOUNDARY STRESSES ALONG BOTTOM OF BLOC

$\sigma_y = -A \sin \alpha x$;
$\tau_{xy} = -B \cos \alpha x$; $A = 2B$
A_{max} = 1000 to 2000 kg/cm²

VARIABLE

...e = σ_{min}
... = σ_{max}
...s = τ_{max} for B = 1.0
... θ = 30°
...rious values of B_{max}

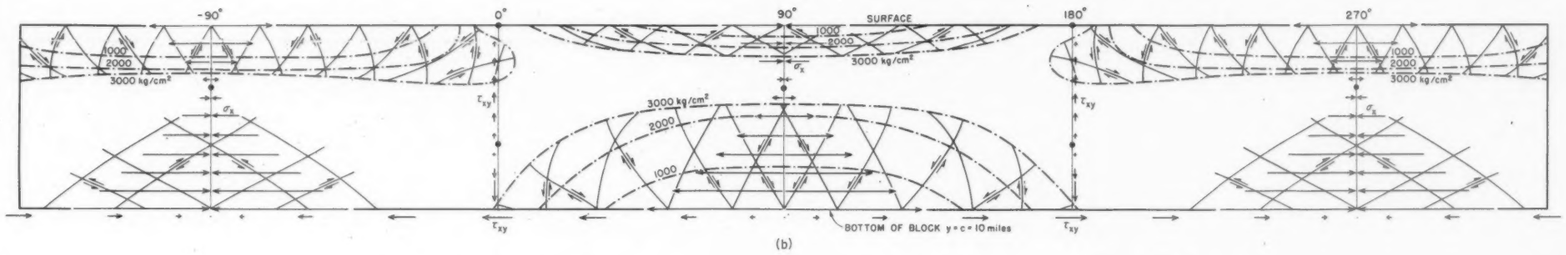

(b)

BOUNDARY STRESSES ALONG BOTTOM OF BLOCK:

$\sigma_y = 0$

$\tau_{xy} = -B \cos \alpha x$

LEGEND

(a) — = Trajectories of maximum principal pressure = σ_{min}
— — = " " minimum " " = σ_{max}
0.5 = Lines of equal maximum shearing stress = τ_{max} for B = 1.0
(b) = Position of potential fault surfaces; θ = 30°
= Boundaries of areas of stability for various values of B_{max}
● = Points of zero shearing stress

B

SUPPLEMENTARY STRESS SYSTEM CONSISTING OF
VARIABLE SHEARING STRESS ALONG BOTTOM OF BLOCK
WAVELENGTH 62.8 MILES; A = 0

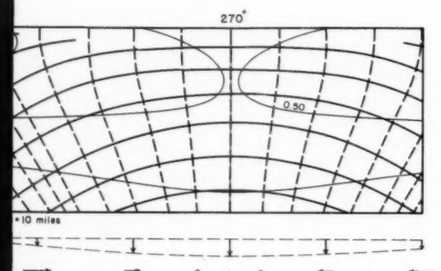

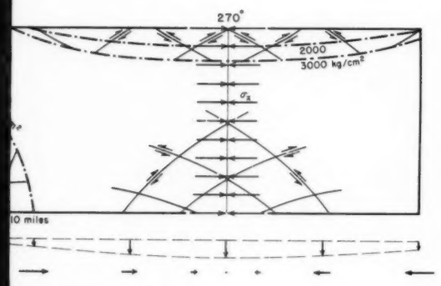

...EGEND

...aximum principal pressure = σ_{min}
...inimum " " = σ_{max}
...maximum shearing stress = τ_{max} for B = 1.0
...ential fault surfaces; θ = 30°
...reas of stability for various values of B_{max}
...shearing stress

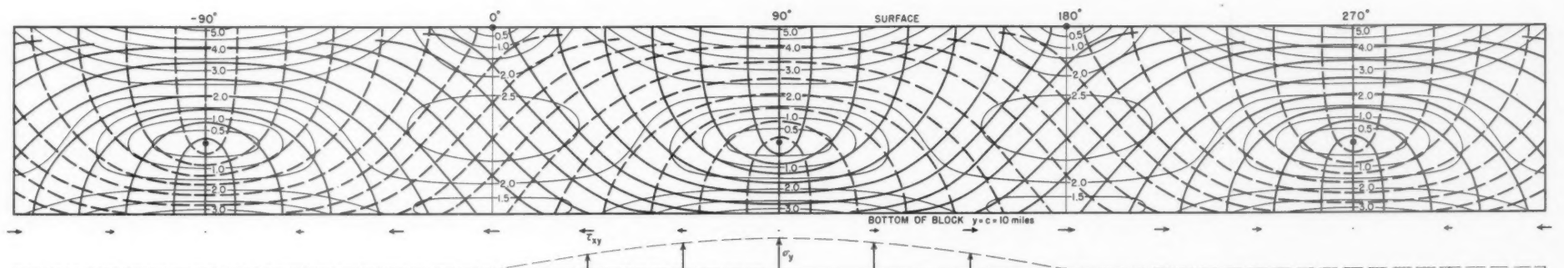

(a)

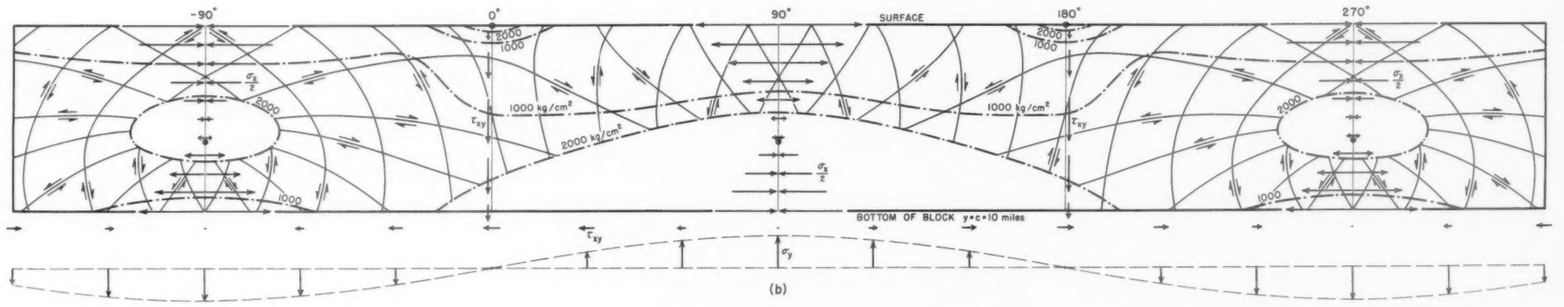

(b)

BOUNDARY STRESSES ALONG BOTTOM OF BLOCK:

$\sigma_y = -A \sin \alpha x$;
$\tau_{xy} = -B \cos \alpha x$; A = 2B
A_{max} = 1000 to 2000 kg/cm²

LEGEND

(a) — = Trajectories of maximum principal pressure = σ_{min}
— — = " " minimum " " = σ_{max}
0.5 = Lines of equal maximum shearing stress = τ_{max} for B = 1.0
(b) = Position of potential fault surfaces; θ = 30°
= Boundaries of areas of stability for various values of A_{max}
● = Points of zero shearing stress

D

SUPPLEMENTARY STRESS SYSTEM CONSISTING OF
VARIABLE VERTICAL AND SHEARING STRESS ALONG BOTTOM OF BLOCK
WAVELENGTH 62.8 MILES; A = 2B

1. SUPPLEMENTARY STRESS SYSTEMS

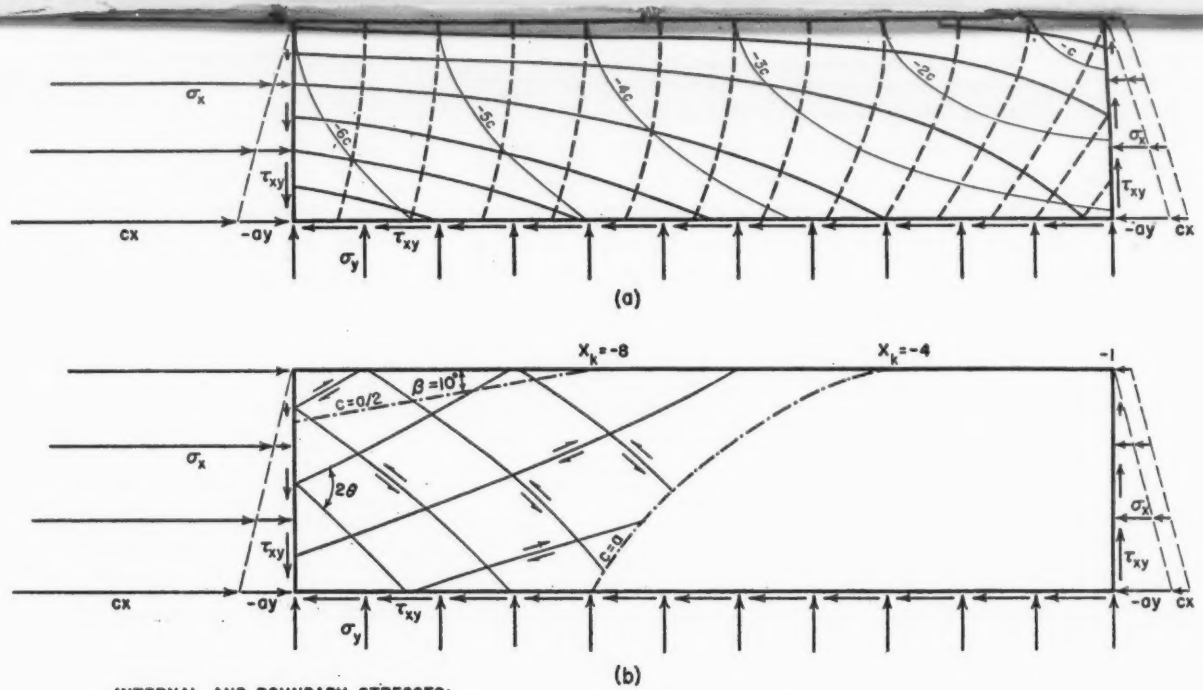

INTERNAL AND BOUNDARY STRESSES:

σ_x = cx − ay

σ_y = − ay

τ_{xy} = − cy

c and a are constants

a = ρg

LEGEND

(a) —— = *Trajectories of maximum principal pressure* = σ_{min}

(a) — — = *" " minimum " " * = σ_{max}

(a) 4c = *Lines of equal maximum shearing stress* = τ_{max}

(b) = *Position of possible thrust-fault surfaces;* θ = 32°

(b) = *Boundaries of areas of stability for various ratios of* a/c

FIGURE 6. SUPPLEMENTARY STRESS SYSTEM CONSISTING OF SUPERIMPOSED HORIZONTAL PRESSURE CONSTANT WITH DEPTH AND WITH CONSTANT LATERAL GRADIENT

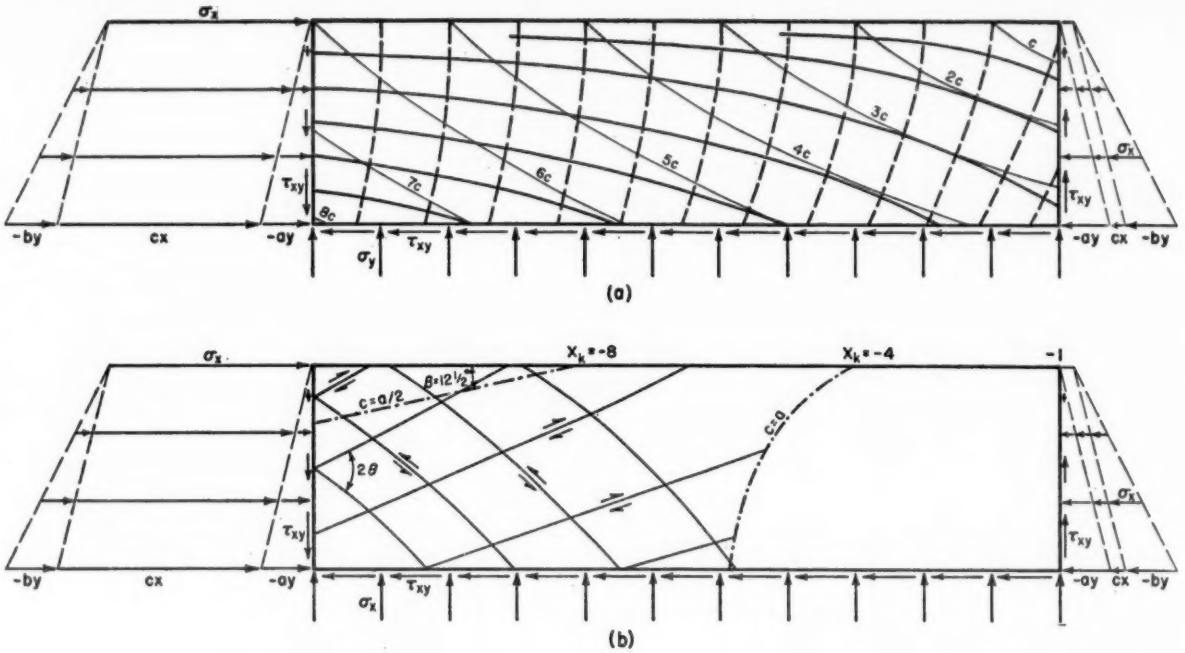

INTERNAL AND BOUNDARY STRESSES:

$\sigma_x = cx-(b+a)y$

$\sigma_x = -ay$

$\tau_{xy} = -cy$

a, b, and c are constants

$a = \rho g$; $-b = c$

LEGEND

(a) —— = Trajectories of maximum principal pressure = σ_{min}

(a) — — = " " minimum " " = σ_{max}

(a) 4c = Lines of equal maximum shearing stress = τ_{max}

(b) ⇌ = Position of possible thrust-fault surfaces; $\theta = 32°$

(b) —·— = Boundaries of areas of stability for various ratios of a/c

FIGURE 7. SUPPLEMENTARY STRESS SYSTEM CONSISTING OF SUPERIMPOSED HORIZONTAL PRESSURE WITH CONSTANT LATERAL AND VERTICAL GRADIENT

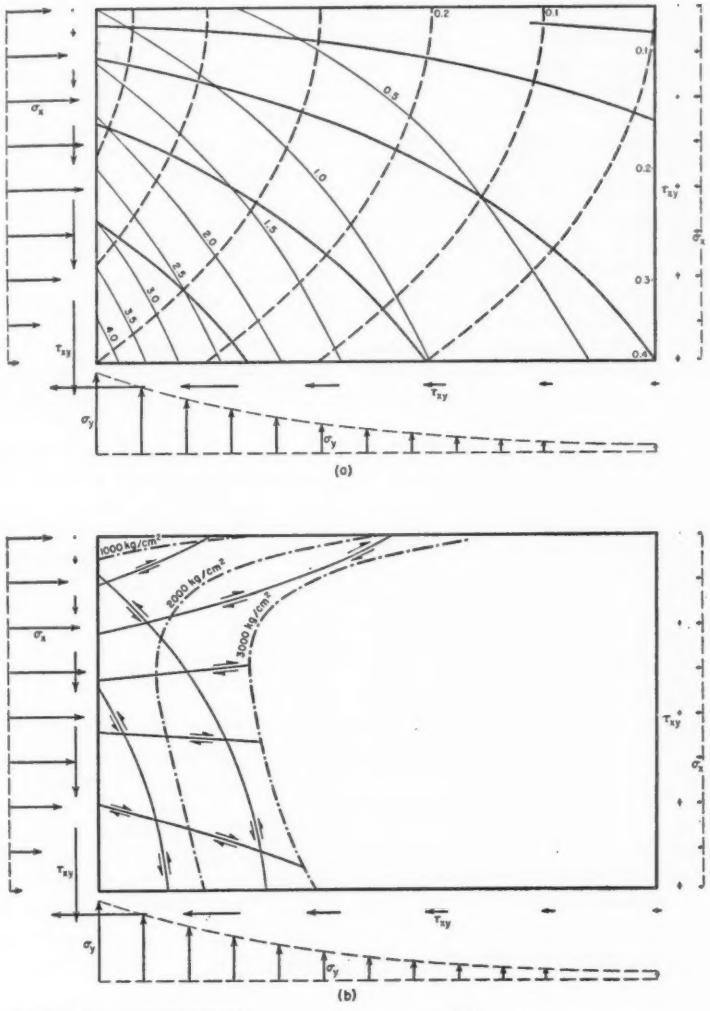

FIGURE 8. SUPERPOSED HORIZONTAL STRESS DECREASING EXPONENTIALLY IN HORIZONTAL DIRECTION

In these equations, b, c, and d are arbitrary constants and may be assigned any value, including zero. Furthermore, any linear combination of equations (10a) to (10c) represents another allowable system.

The simplest case of a supplementary stress

system is given by (10*a*) if we let *b* equal zero. Then the superposed stress is restricted to a constant horizontal component $\sigma_x = d$, the other two components σ_y and τ_{xy} being zero everywhere. From (3) and (5) it follows that the maximum shearing stress is also constant—equal to half the horizontal stress—and that the stress trajectories are everywhere horizontal and vertical, respectively. The associated fault planes will be inclined at angles of about $\pm 30°$ to the horizontal (thrust faults).

We will next examine the stress systems of the first two sub-groups. The constant *d* is now selected to be zero since its contribution has already been discussed. The combination of (10*a*), (10*b*), and the standard state gives the total stress components:

$$\sigma_x = cx + by - ay,$$
$$\sigma_y = -ay,$$
$$\tau_{xy} = -cy;$$

where $a = \rho g$. The term $-ay$ represents the hydrostatic pressure and is the only one appearing in the vertical stress component. The horizontal component σ_x contains two additional terms, the first a linear function of *x* only and the second a linear function of *y* only. Hence σ_x has constant gradients in both the horizontal and vertical directions. The shear stress τ_{xy} is seen to be constant in any horizontal plane; further, it increases vertically at a constant rate which is equal to the lateral gradient of σ_x. The term ky in σ_x appeared previously as a component of the standard state; in the present formulae, it denotes the difference (excess or defect) between the actual magnitude of this stress and that portion of it which is absorbed in the standard state.

Figure 6[1] illustrates the case where the supplementary horizontal pressure is constant with depth ($b = 0$) and Figure 7 where it has a vertical gradient equal to the horizontal one ($b = c$). The external boundary stresses are shown on the end-surfaces and along the bottom of a rectangular block. On the two sides, the horizontal stress σ_x is broken down into its individual components. It is seen that addition of the term *by* does not change the equilibrium of the block in the lateral direction, a fact which explains that the shearing stress along the bottom is the same in both cases.

The trajectories of maximum principal pressure are curved lines, dipping downward away from the area of maximum compression. The curvature is stronger if the vertical gradient of σ_x is small. Since the trajectories are curved, so are the potential fault surfaces. The latter obviously belong to the class of thrust faults. The set dipping towards the area of maximum pressure is slightly concave upwards, the complementary set concave downwards. Thrust faults of the former type are very common in nature and the theoretically deduced curvature is frequently observed. The latter type appears to occur only rarely and little is known regarding the curvature.

The lines of equal maximum shearing stress are expressed in terms of multiples of the constant *c*. The shearing stress naturally increases towards the area of greater horizontal pressure but it also increases with depth, the latter effect being more pronounced if σ_x has a vertical gradient. To determine the boundary of the stable portion of the block, the constant *c* has to be fixed numerically. This is done best by selecting certain values of the ratio c/a, thus expressing the lateral gradient of the superposed horizontal stress in terms of a fraction of the vertical pressure gradient due to weight. In nature this ratio is evidently widely variable with place and time and, in fact, may assume any value from zero up to a magnitude large enough to cause thrusting. The most useful procedure, therefore, consists of assuming several ratios and calculating their respective boundary lines. In both Figures 6 and 7, two such lines are shown corresponding to the ratios $c = a$ and $c = a/2$.

These boundary lines are seen to be dipping towards the area of greater horizontal pressure. The rate of dip is primarily a function of the ratio c/a, being greater the larger this fraction is. It is steep only if the latter is near unity, when the horizontal pressure gradient approaches the magnitude of the vertical pressure gradient due to weight. For smaller values of *c*, the boundary lines are nearly straight and their inclination diminishes rapidly. Numerical examples on the dip β are: for $c = a/2$, β is about 10° in Figure 6 and $12\frac{1}{2}°$ in Figure 7,

[1] Similar to Figure 25 in the companion paper by M. King Hubbert (1951).

for $\alpha = a/10$, β is less than 2° in the former case.

These results suggest the following conclusions. If the supplementary horizontal pressure has only a small lateral gradient, say of the order of half the vertical pressure gradient or less, the potential area of thrusting is confined to a shallow, gently dipping wedge. The resulting deformation will consist of a series of slice-thrusts covering a broad belt but extending only to shallow depth. The presence of a vertical gradient slightly steepens the wedge. However, the boundary becomes very steep or nearly vertical only if the horizontal gradient approaches the magnitude of the vertical increase of the hydrostatic pressure. In that event, thrusting can take place throughout a thick, but probably only narrow, zone of the crust. Such a condition appears to have occurred, for instance, in the marginal belts of several ranges in the Rocky Mountain province.

The boundary stresses of the third sub-group (formulae 10*c*) are also characterized by the fact that the shearing stress is constant in all horizontal planes. Its vertical gradient, however, is now a function of the second order of y, instead of the first order. The shearing stress is balanced by a horizontal pressure, again having constant lateral and vertical gradients but increasing more rapidly in the diagonal direction. This case has not been further analyzed.

The most general expression for the stress systems satisfying the assumption of absence of a vertical stress component is given by the superposition of equations (10*a*), (10*b*) and (10*c*), as follows:

$$\left.\begin{aligned} \sigma_x &= c_1xy + c_2x + by + d; \\ \sigma_y &= 0; \\ \tau_{xy} &= -\frac{c_1}{2}y^2 - c_2y \end{aligned}\right\} \qquad (11)$$

It is seen that the stipulation $\sigma_y = 0$ is associated with two additional general properties of the internal stress system: (1) that the shearing stress is a function of y only, i.e., constant in all horizontal planes, and (2) that σ_x has linear gradients in both the horizontal and vertical directions. That the first two properties are reversible can readily be demonstrated by deriving the stress system based on the assumption:

$$\tau_{xy} = -\frac{\partial^2\Phi}{\partial x \partial y} = -k_1 f(y).$$

Using the same direct integration method as before and satisfying equation (2) and the boundary conditions at the surface, this leads again to equations (11). Hence, the reversed statement: "constancy of the shearing stress in all horizontal planes is associated with absence of a vertical supplementary stress throughout the body," is also true. Thus the heading of this Section could equally well read "Supplementary shearing stress constant in all horizontal planes."

Supplementary Horizontal Stress Decreasing Exponentially in the Horizontal Direction

We have investigated the condition of the presence of a supplementary horizontal stress coupled with absence of a superposed vertical component. In this section we again take a supplementary horizontal stress, but drop the assumption that σ_y be zero throughout the block. Instead, we now impose the condition that σ_x decrease exponentially in the horizontal direction.

For this purpose we take the Airy stress function in the form:

$$\Phi = ce^{x}f(y). \qquad (12)$$

Applying equation (2) to this function yields the differential equation

$$f(y) + 2f^{\text{II}}(y) + f^{\text{IV}}(y) = 0$$

the general solution of which is

$$f(y) = A\sin y + B\cos y + Cy\sin y + Dy\cos y. \qquad (13)$$

Substituting (13) in (12) and differentiating we obtain the stress components (1). The compulsory boundary conditions $\sigma_y = \tau_{xy} = 0$ for $y = 0$ can be taken care of by a proper disposition of the two constants A and B. After eliminating these constants, the stress components become:

$$\begin{aligned} \sigma_x &= ce^{x}\{C(2\cos y - y\sin y) - D(\sin y + y\cos y)\}; \\ \sigma_y &= ce^{x}\{Cy\sin y \qquad\quad - D(\sin y - y\cos y)\}; \\ \tau_{xy} &= ce^{x}\{-C(\sin y + y\cos y) + Dy\sin y\}. \end{aligned}$$

Let:

$$f_1(y) = 2\cos y - y\sin y; \qquad f_2(y) = \sin y + y\cos y;$$
$$f_3(y) = y\sin y; \qquad f_4(y) = \sin y - y\cos y;$$

then the stress components can be written in the form:

$$\left.\begin{aligned} \sigma_x &= ce^x\{Cf_1(y) - Df_2(y)\} = ce^xF_1(y);\\ \sigma_y &= ce^x\{Cf_3(y) - Df_4(y)\} = ce^xF_2(y);\\ \tau_{xy} &= ce^x\{-Cf_2(y) + Df_3(y)\} = ce^xF_3(y). \end{aligned}\right\} \quad (14)$$

The direction of the stress trajectories is given by:

$$\tan 2\beta = \frac{2F_3(y)}{F_1(y) - F_2(y)}. \quad (15)$$

The functions F_1 to F_3 are constant in the horizontal direction since they are functions of y only. Therefore, equation (15) shows that all stress trajectories are parallel curves and the same applies to the fault surfaces under the assumption of constancy of angle between the latter and the directions of maximum principal pressure.

When writing equations (14) in the form:

$$\sigma = c\,\epsilon(x, y),$$

it is evident that the constant c has the dimension of stress. Its value can be selected arbitrarily and determines the absolute magnitude of the stress components, whereas the function $\epsilon(x, y)$ determines their areal variations. The two remaining integration constants C and D are dimensionless and, being likewise fully independent, permit the selection of numerous variations. The degree of variability is further enhanced by the fact that the position of the bottom of the block can be chosen at any desired lower limit of the y functions, the unit of length also being arbitrary. The range of opportunity thus provided can easily be exploited by drawing graphs of the four functions f_1 to f_4 and making visual estimates of the combinations obtainable after multiplication with various constants.

Figure 8 illustrates the case where $C = -1$ and $D = +2$. In this and all succeeding illustrations, only the supplementary boundary stresses are shown; the normal hydrostatic components are omitted to simplify the drawings. The shearing stress acting on the bottom of the block is no longer constant but, like the superposed horizontal stress, increases exponentially towards the pressure area. The same is true for the vertical component which now forms a part of the stress system. All three boundary stresses diminish rapidly away from the area of compression. The zone of potential faulting consists of a narrow, nearly vertical, belt and a shallow outwardly protruding wedge near the surface. Figure 8*b* indicates three boundary lines limiting the area of stability; they correspond to values of the constant c of 1000, 2000, and 3000 kg/cm^2, respectively.

The general fault system in the shallow portion of the unstable segment is similar to that obtained in the preceding stress systems, except for a slight change in attitude. The thrust faults dipping towards the pressure area are less steeply inclined. This divergence increases with depth where, because of a gradual clockwise rotation, the fault surfaces of this set become practically flat and finally even overturned. It appears doubtful, however, that the extreme stage is ever realized, because the sudden decrease of σ_x near the lower left-hand corner of the block does not represent a boundary condition which one would expect in nature. As already stated, we are at liberty to match the bottom of the block with any desired point of the (σ_x, y) curve, for instance, that for which σ_x reaches a maximum. In that case the lateral pressure increases throughout the entire thickness of the block, thus providing a stress system which fully satisfies our intuitive concept of geological probability. Figure 8 demonstrates that even within these limitations the thrust planes reach a practically horizontal attitude (in the vicinity of approximately half of the total depth to which calculations were carried out).

It is thus evident that stress systems of this type produce thrust faults which are only gently inclined at shallow depth and become nearly horizontal at greater depth. Such attitudes are frequently observed in nature and are usually interpreted to indicate subsequent tilting of the fault surfaces. It has been shown here that the gently inclined attitudes may equally well be explained as original features of the stress system.

Variable Vertical and Shearing Stress Acting on the Bottom of a Block

The preceding two sections were principally concerned with various forms of horizontal compression acting on the two sides of a block. We now focus on stresses acting on the bottom of a block. These may be superposed vertical stresses, shearing stresses, or a combination of both. It is evident that a vertical component which is constant laterally is of no interest for geological purposes. Such a condition may exist within a limited width of the crust, but it then forms only a part of a broader system in which these stresses eventually die out sideways. Hence, only a laterally variable vertical component will be investigated. The most suitable form of lateral variation is that of a sinusoidal curve. This is the most convenient assumption from the mathematical standpoint and in all probability also forms the most satisfactory approximation to many actual cases of differential vertical uplift.

Examples of both constant and variable shearing stresses along the bottom of a block were already encountered in association with superimposed horizontal pressures; however, if variable, they had a strictly unidirectional gradient. This property renders them inapplicable for many important phenomena, such as the drag produced along the bottom of the crust by the action of convection currents in the underlying substratum. The treatment of this problem likewise leads to a sinusoidal form of the primary boundary stresses.

To obtain stress systems of the desired type we select the Airy stress function in the form

$$\Phi = \sin \alpha x \cdot f(y), \tag{16}$$

where f is a function of y only and

$$\alpha = \frac{2\pi}{l}$$

Application of equation (2) to this stress function yields the following equation for $f(y)$:

$$\alpha^4 f(y) - 2\alpha^2 f^{II}(y) + f^{IV}(y) = 0. \tag{17}$$

The general solution of this differential equation is (Timoshenko, 1934, p. 45)

$$\left.\begin{aligned} f(y) = {} & C_1 \cosh \alpha y + C_2 \sinh \alpha y \\ & + C_3 y \cosh \alpha y + C_4 y \sinh \alpha y. \end{aligned}\right\} \tag{18}$$

The stress components (1) are obtained by inserting this function of y into the stress function (16) and subsequent differentiation. They are:

$$\begin{aligned} \sigma_x &= \sin \alpha x\{C_1\alpha^2 \cosh \alpha y + C_2\alpha^2 \sinh \alpha y \\ &\quad + C_3\alpha(2 \sinh \alpha y + \alpha y \cosh \alpha y) \\ &\quad + C_4\alpha(2 \cosh \alpha y + \alpha y \sinh \alpha y)\} \\ \sigma_y &= -\alpha^2 \sin \alpha x\{C_1 \cosh \alpha y + C_2 \sinh \alpha y \\ &\quad + C_3 y \cosh \alpha y + C_4 y \sinh \alpha y\} \\ \tau_{xy} &= -\alpha \cos \alpha x\{C_1\alpha \sinh \alpha y + C_2\alpha \cosh \alpha y \\ &\quad + C_3(\cosh \alpha y + \alpha y \sinh \alpha y) \\ &\quad + C_4(\sinh \alpha y + \alpha y \cosh \alpha y)\} \end{aligned}$$

The mandatory boundary conditions at the surface are satisfied if we let:

$$C_1 = 0; \qquad C_2 = -\frac{C_3}{\alpha}$$

This imposition reduces the stress components to the form:

$$\left.\begin{aligned} \sigma_x &= \alpha \sin \alpha x\{C_3(\sinh \alpha y + \alpha y \cosh \alpha y) \\ &\quad + C_4(2 \cosh \alpha y + \alpha y \sinh \alpha y)\}; \\ \sigma_y &= -\alpha \sin \alpha x\{-C_3(\sinh \alpha y - \alpha y \cosh \alpha y) \\ &\quad + C_4 \alpha y \sinh \alpha y\}; \\ \tau_{xy} &= -\alpha \cos \alpha x\{C_3 \alpha y \sinh \alpha y \\ &\quad + C_4(\sinh \alpha y + \alpha y \cosh \alpha y)\}. \end{aligned}\right\} \tag{19}$$

The remaining two integration constants C_3 and C_4 are available for suitable selections of the boundary stresses. From the form of equations (19) the proper choice evidently consists of functions of the type

$$\left.\begin{aligned} \sigma_y &= -A \sin \alpha x; \\ \tau_{xy} &= -B \cos \alpha x; \end{aligned}\right\} \tag{20}$$

where A and B are arbitrary constants. These boundary stresses are placed along the bottom of a block, the position of which is determined by $y = c$, c being likewise a constant. Substituting functions (20) for the left-hand sides of the corresponding equations (19) and replacing y by c, we obtain two equations from which the as yet unassigned integration constants C_3 and C_4 can be calculated in terms of the remaining constants α, c, A and B. They can then be eliminated from equations (19).

Performing these steps we arrive at the following final expressions for the stress components:

$$\left.\begin{aligned}\sigma_x &= \sin\alpha x\{-k_1 f_1(y) + k_2 f_2(y)\} = \sin\alpha x F_1(y);\\ \sigma_y &= \sin\alpha x\{-k_1 f_3(y) - k_2 f_4(y)\} = \sin\alpha x F_2(y);\\ \tau_{xy} &= \cos\alpha x\{k_1 f_4(y) - k_2 f_1(y)\} = \cos\alpha x F_3(y);\end{aligned}\right\} \quad (21)$$

where:

$$\left.\begin{aligned}f_1(y) &= \sinh\alpha y + \alpha y\cosh\alpha y;\\ f_2(y) &= 2\cosh\alpha y + \alpha y\sinh\alpha y;\\ f_3(y) &= \sinh\alpha y - \alpha y\cosh\alpha y;\\ f_4(y) &= \alpha y\sinh\alpha y;\end{aligned}\right\} \quad (22)$$

and:

$$\left.\begin{aligned}k_1 &= \frac{A\alpha c\cosh\alpha c - B\alpha c\sinh\alpha c + A\sinh\alpha c}{\sinh^2\alpha c - \alpha^2 c^2};\\ k_2 &= \frac{A\alpha c\sinh\alpha c - B\alpha c\cosh\alpha c + B\sinh\alpha c}{\sinh^2\alpha c - \alpha^2 c^2}.\end{aligned}\right\} \quad (23)$$

Equations (21) represent the general solution for the internal stress components produced by sinusoidal boundary stresses acting on the bottom of a block.

It can easily be verified that equations (21) satisfy the imposed boundary conditions, both the mandatory ones at the surface, as well as the selective ones at the bottom. All three stress components are seen to vary in the horizontal direction according to sinusoidal functions, and in the vertical direction according to the more complicated hyperbolic functions f_1 to f_4 (equations 22). The latter are multiplied by two constant factors, k_1 and k_1 which, in turn, are expressions of four other constants, α, c, A, and B (equation 23). Since α is defined by $\frac{2\pi}{l}$, the terms αc, αy, and functions thereof, are dimensionless, whereas the constants A and B and, therefore, k_1 and k_2, have the dimensions of stress (m, l^{-1}, t^{-2}). The latter result is, of course, also directly obtainable from equations (20). The significance of the four constants is:

$c = y_c$ is the depth of the bottom of the block along which the boundary stresses are acting;

$l = \frac{2\pi}{\alpha}$ is the distance, in the horizontal direction, of a full wave length of the sinusoidal variations of the stress components;

A and B represent the maximum values of the supplementary vertical and shear components at the bottom.

All four constants are mutually independent and may be assigned any desired value. For instance, any combination of thickness and lateral extent (wave length) of the block is permissible. The same applies to the ratio of the amplitudes of the two supplementary boundary stresses. Letting A equal zero yields a case of pure drag along the bottom, whereas B equal zero corresponds to differential vertical uplift alone. Though it is questionable that these latter conditions exist in nature, or are even closely approached, it is of interest to examine the general behavior of these two extreme cases. On the whole, it is seen that equations (21) provide the solution for a substantial variety of situations.

The form of the stress trajectories is given by:

$$\tan 2\beta = \frac{1}{\tan\alpha x}\,\frac{2F_3(y)}{F_1(y) - F_2(y)}. \quad (24)$$

This equation shows that, for values of x denoting uneven multiples of a quarter wave length ($x = \frac{l}{4}, \frac{3l}{4}$ etc.), the two principal directions are vertical and horizontal, respectively, and for values of x denoting even multiples of a quarter wave length ($x = 0, \frac{2l}{4}$ etc.), they are both inclined at 45°. For all other values of x, the directions of the trajectories are complicated functions of y. In the horizontal direction they are constant for those specific depths for which either F_3 or $F_1 - F_2$ are zero. The former case always includes the surface of the block, where the trajectories are horizontal and vertical; the latter, where the trajectories are at 45°, is only occasionally encountered. Of special importance in the construction of the stress diagrams are those points for which the right-hand side of equation (24) is indeterminate (for instance, because of the condition of zero over zero). These are singular points for which the directions of the principal stresses are undefined. They occur at places where the shearing stress is zero. If located internally they are associated with a 90-degree turn of the stress trajectories when passing the point in a vertical or horizontal direction. Owing to the complexity of the expressions for the stress components, the complete solution of equation (24) and the

general equations (3) and (4), is best carried out by numerical and graphical methods.

A series of specific examples is shown on Plate 1. The boundary stresses along the bottom of the block are clearly illustrated in each case. In all instances, a full wave length of the sinusoidal stress variations is shown, but the lateral extent of the block is left undetermined. It should be remembered that we are at liberty to terminate the blocks at any desired place by the simple expedient of applying the appropriate boundary stresses. We might be interested, for instance, in a full wave length of the diagram, or in any one of several significant portions, such as the positive or the negative zone of the supplementary vertical stress. It will be seen later, however, that in some systems the associated horizontal stress component σ_x varies in the vertical direction in a manner which probably excludes it from consideration as a primary boundary stress. Its role should then be restricted to that of a purely internal stress. In such cases, the logical choice of the lateral limits of the block is restricted to the 0- and 180-degree positions (Pl. 1, B and D). To facilitate this aspect of the analysis, the horizontal and lateral shearing stress components have been added to the diagrams at the most important positions. From equations (21), it is seen that σ_z is zero for all points $x = 0$ or $l/2$ but reaches maximum values (positive or negative) for all points $x = l/4$, $3l/4$ etc. The relations are similar for the shear stress components, except for a phase change of one-quarter of a wave length.

The boundary lines segregating areas of stability from those subject to faulting were again calculated for several values of the maximum supplementary boundary stresses, the usual selections being 1000, 2000, and 3000 kg/cm^2. In this connection, a remark concerning the symmetry of the diagrams is in order. Equations (21) show that all quantities which depend solely upon the supplementary stress components have the full degree of symmetry characteristic of the trigonometric functions. These include the stress trajectories, the lines of equal maximum shearing stress and the attitudes of the potential fault surfaces. Conversely, the boundary curves of the stable areas do not display this symmetry between the positive and negative halves of a full wave length. The reason can be seen from a study of Figure 5. For any two points half a wave length apart, σ_{min} and σ_{max} change sign, whereas the line representing the standard state always remains negative. Hence, there is a switch in position between the two principal stresses with respect to the line representing the hydrostatic pressure. This causes a completely different distribution between the stable and unstable segments in the positive and negative half wave length. The only exception is for the points $x = 0$ and $l/2$, for which the interchange is of no consequence due to the fact that $\sigma_{max} = -\sigma_{min}$. This lack of symmetry of the boundary lines represents a striking feature of the diagrams. It is another consequence of the fact that the occurrence of faulting is a function not only of the maximum shearing stress but also of the total confining pressure. Gravity once more exerts a decided influence upon the results.

Plate 1, A represents an example of a relatively narrow wave length. The selected constants are: $l = 31.4$ miles, $c = 10$ miles, and $A = B$. The wave length here chosen roughly equals the distance between adjacent mountain ranges in portions of the Basin-and-Range province, notably Nevada. This statement is made to facilitate a mental association of the selected width with certain well-known structures. Although the diagram covers the two adjacent negative quadrants, we shall limit our attention to the positive half wave length. The supplementary stress system is composed of a vertical pressure gradually decreasing from a maximum value at the center ($\alpha = 90°$) to zero at both ends ($\alpha = 0$ and $180°$), and of a bottom shear stress increasing from the center towards both ends. The two primary stresses set up a horizontal tensile component σ_x which is nearly constant with depth and has the same lateral distribution as σ_y. Only a downward-directed shearing stress acts on the two sides of the block. The necessity of its presence is immediately realized from a consideration of the equilibrium requirement in the vertical direction; it counteracts the upward push at the bottom due to the superposed vertical pressure.

The stress trajectories are vertical and hori-

zontal in the central portion of the block, but gradually turn into a 45-degree position towards both ends, except within a thin zone immediately below the surface. This rotation is associated with corresponding changes in the attitude of the fault surfaces. In the central upper portion of the block, normal faults occur, having the characteristic dips for this class of faults. Away from the center, the dip of one of the two sets gradually increases, finally becoming vertical, or even slightly overturned, near the ends. The complementary set decreases in dip, changing from a normal 60° at the center to as low as 15° in the deeper end portions. These changes in attitude do not apply to the surface, where the directions of the stress trajectories remain unaltered, because of the required boundary conditions. There is, however, a rapid transition with depth from this normal position along the surface into the significant changes in orientation below.

During the gradual build-up of a stress system of this type (lower diagram of Pl. 1, A), instability with resultant faulting is first reached in a broad, but relatively thin, layer below the surface. With continued intensification of the primary stresses, this zone expands with depth and, to a lesser degree, sideways (at the surface it never reaches the two endpoints, since they represent singular points of zero shear stress). When their maximum value has attained a magnitude of the order of 3,000 kg/cm^2, it has spread out to embrace nearly the full depth of the outer portions of the block, but it does not yet cover the deeper central portion where the maximum shear stress is still below the strength. The process of this gradual expansion of instability is illustrated graphically by the three boundary lines corresponding to values of 1000, 2000 and 3000 kg/cm^2, respectively, of the maximum value of the uplifting force at the bottom.

The changes in attitude of the normal faults associated with this stress system are of considerable interest. Faults which are steeply dipping, vertical, or even slightly overturned, are frequently observed in areas where the dominating tectonic force appears to have been a differential vertical uplift. Numerous examples of this type have been described, for instance, from the Basin-and-Range province and from those portions of the Rocky Mountains in which vertical deformation predominates. If the dip is less than 90°, such faults are still assigned to the class of normal faults; if overturned, they are usually designated as reverse faults. Anderson has emphasized that faults of this nature belong in many instances to an entirely different class, the transcurrent or lateral class. This is often, but by no means always, true. An alternative explanation, applicable to those cases where lateral displacement is lacking, is provided by the present analysis. It shows that steeply dipping normal faults and reverse faults can be the direct product of an original stress system such as that here analyzed. They occur on the flanks of the uplift, beginning at a shallow depth. To be observable at the present surface, we merely have to assume that the uppermost layer has since been removed by erosion. The rather wide occurrence of such faults is not unexpected in view of the probability that the causal stress system is frequently realized in nature. However, this system is essentially of local character, which explains the fact that near-vertical normal faults and reverse faults form no part of Anderson's classification, based exclusively upon regional stress systems.

The complementary set of low-angle normal faults also deserves some attention. Faults of this type appear to be rare and are seldom mentioned in the literature. An outstanding case, however, has been described by C. R. Longwell from the Desert and Sheep ranges in southern Nevada (Longwell, 1945). Here Longwell found the presence of an extensive system of low-angle normal faults, all located on the flanks of a major anticline and dipping towards its axis. The range of the dips is mainly from 10° to 25°, and the form of the fault surfaces is further characterized by a slight upward concavity. This combination of facts agrees remarkably well with the general behavior of the low-angle normal faults emerging at the surface inside the positive quadrants. The corresponding dips in Plate 1, A are not quite as low as those described by Longwell from southern Nevada, but it can logically be explained by assuming a further flattening due to a subsequent rise of the central portion of the uplift.

Another characteristic feature shown on the diagram is the reversal in curvature of the low-dipping normal faults with depth. Its verification in nature would be contingent upon finding an example similar to the Desert-Sheep ranges, but exposed at a lower level. No clear-cut example of a combination of the near-vertical and low-angle, normal faults is known to the author, probably because of the protective influence of preceding fractures. The question of why very steep normal faults occur much more frequently than flat ones is less easily answered.

Plate 1, B–D presents a series of examples with a broader wave length. While the thickness of the block is the same as in the preceding case (c = 10 miles), the wave length is now twice as large, 62.8 miles. This distance is more comparable to that between adjacent ranges in certain portions of the Rocky Mountains. The difference between the three cases is in the ratios of the superposed vertical and shear-stress components. They are: $A = 0$ in Plate 1, B, $A = B/2$ in Plate 1, C and $A = 2B$ in Plate 1, D.

The results in the second case (Pl. 1, C) are quite similar to those in the preceding example. Evidently, the doubling of the wave length is roughly compensated by a reduction of the ratio A/B by half. The only notable difference lies in the relative proportions of the stable and the unstable segments. It is seen that for equal values of B_{max}, the depth penetration of the faulted portions is much greater in Plate 1, C than in Plate 1, A. For B_{max} = 3,000 kg/cm^2, it now embraces the entire positive half of the wave length, excepting two small areas in the immediate vicinity of the corners of zero shearing stress.

The negative half of the wave length illustrates the conditions due to the presence of a variable vertical tensile stress acting on the bottom of the block, in combination with a shear stress component of equal size but opposite directions as compared with the positive quadrants. There is, of course, no absolute tension at this depth, the supplementary tensile stress being always smaller than the standard state. It represents a partial relief of the pressure due to the weight of the overburden. The boundary stresses at the bottom set up a horizontal compression which may produce thrust faults within a thin layer below the surface.

Major changes in the character of the stress system accompany alterations of the above ratio A/B in either sense. Although it is doubtful whether these cases still fall within the domain of geological reality, they demonstrate the nature of the changes in both directions. Plate 1, B represents the extreme case where the supplementary stress applied to the bottom of the block consists of a sinusoidal shear stress only, A being zero. Now the internal horizontal stress component is no longer approximately constant with depth, nor even of uniform sign. At the 90-degree position σ_x changes from a maximum compressive stress at the surface to a maximum tensile stress at the bottom; at 270°, the signs are reversed. At some particular depth along these positions, singular points of zero shearing stress occur, accompanied by a 90-degree turn in the direction of the stress trajectories. A second pair of singular points is found at the 0 and 180-degree positions. The latter points are further characterized by the fact that the horizontal plane containing them is, like the surface, a principal plane where all trajectories are vertical or horizontal. The 90-degree switch here takes place in the horizontal direction.

A peculiar and important feature of a stress system of this type is that it produces two layers of faulting, separated by an intervening stable zone. Corresponding to the described variations in σ_x in the first half wave length, there is a zone of normal faulting in the lower part of the block, underlying a thin zone of thrusting in the uppermost portion. In the second half wave length the distribution is reversed, but thrusting in the lower portion does not occur unless the boundary stress at the bottom reaches very high values, exceeding 3,000 kg/cm^2 (although these areas are essentially stable, the attitude of a few potential fault surfaces has been indicated in the diagram). Conversely, at the 90-degree position, the strength limit at the bottom is reached for comparatively small values of B_{max}, due to the large tensile stress component.

The effect of a change in ratio in the other direction is illustrated in Plate 1, D. Here the ratio A/B is equal 2, the vertical stress com-

ponent now being the larger one. Although the shear stress component is still of appreciable magnitude, the resulting effects are equally pronounced as in the preceding case. They are also quite similar, though of opposite sense. The horizontal component σ_x again has a large vertical gradient, accompanied by a change in sign and by the occurrence of singular points. (They are absent, however, at the 0 and 180-degree positions.) The distribution of faulting is the reverse of that encountered in Plate 1, B. The upper portion of the first half wave length is a zone of normal faulting, whereas the lower portion is stable up to very large magnitudes of the boundary stresses. The second half wave length is roughly divided into three parts, namely, an upper layer of thrusting, an intermediate stable one, and a lower one of normal faulting. One important difference between the two cases—aside from their opposite character—lies in the relative proportions of the stable areas. This is especially marked in the vicinity of the 0- and 180-degree positions, where almost the entire thickness of the block is stable in Plate 1, B and unstable in Plate 1, D. In the latter case, the faulting here encountered is quite similar to that previously found in Plate 1, C, one set consisting of nearly vertical normal or reverse faults and the complementary set of gently dipping normal faults.

The stress system illustrated in Plate 1, D is obviously due to tectonic forces causing differential uplifts and depressions in adjacent belts of the crust. The former correspond to the positive, the latter to the negative half wave lengths of the diagrams. The primary vertical stresses applied at the bottom—representing an uplifting force in the positive belts and a partial relief of pressure in the negative zones—are probably accompanied by shear stresses of smaller but still appreciable magnitude. Possibly the ratio selected in Plate 1, D is already weighted too strongly in favor of the vertical component to be geologically significant. Diagrams B and D are nonetheless of interest due to the result that a departure in either direction from a certain "balanced" ratio produces stress systems in which a zone of thrusting may occur above a zone of normal faulting and vice versa, the two faulted layers being separated by a stable zone.

Convection Currents

Another important usefulness of the equations derived in the preceding section (equations 20 to 23) consists of their application to convection currents. Several authors (Griggs, 1939; Vening Meinesz and others, 1948), have demonstrated the likelihood of a periodic existence of large-scale convection currents in the weak substratum underlying the crust of the earth. Griggs shows that of all the primary forces so far suggested as the basic cause for mountain building, only two are potentially of sufficient magnitude to provide acceptable working hypotheses. These are (1) lateral compression due to thermal contraction, and (2) the viscous drag exerted on the bottom of the crust by convection currents in the substratum. He rejects the first one on account of other difficulties, but demonstrates the adequacy of the second on the basis of theoretical considerations, experimental data, and the results obtained from an ingenious scale model with dimensionally correct physical properties. In view of the results of these and related investigations, the effect of convection currents on the deformation of the crust has become of considerable geological interest.

The shearing stress exerted on the bottom of the crust by the viscous flow in the substratum is evidently best expressed in the form of a sinusoidal curve, the half wave length of which represents the width of the convection cell. Hence, it conforms to the second of the two primary boundary stresses analyzed in the preceding section (equations 20). Furthermore, it appears logical to assume that the region of the crust above the rising current endures a supplementary upward pressure, and the portion above the sinking column experiences a downward drag causing a reduction in the hydrostatic pressure. Therefore, the first of the two boundary stresses of equations (20) is probably also effective. This relationship between the location of the convection cells and the boundary stresses acting on the bottom of the crust is schematically illustrated in Figure 9. On the other hand, the numerical value of the ratio of the two stresses A/B is not safely determinable from qualitative considerations. Whatever it may be, equations (20) to (23) provide the basic solution for the determination

of the stress distribution in the crust due to the action of convection currents in the substratum.

The selection of the critical constants is as yet highly speculative. In a recent paper on convection currents, Vening Meinesz (1948, p. 200) discusses an apparent example from the Indonesian Archipelago and assumes the following constants: depth of crust $c = 30$ kilometers, distance between rising and sinking currents $l/2 = 340$ kilometers, and maximum shear stress at the bottom of the crust $B = 3{,}320$ kg/cm^2. This case, making the further assumption $A = 0$, has been calculated and was found to yield a stress system almost identical to that shown in Plate 1, B. It is not reproduced here since the only essential difference between the two pictures consists of a reduction in the ratio of thickness over wave length by the order of about three to one. A further reason for this omission lies in the uncertainty regarding the proper ratio A/B. The presence of an associated vertical stress component being surmised, the correct solution may correspond more probably to a flattened-out version of Plate 1, C or to another closely related system.

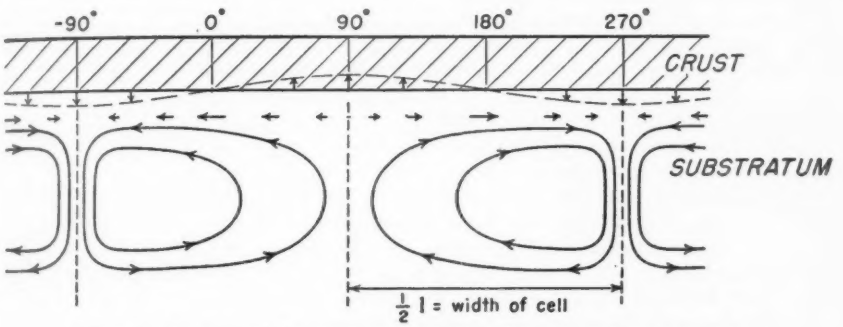

FIGURE 9. CONVECTION CURRENTS AND BOUNDARY STRESSES AT BOTTOM OF CRUST

CONCLUSIONS

A superposed horizontal compression with constant lateral and vertical gradients is always accompanied by a shear-stress component being constant in all horizontal planes. The associated thrust-fault surfaces are slightly curved, concave upwards for the set dipping towards the region of increased compression. If the lateral gradient of the superposed horizontal pressure is small, say of the order of half, or less, of the vertical pressure gradient due to weight, then the potential zone of faulting is limited to a thin wedge below the surface in which numerous shallow slice thrusts are expected to occur. If the gradient is sufficiently large (approximating the vertical gradient of the hydrostatic pressure), thrust faults may penetrate to great depths, but may then be confined to a comparatively narrow zone. The same is true if the superposed horizontal compression has an exponential—instead of a linear—rate of decrease. It is then associated with vertical and shear stress components likewise decreasing exponentially in the horizontal direction. The inclination of the resulting thrust-fault surfaces diminishes rapidly with depth. Hence, a gently dipping, or even horizontal, attitude may not necessarily imply a subsequent rotation but can also result directly from a local stress system of this type.

A laterally variable vertical boundary stress acting on the bottom of a block is most likely associated with a corresponding shear-stress component, the latter being 90° out of phase if the vertical component is assumed in the form of a sinusoidal curve. For certain "balanced" ratios of the two components, this combination causes a supplementary horizontal tensile stress in the belt subjected to the increased upward pressure and a corresponding compressive stress in the adjacent depressed belts. The boundary zones between these belts are characterized by absence of a superposed horizontal pressure and the occurrence of maximum shear-stress components. This causes a

45-degree rotation of the stress trajectories, which, in turn, leads to a pronounced change in the attitude of the fault surfaces. The standard normal faulting occurs over the central uplifted portion, but towards both flanks one of the two sets gradually changes to very steep, vertical, and finally overturned positions, whereas the complementary, but rarely realized, set of normal faults assumes unusually low inclinations. Thus the nearly vertical normal faults, so frequently encountered in tectonic provinces characterized by differential vertical uplift, are explained as a primary feature of such stress systems. The anomalous attitudes are caused by the described rotation of the stress trajectories. They cannot be ascribed to variations in the ratio of supplementary horizontal and vertical pressures, as is occasionally expressed in the literature, based on a false application of the methods of vector analysis. On the other hand, as Anderson has pointed out, vertical and reverse faults are in numerous instances not variations of normal faults but belong to the dynamically entirely different class of transcurrent faults.

A pronounced departure of the ratio of the two primary stress components in either direction from the discussed balanced condition produces theoretically interesting cases which may, or may not, be realized in nature. One of the principal features of these systems is the coexistence of two diverse zones of faulting at different levels in the crust, one situated above the other but separated from it by an intervening zone of stability.

Finally, the equations derived provide the basic solution for the stress distribution in the crust caused by convection currents in the substratum. A detailed application to this phenomenon must await a more secure knowledge of the pertinent constants.

References Cited

Anderson, E. M. (1942) *The dynamics of faulting*, Oliver and Boyd, London, 183 pages.

Griggs, David (1939) *A theory of mountain building*, Am. Jour. Sci., vol. 237, p. 611–650.

Hubbert, M. King (1951) *Mechanical basis for certain familiar geologic structures*, Geol. Soc. Am., Bull., vol. 62, p. 355

Jeffreys, Dr. H. (1936) *Note on fracture*, Royal Soc. Edinburgh, Pr., vol. 56, pt. 2, p. 158–163.

Longwell, C. R. (1945) *Low-angle normal faults in the Basin and Range Province*, Am. Geophys. Union, Tr., vol. 26, pt. 1, p. 107–118.

Timoshenko, S. (1934) *Theory of elasticity*, Eng. Soc., Mon., 403 pages.

Vening Meinesz, F. A. (1948) *Major tectonic phenomena and the hypothesis of convection currents in the Earth*, Geol. Soc. London, Quart. Jour., vol. 103, pt. 3, p. 191–207.

Shell Oil Co., Shell Building, Houston, Texas

Manuscript Received by the Secretary of the Society, September 23, 1949

BULLETIN OF THE GEOLOGICAL SOCIETY OF AMERICA
VOL. 62, PP. 399-416, 1 FIG., 1 PL. APRIL 1951

MEASUREMENT OF PALEOTEMPERATURES AND TEMPERATURES OF THE UPPER CRETACEOUS OF ENGLAND, DENMARK, AND THE SOUTHEASTERN UNITED STATES

BY H. C. UREY, H. A. LOWENSTAM, S. EPSTEIN, AND C. R. MCKINNEY

ABSTRACT

Since the abundance of the O^{18} isotope in calcium carbonate varies with the temperature at which it is deposited from water, the variation in abundance can be used as a thermometer. This paper discusses the following problems: (1) the magnitude of the effect expected, (2) the mass spectrometer of high sensitivity, (3) the preservation of the record during geological time, (4) the constancy of the isotopic composition of the ocean, (5) the impossibility of using skeletons of air breathing animals, and (6) the temperature of marine animals relative to their surroundings.

A Jurassic belemnite is used to show that the record has been retained since Jurassic times, and belemnites of the Upper Cretaceous of the United States, England, and Denmark are used to determine the temperature of this time at these localities. The temperatures are about 15°–16°C and indicate nearly uniform temperature over this latitudinal belt. Because of the possible variation in O^{18} content of the oceans and the limited number of samples, these temperatures are regarded as preliminary.

CONTENTS

	Page
Introduction	399
Acknowledgments	400
Fractionation of isotopes in chemical processes	400
Problem of measuring paleotemperatures	401
Measurements of isotope composition, and temperatures of the Upper Cretaceous	406
Discussion of the North American temperatures	414
References cited	416
Addendum	416

ILLUSTRATIONS

Figure	Page
1. Cretaceous sections for localities studied	413

Plate	Facing page
1. Seasonal growth of a Jurassic belemnite	406

INTRODUCTION

Geologists have drawn many conclusions from the purely qualitative evidence of geological studies in regard to the past climatic conditions on the earth. These deductions are based upon a great variety of evidence, and the ability of the geologists to deduce as much as they have in regard to these conditions excites the wonder and admiration of all the uninitiated who examine their work even casually. Palm trees do not grown in Spitzbergen, according to all our evidence, unless the weather is mild—about the same as that of Florida. Heavy shells are deposited in warm water, and thin shells in cold water. Tree rings are definite evidence of seasons.

During the last 15 years a number of people have studied chemical properties of isotopic substances. These studies include the demonstration of differences in the chemical properties of the hydrogen isotopes, the first calculations of such differences in the case of other of the lighter isotopes, extensive applications of such differences to the separation of isotopes and considerable evidence of such differences from surveys of the abundances of the lighter isotopes in nature. From the standpoint of the natural abundances the early demonstration that deuterium was not constant over the surface of the earth, the demonstration by Dole (1935, p. 2731; 1936, p. 268) that oxygen also varies, particularly in the air, and the variation of carbon from inorganic and organic sources by Nier (Nier and Gulbranson, 1939, p. 697; Murphy and Nier, 1941, p. 771) contributed to geology. Recently Thode, MacNamara, and Collins (1949, p. 361) have dem-

onstrated substantial variations of the sulfur isotopic abundances, and Thode, MacNamara, Lossing, and Collins (1948, p. 3008) have demonstrated such variations in boron. The present paper presents a way in which the natural variations in the abundances of the lighter isotopes makes possible, in principle at least, quantitative measurement of paleotemperatures.

Acknowledgments

We are indebted to The Geological Society of America and to the American Petroleum Institute for grants which have made this work possible, and we wish to extend our most sincere thanks for this help. During recent months the work has also been supported under Task Order XXVIII, Contract N6ori-20 of the Office of Naval Research.

Fractionation of Isotopes in Chemical Processes

Differences in the chemical properties of the elements, such as differences in vapor pressures and in equilibrium constants of exchange reactions, are at least partially responsible for these variations in the lighter isotopes in nature. Quite certainly the variation of the hydrogen and oxygen isotopes in the fresh waters of the earth as compared with the sea is due to the difference in vapor pressures of the varieties of water containing hydrogen and deuterium or the three oxygen isotopes, oxygen 16, 17, and 18. The variation in the abundance of the carbon isotopes discovered by Nier cannot certainly be assigned to this cause. He found that carbon 13 exists in organic matter in a decreased abundance as compared with the carbon in carbonates. Whether the photosynthetic process concentrates the carbon isotopes by some equilibrium or near-equilibrium process is not certain. Since the oxygen isotopes of the air are not in equilibrium with the oxygen isotopes of the sea or fresh water, this effect is probably also produced by the photosynthetic process or by the oxidation of organic matter by atmospheric oxygen,[1] and if a vital selection of the isotopes occurs in the case of one of these isotopes it may well do so in others.

Variation in isotopic abundances which are due to differences in thermodynamic properties —*i.e.*, processes which are in equilibrium or very close to equilibrium—are understood in principle and in many cases in detail. On the one hand, it is necessary to know the quantum states of these molecules, and on the other it is necessary to have the exact theories of statistical mechanics in order to relate these quantum states to the physical chemical properties. For Molecules in the neighborhood of ordinary temperatures and above, it is unnecessary to consider the rotational quantum states, since these are very close to classical at these temperatures in the case of all molecules except those involving the hydrogen isotopes. In this case the entire difference in the chemical properties resides in the differences in the vibrational energy levels. A great many calculations covering exchange reactions of the lighter elements were made by Urey and Greffi (1935, p. 321) and have been recalculated by Urey (1947, p. 562), together with the mathematical formulae and spectroscopic data by which the calculations are made. In general differences of a few per cent in the ratio of isotopes in two chemical compounds which are brought to equilibrium with each other with respect to the exchange of isotopes are possible for elements even as high in the periodic system as chlorine. The heavier elements can be expected to show but very slight effects of this kind. The calculations indicate that there

Table 1.—Calculated Fractionation Factors for O^{16} and O^{18}*

t°C	$CO_3^= - H_2O(l)$	$SO_4^= - H_2O(l)$	$PO_4^{\equiv} - H_2O(l)$
0	1.0220	1.0204	1.0104
25	1.0176	1.0157	1.0087
Ratio K_0/K_{25}	1.0044	1.0047	1.0017

* McCrea (Doctoral Dissertation, Chicago, 1949) by attempting to include the effects of the potential fields in crystals instead of assuming no such fields as was done by Urey (1947) secures slightly different values for the $CO_3^=$ — H_2O constants.

[1] However, Dole has recently proposed other explanations for this effect (1949, p. 77).

should be differences in the ratio of the oxygen isotopes in water and carbonate ion, water and sulfate ion, and water and phosphate ion, (Table 1).

In these calculations the results are reported for equilibrium between liquid water and the carbonate ion rather than between the gaseous water and the carbonate ion. A slight difference of a few per cent is expected in the isotopic composition, and slight temperature coefficients are predicted. The calculations show that this difference for the carbonate-water equilibrium shoud amount to about 0.44 per cent in 25°C, or 0.176‰ per degree C. The calculations are not exact because experimental data do not supply us with the vibrational energy levels for those molecules containing oxygen 18, and hence the vibrational frequencies of these molecules must be calculated from the known vibrational frequencies of the more abundant oxygen 16 varieties. The calculation depends upon a choice of constants. In fact, in the case of the carbonate ion five constants are needed to describe the potential energy function to the precision of quadratic terms in the co-ordinates, whereas only four independent frequencies are available for the calculation of these constants from the observed vibrational frequencies of the CO_3^{-16} ion. A similar situation exists in the phosphate and sulfate ions.

If a relation exists between the oxygen abundances in these compounds, and temperature, and the water in which the compounds were deposited, it should be possible to set up a thermometer for present-day organisms living in the sea, if the isotopic composition of the water is known not to differ from the mean of the present seas, or, in case it does, if both the isotopic composition of the carbonate and water are determined. Thus it would only be necessary to establish an empirical temperature scale and to measure the isotopic abundances of oxygen in a shell deposited by an animal in the sea in order to determine the temperature at which deposition took place. This application may be of interest in some cases, as for example in determining the temperature history of an animal, but the process which we describe is difficult, and wherever possible ordinary thermometers are likely to be considerably more convenient. On the other hand, these effects may be preserved during geological time, and hence this method affords a possible method for measuring paleotemperatures.

Problem of Measuring Paleotemperatures

Since the predicted temperature coefficient for the ratio of oxygen isotopes in calcium carbonate relative to water is small, mass spectrometers of very great precision and sensitivity are needed for this problem. It would be desirable to measure paleotemperatures within less than a degree Centigrade, which corresponds to a change in the atomic weight of oxygen in the calcium carbonate of 7×10^{-7} atomic weight units, or a change in the abundance of oxygen 18 by 1 part in 2.5 million of oxygen. We have set 0.01 per cent or better, corresponding to about 0.5°C or 1°F, as our objective in these experiments. As measurements of the ratio of isotopes have been conducted in the past, reports in the literature of 0.1 per cent or 1‰ are about as high a precision as has been attempted. Hence the first problem in the application of this method to paleotemperatures is the construction and operation of very sensitive mass spectrometers.

Since we have examples of animals and plants laying down isotopes out of equilibrium with their surroundings, as for example the carbon of organic material, we may well ask whether the deposition of calcium carbonate by an animal or a plant occurs so as to leave the oxygen isotopes in equilibrium with the water from which deposition takes place; that is, we may ask whether there is a *vital effect*. Probably the equilibrium deposition should be closely approximated in many cases, for the calcium carbonate deposited is constantly bathed with water from the surroundings and hence may exchange its oxygen with the surrounding water during the deposition process. However, one could quite readily imagine mechanisms which would involve the deposition of organic oxygen and thus invalidate these assumptions. The whole question could be answered only by experiment, so far as we can judge from the present state of our knowledge of the physiology of deposition of such substances. The question of deposition of phosphate on the other hand would appear to be

even more doubtful than the deposition of carbonate, since phosphate ion does not exchange its oxygen with water in which it is dissolved, and hence perhaps the phosphate deposited by animals generally does not have its oxygen in equilibrium with its surroundings. Since phosphate is so intimately involved in biochemical reactions, its oxygen may be brought to equilibrium with water by them. Only careful experimentation can determine. the feasibility of the phosphate thermometer.[2]

Animals rarely deposit sulfate, and it is not an important substance for investigations of the type we envisage immediately. Silica is often deposited by plants and animals as a hydrous silica. Since the relative proportions of water and silica might change the relative abundance of the oxygen isotopes, this does not appear to be a very promising line of attack, though again experiments should be made to determine whether there is any possibility of using a silicate thermometer. Of the possible thermometers—that is, the carbonate, phosphate, sulfate, and silica the carbonate thermometer seems the most likely to give satisfactory results. A combination of the carbonate and phosphate would eliminate the water, and hence the isotopic variation of water always present in brackish water and fresh water would be eliminated. Dr. Martin Steinberg is investigating the possibilities of this thermometer.

Assuming that the shell is laid down in equilibrium with the water, the next important question is whether this composition is preserved during geological time. In the first place, if radical metamorphosis takes place, as for example the conversion of limestone to dolomite, no satisfactory record of the isotopic abundance can be expected, for the disolved carbonate should exchange with the water in which it is dissolved and then be redeposited with the composition partially dependent on its original composition and partially on the water which was the means of redeposition. Also, if aragonite is converted to calcite through solution in water, the record would be destroyed, but, if recrystallization without the possibility of exchange occurs, the record might be preserved.

The second important method for destruction of the temperature record is diffusion through the solid state. Shells as usually deposited appear to be fairly compact, but microscopic examination shows that they consist mostly of very small crystals, often with definite canals through the shell, as for example in the case of the brachiopods or the echinoderms. Thus in considering the problem of diffusion it is not the gross size of the shell that is important, but rather the small microscopic particles, since in the course of geological time water would probably pass through the shell by hydrodynamic flow, or diffusion in the liquid would bring the isotopic composition of water within the shell to that of water in which it is immersed. The diffusion problem for considering this situation exactly would be very complicated. Assuming that the initial conditions are that (1) at the surface of the crystals the composition is that required for equilibrium with the surrounding water, and that it remains so throughout the diffusion process, and (2) that initially the composition of the crystal differed from that which would be in equilibrium with the water in which it has been immersed during the time since the shell was formed, and that it changes from this initial condition in accordance with the diffusion laws at some constant temperature, a calculation can be made which relates the size of the crystal, the time, and the coefficient of diffusion to the composition of the shell remaining. The fraction of the excess mean concentration over that in equilibrium with the surrounding water, assuming that the coefficient of diffusion is the same in all directions, is

$$\frac{Q}{Q_0} = \frac{512}{\pi^6}\left\{\sum_{m=0}^{\infty}\frac{1}{(2m+1)^2}\,e^{-a(2m+1)^2}\right\}^2,$$

where $a = \dfrac{D\pi^2 t}{l^2}$, D is the diffusion coefficient, t the time, and l the length of the edge of the cube.

If we require that the crystal shall retain its

[2] Dr. Mildred Cohen (private communication) informs us that she has found that some enzymatic hydrolyses of phosphoric esters split the oxygen phosphorus bond though others do not. Hence a mechanism is available which may establish equilibrium between water and phosphate in animal bodies.

original composition within some arbitrary percentage, the value of $\frac{D\pi^2 t}{l^2}$ can be estimated from this equation. (If one uses different values of D for different axes, the result is the same as though different lengths were used for the direction parallel to the axis and for the two directions perpendicular to this.)

TABLE 2.—VALUES OF Q/Q_0 FOR VALUES OF a*

$a = \frac{D\pi^2 t}{l^2}$	$\frac{Q}{Q_0}$
0.1	0.461
0.05	0.590
0.01	0.795
0.005	0.854
0.001	0.915
0.0001	0.964
0.00001	0.972

* We are indebted to Mr. L. G. Montet for the numerical results given in this table.

Table 2 gives a few values of a for a few values of Q/Q_0.

The coefficient of diffusion of one ion can be calculated from the electrical conductivity providing the current is carried by that ion and not by the other. Joffe (1923, p. 461) concluded that only the calcium ion carries the current, but to what extent the carbonate ion carries current was not determined except that its contribution was not detected. If we assume that the carbonate ion carries some fraction, δ, of the current, the coefficient of diffusion of the carbonate ion can be calculated from the resistivity of calcite from the equation,

$$D = \frac{RT\delta}{n^2F^2C\rho},$$

where n is the number of charges on the ion—*i.e.*, 2—, F is the faraday, 9650 EMU, C is the number of gram molecules of carbonate ions per cm³, ρ is the specific resistance in absolute units, and δ is the unknown fraction of the conductivity due to carbonate and assumed to be 0.01 here. If ρ is in ohms, this formula must be multiplied by 10^{-9}. Curie (1889, p. 385)[1] measured the specific resistance of calcite, and his values and the values of D calculated from them are given in Table 3.

Using the first two values of $D_{CO_3^{--}}$ in the table, we can estimate the time required for diffusion to destroy the record. Thus at 20°C a crystal of 1 mm. dimensions will retain 96.4 per cent of the original concentration relative to the equilibrium concentration of a changed environment for 2.3×10^{15} seconds (7×10^8 years), while at 100°C the same crystal will retain this record only 2.1×10^{11} seconds (6.4×10^4 years). Crystals of this size will not lose the temperature record due to diffusion in times sufficiently long to be of considerable interest, and the coefficients of diffusion may be even smaller than those given in Table 3.

TABLE 3.—MEASURED SPECIFIC RESISTANCE OF CALCITE AND CALCULATED COEFFICIENTS OF DIFFUSION

	t°C	ρ	$D_{CO_3^{--}}$
∥ axis	20	5.5×10^{14}	4.4×10^{-23}
	100	5×10^{11}	4.8×10^{-20}
	160	3×10^{10}	8.1×10^{-19}
⊥ axis	15	9.5×10^{15}	2.5×10^{-24}
	100	2.4×10^{12}	1.0×10^{-20}
	150	1.3×10^{11}	1.9×10^{-19}

A shell may grow a centimeter per year or 3×10^{-3} cm. per day within an order of magnitude. For simplicity we assume that the concentration of O^{18} with distance due to daily variation of temperature varies according to a cosine law. Then the diffusion equation gives

$$C = e^{-D\pi^2 t/l^2} \cos \pi \frac{x}{l},$$

where we take the mean concentration as zero. If we can detect a concentration difference equal to 0.5 of the original difference between maximum and minimum, *i.e.*, at $x = 0$ and $x = l$, we have

$$ln\ 2 = \frac{D\pi^2 t}{l^2}.$$

Substituting $D = 4.4 \times 10^{-23}$ and $l = 3 \times 10^{-3}$, the time becomes 1.4×10^{16} or half a billion years. If we ask for 0.75 of the original

[1] *See* Landolt-Bornstein Tabellen II, 1062 (1923).

variation the time becomes fifty milion years. Thus even a daily variation of temperature might be partially preserved.

There is the question of whether the isotopic composition of the ocean has remained constant during geological time. Such a change would be produced, if igneous rocks of one isotopic composition are weathered and sedimentary rocks of another composition are produced. At high temperatures the isotopic compositions of all chemical substances should be the same, and, if this temperature was that of molten lava or higher, differences in isotopic composition of water and silicates should not be large and at least they should be less than at lower temperatures. The calculations referred to above show that O^{18} concentrates preferentially in the solid phases and not in the water, and it can be expected that this will be true with respect to the silicate rocks. Thus 0^{18} should enter the sedimentary rocks and its concentration in the oceans should decrease with time. Assuming that the ratio of concentration in water and silicates is the same as for sulfate and water at 25°C, namely, 1.016, and that 600 g. of rock have been eroded for each 1000 g. of water (Goldschmidt, 1933, p. 112), it is easily shown that the water should have changed its ratio of oxygen isotopes by 3.8‰ due to this cause. Dr. P. Baertschi has shown that there are differences between ocean water on the one hand and the Disco Island Greenland basalt containing native nickel-iron and other igneous rocks, and, on the other hand, sedimentary rocks of just the kind and magnitude predicted, though the total difference between ocean water and sedimentary rocks is not 16‰ as predicted. These results will be published elsewhere.

It is of interest to inquire as to the time at which these changes took place. The carbonate equilibrium should have taken place early in the earth's history, and largely since then no important change in the O^{18} content of carbonates occurred. The shales which make up much of the sedimentary rocks should exchange their oxygen with water less readily than the carbonates, but no information is available. Baertschi finds that sandstones have an increased O^{18} content relative to the Greenland basalt and thus may have exchanged their oxygen to some extent, though the difference is small enough to be explained by equilibrium differences in concentrations between the silica and other phases of igneous rocks. Perhaps it is a conclusion based on little more than prejudice, but we believe that it is most likely that the major part of this change occurred before the Cambrian. Until more data are available we will make no correction for this effect.

If the water of the oceans has been steadily produced during the earth's history from plutonic activity, as maintained by some (W. W. Rubey, private communication), the entire problem of the isotopic composition of the oceans must be considered from this point of view and must involve measurements on the O^{18} and D concentrations in waters which might be expected to be juvenile, as from geysers, hot springs, and volcanoes. Such measurements have not been made, but are desirable from the standpoint of the work presented here as well as for the evidence they might give relative to this suggestion in regard to the origin of the earth's water.

The oxygen of the air has a higher isotopic composition than that of the sea and fresh water. The difference in isotopic composition amounts to about 2 per cent for air oxygen as compared with the sea. All animals use atmospheric oxygen, and hence produce water that contains an increased concentration of oxygen 18. In the case of marine animals having gills which exchange water between the sea and their blood stream, it can be expected that in spite of the oxidation processes taking place within their bodies the water content of their bodies will be very close to that of the sea. One can reason that this must be true, for the water oxygen must pass through the gills approximately as readily as does the elementary oxygen, and since the amount of water present at the surface of the gills is larger than the amount of oxygen by a factor of about 10^5, the rate of transfer of the water oxygen must be much more rapid than the transfer of elementary oxygen, and hence the isotopic composition of the blood stream must remain close to that of the sea. On the other hand, either marine or land animals that breathe air are suspect for our purposes, since atmospheric oxygen is high in oxygen 18 (*i.e.*, plus $\backsim$ 20‰). Land animals

drink fresh water with a decreased concentration of oxygen 18, and animals of the sea eat food containing a very considerable amount of water of the composition of water of the sea. Without knowing the relative importance of these factors it is difficult to have any confidence in any measurements made on air-breathing marine animals, and even less on land animals. It would be possible to investigate the blood of marine reptiles or mammals to determine how nearly the oxygen 18 content of their blood agrees with that of the sea. This has not yet been done.

The question arises as to whether marine animals maintain their body temperature above that of the surrounding sea. They do not. The source of heat is the combustion of food by oxygen received through the membranes of gills, usually, or of the general body surface. The membrane through which the oxygen diffuses is the same as that through which heat is lost to the surroundings. The transport of oxygen determines the rate of heat production, and this must equal the rate of loss by thermal conduction. Assuming the maximum concentration of oxygen in sea water—*i.e.*, 6 ml. per liter—and that the oxygen combines with sugar to produce 56,000 calories per gram atom of oxygen, and knowing the coefficient of diffusion of oxygen in water and the coefficient of conduction of heat in water, we can set up the following equation:

$$56{,}000D\frac{\Delta C}{\Delta l} = K\frac{\Delta t}{\Delta l},$$

where D is the coefficient of diffusion, K the coefficient of thermal conduction, ΔC the concentration difference of oxygen between the blood stream and the water and not greater than that corresponding to 6 ml. per liter, or .0005 gram atoms per cm^3, Δt the difference in temperature between the water and blood stream, and Δl the membrane thickness through which both diffusion and heat conduction take place. The quantity Δl is unknown, but is the same for both processes and can be cancelled from the equation and the equation solved for Δt. Substituting $D = 2 \times 10^{-5}$ cm^2sec^{-1} and $K = 1.42 \times 10^{-3}$ cal. $cm.sec^{-1}{}^{\circ}C$, we find that $\Delta t = 0.38°C$. This is the maximum difference in temperature possible under normal aerobic conditions. Animals can expend energy for limited periods of time under anaerobic conditions and thus raise their temperature above that calculated here, but such periods would seem to be negligible.

The preparation of carbon dioxide gas for use in the mass spectrometer has constituted one of the most difficult problems in this research. It is so intimately related to the problem of the empirical temperature scale that both these problems and related ones will be discussed in a separate paper. Impurities in the carbon dioxide must not produce peaks at masses 44 and 46 such that the ratio of intensities of these masses is changed by more than one part in 10^4, which means an impurity in mass 44 of less than this amount and in mass 46 of less than one in 2.5×10^6. We are fortunate in using a relatively clean part of the mass spectrum. The carbon dioxide is prepared from calcium carbonate by the action of orthophosphoric acid to which phosphorus pentoxide is added to bring the concentration to approximately 100 per cent. To this enough chromic oxide is added to give a slight permanent red tint, and the excess oxide is reduced with hydrogen peroxide and the excess decomposed by heating. The calcium carbonate sample is first heated in a stream of carbon dioxide-free helium for 15 minutes at approximately 475°C in order to destroy organic matter. Approximately 9 cc. of the phosphoric acid and 50 mg. of the calcium carbonate are put in separate arms of a reaction vessel, evacuated, and brought to 25°C in a thermostat. The acid is then poured onto the carbonate. A vigourous evolution of carbon dioxide results, sometimes with a little froth which breaks during half an hour in the thermostat. The gas is then transferred to sample tubes and analyzed on the mass spectrometer. All stop cocks and tapered joints are greased with Apiezon *N* cock grease. We have never detected any effect of impurities due to this material.

With this procedure reproducible analyses are secured for both recent specimens and fossils. Using the shells of present-day marine animals grown at known temperature and correcting for the variation of isotopic composition of the various sea waters, the following equa-

tion for temperature is secured (Epstein, Buchsbaum, Lowenstam, and Urey, 1950):

$$t = 11.88 - 5.91\delta,$$

where t is measured in °C, and δ is the difference in ‰ between the ratio of O^{18} to O^{16} in a standard working gas, and this ratio for the sample, *i.e.*,

$$\delta = \left(\frac{R_{sample}}{R_{standard}} - 1\right) 1000,$$

where R_{sample} and $R_{standard}$ are the ratios of $CO^{16}O^{18}$ to CO_2^{16} for the sample and reference gas respectively. The reference gas is carbon dioxide prepared from *Belemnitella americana* from the Peedee formation of South Carolina. The slope of this curve agrees within the limits of error with that secured by McCrea (1949; 1950, p. 849) from inorganic crystals of calcium carbonate grown at constant temperature. This equation is believed to be accurate to ±1°C if the calcium carbonate were deposited in sea water of the mean isotopic composition of sea water of salinity 34.8‰. If the calcium carbonate was deposited in water of other isotopic composition, appropriate corrections must be made. The maximum variation in temperature for fully marine conditions due to the variation of isotopic composition of the oceans is ±4.5°C.

The variation of isotopic composition of the present oceans, as discussed by Epstein, Buchsbaum, Lowenstam, and Urey (1951), presents the greatest difficulty so far encountered in the measurements of paleotemperatures. These authors point out that isotopic composition varies approximately linearly with salinity. Their data on surface waters are not very extensive, but this rough linear relation applies also to surface waters. The isotopic composition varies in a rough linear way with the temperature of surface waters. This indicates that, if no correction for the isotopic composition were made, a temperature of 30°C would be read as about 25°C, while a temperature of 10°C would be read as 15°C. High temperatures would be read too low, and low temperatures too high. However, no correction to past temperature determinations can be made by use of their curve because (1) A general average change in the earth's temperature would not change the average isotopic composition of the oceans, and hence a measured isotopic composition could not be corrected with their curve. (2) The slope of the curve of O^{18} composition vs. temperature is due to evaporation and condensation of water, and hence can be expected to be greater in times of high precipitation and lower in those of low precipitation. In general one would expect that high rates of evaporation and precipitation would accompany higher average temperatures of the earth's surface. However, we have the phenomena of glacial periods which somehow appear between limits of extremely low and extremely high temperatures, and these make estimates in regard to the relation of temperature to precipitation very difficult. For the present we do not attempt to estimate the correction for isotopic variations in the sea, but this problem is being studied from several angles and it is hoped that corrections can be applied in the future.

Measurements of Isotopic Composition, and Temperatures of the Upper Cretaceous

In considering geological specimens for our first attempts at measuring these temperatures, we have been guided by our considerations of probable diffusion of the carbonate in solid calcium carbonate and the improbability that recrystallized carbonates would retain the record. Since aragonite is unstable and commonly recrystallized, all recrystallized aragonitic shells will probably lose the record.

A study of fossil carbonate shells indicated that the belemnites would be the most likely to retain the record. These have a very compact structure with calcite crystals megascopically visible and so closely fitted together that internal reflections do not occur since the specimens are characteristically translucent. The polarizing microscope shows that the calcite crystals are arranged with their axes perpendicular to the axis of the guard. The orientation

Plate 1.—Seasonal Growth of Jurassic Belemnite

Figure 1.—Cross Section of a Jurassic Belemnite
Showing relation of samples to growth rings. *W* and *S* refer to winter and summer regions respectively.
Figure 2.—Variation of Temperature and C^{13} Content with Radius of Jurassic Belemnite

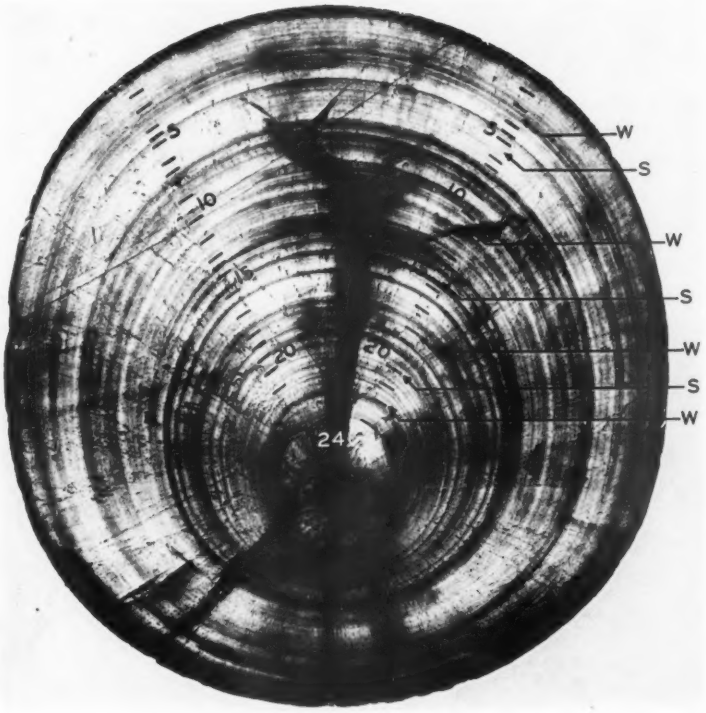

FIGURE 1

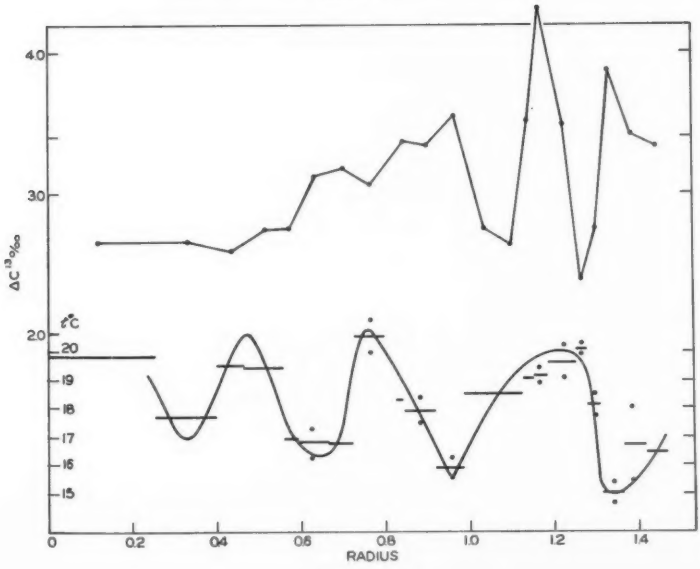

FIGURE 2

of the crystal axes and the shape and size of the crystals are evident.

Several paleontologists advised investigation of the possibility that various representative species of the genus *Inoceramus* might retain the temperature record. These fossils show evidence of massive calcite crystals of substantial size, though they are opaque. The calcitic layer of the shell is also present in many present-day mollusks, though usually not developed to the remarkable extent that it is in this extinct group. Experiments in progress confirm our expectation that this group retains the temperature record.

In the belemnites, a particularly convincing test for the durability of the record has been made. A Jurassic belemnite[4] approximately 2.5 cm in diameter, brownish and translucent, with very well-defined growth rings, has been investigated for a seasonal effect and bilateral symmetry of isotopic constitution both with respect to carbon and oxygen. A flat disk about 3 mm. thick was cut from the specimen, polished, and photographed in transmitted light (Pl. 1, fig. 1). Samples of carbonate were ground from the specimen following the growth lines from each side of the disk, as shown by the numbered rings shown in the photograph. In some cases right and left samples were not taken and analyzed, either because of accident in the cutting or preparation or because the samples were combined to secure sufficient carbonate for our samples. In one case both the right and left samples were lost.

TABLE 4.—ANALYSES OF A JURASSIC BELEMNITE

Ring No.	$\delta(C^{13})$			$\delta(O^{18})$			t°C
	R	L	Av.	R	L	Av.	
1	3.3_4	2.5_0		-0.6_5	-1.8_4	-0.6_5 (?)	$15._7$
2	3.5_7	3.3_5	3.4_1	-0.4_7	-0.9_5	-0.7_1	$16._1$
3	3.8_2	3.9_4	3.8_8	-0.4_6	-0.3_0	-0.3_8	$14._1$
4	2.6_5	2.8_8	2.7_6	-1.0_4	-0.8_9	-0.9_6	$17._5$
5	2.4_1	2.3_7	2.3_9	-1.3_2	-1.3_7	-1.3_5	$19._9$
6	3.2_7	3.6_9	3.4_9	-1.3_7	-1.1_5	-1.2_6	$19._3$
7	4.2_4	4.3_9	4.3_2	-1.2_1	-1.1_4	-1.1_7	$18._8$
8	3.5_2	—	3.5_2	-1.1_4	—	-1.1_4	$18._6$
9	2.6_5	—	2.6_5	-1.0_4	—	-1.0_4	$18._6$
10	—	2.7_5	2.7_5	—	-1.0_5	-1.0_5	$18._1$
11	3.4_6	3.6_2	3.5_4	-0.6_2	-0.4_9	-0.5_5	$15._1$
12	3.2_9	3.4_9	3.3_4	-1.0_3	-0.8_5	-0.9_4	$17._4$
13	3.3_7		3.3_7	-0.8_9		-0.8_9	$17._1$
14	—		—	—		—	—
15	3.0_8	3.0_9	3.0_7	-1.5_4	-1.3_1	-1.4_2	$20._3$
16	3.1_8		3.1_8	-0.7_1		-0.7_1	$16._1$
17	3.0_9	3.1_6	3.1_2	-0.8_3	-0.6_4	-0.7_3	$16._2$
18	2.7_5		2.7_5	-0.7_5		-0.7_5	$16._2$
19, 20	2.7_4		2.7_4	-1.2_1		-1.2_1	$19._0$
21	2.5_9		2.5_9	-1.2_4		-1.2_4	$19._2$
22, 23	2.6_8		2.6_8	-0.8_9		-0.8_9	$17._1$
24	2.6_8		2.6_8	-1.3_0		-1.3_0	$19._6$
							Av. $17._6$

The samples were analyzed for the C^{13} and O^{18} isotopes (Table 4).

The right and left samples of the outermost ring do not agree either in C^{13} or O^{18}, and the check for the two samples of the second ring is rather bad for the O^{18}. Otherwise the agreement on the two sides lies within 0.2‰. Considering probable errors of measurement, and the difficulty of cutting samples of the same thickness from the two sides, the agreement is very satisfactory. A radial variation of isotopic composition occurs both in the carbon and oxygen isotopes. The variation of the carbon isotopes does not correlate with any

[4] Unfortunately, we do not know the species of this specimen. It was collected along with others on the Island of Skye by Dr. Cyril S. Smith, who kindly made them available to us. The specimens are of various shapes and sizes and do not appear to be a single species. As nearly as we can learn they are Jurassic, probably from the Oxford clay.

other variable found either in fossil or present-day specimens, and the variation in this specimen is of the order found in present-day specimens. The erratic variation is probably due to fractionation of the carbon isotopes by plants and the large effect that this has on the very small amount of carbon in the sea (approximately 28 mg. per liter).

Figure 2 of Plate 1 plots temperatures deduced from our O^{18} abundances against a radius measured along a line from the center of growth outward. The temperatures are plotted as horizontal lines over the range of the radius for which they are the mean temperature. The true temperature curve should intercept equal areas above and below these lines. Such a curve is drawn trying to take account of this requirement and the uncertainty of the data. Where analyses for both the right and left sides are available the line is the average, and points above and below represent the two data. The plot of δ (C^{13}) is also given and shows no correlation with the seasons. The lack of structure at the smaller radii is probably due to the fact that the samples are too thick to show the variations that may exist.

It seems difficult to believe that any "accidental" process of diffusion or exchange could have produced such a distribution of carbon and oxygen isotopes, and we conclude that the record has been substantially preserved for over a hundred million years by this belemnite. In our work on other belemnites, we have never had any reason to doubt the isotopic record providing the specimen was translucent.

This Jurassic belemnite records three summers and four winters after its youth, which was recorded by too small amounts of carbonate for investigation by our present methods; warmer water in its youth than in its old age, death in the spring, and an age of about four years. The maximum seasonal variation in temperature is about 6°C. The mean temperature was 17.6°C.

Dr. C. J. Stubblefield of the British Museum has very kindly co-operated in securing specimens of belemnites, oysters, and brachiopods from the Upper Cretaceous Chalk of England. Thus we have well-preserved specimens imbedded in a matrix which has been modified but slightly with time. Table 5 lists the specimens secured from him and his record of the places and zones from which they originate.

Dr. J. Troelsen of the Mineralogical and Geological Museum of Copenhagen also supplied us with three belemnites from the lower and upper Maestrichian of Denmark. The data regarding their collection are as follows:

1. *Belemnitella mucronata*, Upper Maestrichian, 17m. below the top of the white chalk, Stevns, Denmark.
2. *Belemnitella mucronata*, Upper Maestrichian, 30–40 mm. below the top of the white chalk, Stevns, Denmark.
3. *Belemnitella mucronata*, Lower Maestrichian (white chalk), Møen, Denmark.

In studying the isotopic composition of these specimens we first removed carefully the chalk from the specimen. In the case of the belemnites the surface layers and any chalky infiltrations in cracks of the specimen were carefully removed. When possible a complete cross section of the guard was used to secure a true average temperature. In any case a piece of the solid clear calcite was gound to a fine powder and carbon dioxide prepared from these samples. In the brachiopods and oysters the chalk again was carefully removed, and parts of the clean shells were gound to fine powder and used for the preparation of the carbon dioxide samples. Whenever the chalk was available samples of the chalk in the immediate neighborhood of each specimen were analyzed. The results of the carbon and oxygen analyses for the English samples are recorded in Tables 6 and 7. In these tables the zones have been numbered as indicated in Table 5.

The oysters, brachipods, and their chalks agree in O^{18} composition only very roughly, and their C^{13} concentrations do not agree within the limits of our measurements. The belemnites do not agree in O^{18} concentrations with their chalks nor with the oysters and brachiopods. We conclude that only the belemnites retain the temperature record. Probably the crystals of the other specimens are so small and the structure so open that diffusion has destroyed the record. In other studies now in progress we have found that a chalky belemnite—*i.e.*, one that has lost its translucent character—agrees in isotopic composition with its surrounding chalk.

TABLE 5.—BELEMNITES, OYSTERS, AND BRACHIOPODS FROM UPPER CRETACEOUS CHALK

All the localities are in Hampshire except the *Ostrea lunata* zone, which comes from Trimingham. The numbers of the localities refer to *The Stratigraphy of the Chalk of Hants*, by R. M. Brydone, Publication Dulau, London 1912

	Zone		Rhynchonellids	Oysters	Belemnites
Senonian	UPPER CHALK	1. *Ostrea lunata*	Trimingham	Trimingham	Trimingham
			Group of "*Rh.*" *plicatilis* (J. Sowerby)	*Ostrea vesicularis* Lamarck	*Belemnitella mucronata*
			" 1153	1153	1145
		2. *Belemnitella mucronata*		*Ostrea semiplana* (J. de C. Sowerby)	*Belemnitella mucronata*
			" 1086	1153	1150
		3. *Actinocamax quadratus*		*Ostrea vesicularis* Lamarck	*Actinocamax quadratus*
			" 1046	1067	1040a
		4. *Offaster pilula*		*Ostrea incurva* Nilsson	*Actinocamax* sp.
			" 918	889	
		Offaster pilula 5. *Echinocorys scutata* var. *depressula*		*Ostrea canaliculata* (J. de C. Sowerby)	
			" 838	838	817
		6. *Marsupites testudinarius*		*Ostrea semiplana* (J. de C. Sowerby)	*Actinocamax* sp.
		7. *Uintacrinus westfalicus*		278	
		8. *Micraster coranguinum*	" 322	*Ostrea boucheroni* Coquand	295
				138	*Actinocamax* sp.
		9. *Micraster cortestudinarium*	" 138	*Ostrea vesicularis* Lamarck	
		10. *Holaster planus*	" 116	116	
Turonian	MID-DLE CHALK	11. *Terebratulina lata*		" 116	
		12. *Inoceramus labiatus*	80		
			"*Rh.*" *cuvieri* d'Orbigny		
Cenomanian	LOWER CHALK	*Holaster subglobosus* 13. *Actinocamax plenus*		" 34	54
		14. *Schloenbachia varians*	21		*Actinocamax plenus*
			"*Rh.*" *mantelliana* (J. de C. Sowerby)		

TABLE 6.—THE QUANTITY $\delta(C^{13})$ FOR UPPER CRETACEOUS OF ENGLAND

Zone	Brachiopod		Oyster		Belemnite	
	Specimen	Chalk	Specimen	Chalk	Specimen	Chalk
1	1.3_9	0.9_4	0.7_9	0.7_1	0.4_8	1.6_4
2	2.8_3	1.8_7	2.6_0	1.5_5	2.1_1	1.3_9
3	2.5_8	1.6_1	1.8_0	1.7_6	1.1_2	1.3_2
4	2.9_0	—	2.2_6	1.7_2	0.9_2	—
5	2.4_0	1.8_0	1.6_8	1.1_9	—	—
6	2.3_2	1.6_7	1.8_7	1.6_7	1.8_5	—
7	—	—	—	—	—	—
8	—	1.5_8	1.6_7	1.5_2	—	—
9	1.5_2	0.7^5	2.0_9	1.0_4	—	—
10	1.9_7	1.1_7	1.3_0	0.9_0	—	—
11	—	—	1.2_2	1.2_2	—	—
12	—	—	—	—	—	—
13	—	—	2.8_4	2.8_1	3.2_0	—

Some specimens of Table 5 were not used because of bad preservation.

constant composition had been reached, all the analyses should be identical, and thus we conclude that this is not the case.[5]

The oxygen analyses for the Danish specimens together with derived temperatures are given in Table 8. The specimens are numbered as given previously.

Upper Cretaceous paleotemperature data for North America were secured from the *Exogyra costata* zone of a number of widely scattered outcrops of the Gulf Coast and Eastern Seaboard of the United States between western Tennessee and northeastern Mississippi northeastward to New Jersey.[6] The specimens from Tennessee were derived from the sandy marls of the basal third of the exposure on Dave Weeks' place, 3½ miles south of Enville, McNair County, the type locality of the Coon Creek tongue of the Ripley formation (Wade,

TABLE 7.—THE QUANTITY $\delta(O^{18})$ FOR UPPER CRETACEOUS OF ENGLAND

Zone	Brachiopod		Oyster		Belemnites		Belemnite Temperature
	Specimen	Chalk	Specimen	Chalk	Specimen	Chalk	
							°C
1	-1.4_8	-2.3_9	-1.8_5	-2.2_6	-0.5_5	-1.8_9	$15._0$
2	-1.9_3	-2.9_0	-2.6_9	-2.9_2	-0.4_2	-2.5_2	$14._4$
3	-2.4_0	-2.4_6	-2.9_9	-2.6_6	-1.2_4	-3.8_5	$19._2$
4	-1.9_5	—	-1.9_1	-2.6_0	-1.2_6	—	$19._3$
5	-2.4_3	-2.2_0	-2.7_3	-2.7_4	—	—	
6	-2.1_0	-2.4_6	-2.4_4	-2.5_6	-2.0_3	—	$23._8$
7	—	—	—	—	—	—	
8	—	-2.6_8	-2.8_9	-2.3_5	—	—	
9	-2.8_3	-2.9_4	-2.0_2	-2.5_9	—	—	
10	-2.6_0	-2.4_7	-3.6_8	-2.7_5	—	—	
11	—	—	-3.6_2	-3.1_6	—	—	
12	—	—	—	—	—	—	
13	—	—	-1.8_9	-3.5_4	-0.4_0	—	$14._2$
14	—	—	—	—	—	—	

Present-day specimens show marked variation in C^{13} concentrations even when they grew in the same region at the same time. Thus the samples considered here should have had identical or nearly identical O^{18} concentrations, but not identical C^{13} concentrations when first buried. If both the oxygen and carbon concentrations changed with time we would expect that the oxygen concentrations would tend to change by comparable amounts, and hence remain somewhat the same as observed. On the other hand the carbon concentrations should show no such approximate agreement. If complete equilibrium with water and carbon of

1926). Though belemnites do not occur in these deposits, depriving us of our reliable standard

[5] We have analyzed a few samples of ooze from the Pacific and Atlantic Oceans in co-operation with W. F. Libby and J. R. Arnold, who are working on C^{14} concentrations in such materials. We are unable to interpret the results in any consistent way as yet, and evidently more data are required.

[6] The specimens from Western Tennessee, Mississippi, North Carolina, and South Carolina were collected by H. C. Urey and H. A. Lowenstam. We are indebted to Dr. L. W. Stephenson for advising us on certain collecting localities in South Carolina, to Dr. Horace C. Richards who guided us to the New Jersey outcrops, and to Mr. P. A. Bethany of Macon, Mississippi, who advised us on and collected with us from the outcrops of the Macon area.

for comparison, the excellent shell preservation of all the molluscan elements with originally aragonitic shells, elsewhere in the outcrop areas preserved only as casts, implied exceptionally favorable burial conditions suggestive of preservation of original isotopic abundances. The specimens analyzed from northeastern Mississippi were secured from the Prairie Bluff Chalk, at two localities, the glades on the Vanny Jackson farm west of the Rocky Hill Church road, 3.6 miles north-northeast of Starkville, Octibbeha County, which is the general area of fossil locality 6846 of Stephenson and Monroe (1940), and from glades on the A. Lindley farm 4 miles southwest of Macon, Noxubee County (Stephenson and Monroe's 1940 collecting locality 17242, 17484). At both localities, the specimens were found loose in the residual fossil concentrations which littered the glades, since Prairie Bluff specimens satisfactorily preserved and located *in situ* were unavailable. The positions marked 10 feet and 13 feet above the base of the Prairie Bluff formation in Table 9 for the specimens from the Lindley locality refer to collecting levels on the glade and not to stratigraphic positions. Despite the rich assemblages in the glade concentrations, only originally pure calcitic skeletal forms on the calcitic layer of calcite and aragonitic interlayered shells are preserved as such, reducing the number of potential elements for paleotemperature determinations to crinoidal remains, echinoids, *Terebratulina floridana*, Ostreidae, and Pectinidae among the pelecypods and guards of *Belemnitella americana*, the balance consisting of molds, prevalently in phosphatic form. Shark teeth occur with the invertebrate assemblages composed of carbonate skeletons and furnish source material for a possible future check of the carbonate thermometer by the phosphate thermometer.

The South Carolina specimens were secured *in situ* from the basal section of the Peedee formation which is well exposed in the west bank of the Peedee River at Burches Ferry, 15½ miles from Florence. This is the locality from which Stephenson (1923) described and figured a number of well-preserved specimens of *Belemnitella americana* and described a new species. At the time of our visit, the river was low enough to expose a total of 13½ feet of Peedee strata, consisting of calcareous, argillaceous, glauconitic sand above 3½ feet of the shales of the Black Creek formation. *Belemnitella americana* was found in small numbers through the entire local Peedee section; it was concentrated in conspicuous numbers in a narrow 9-inch zone, 57 inches above the base of the formation.

TABLE 8.—OXYGEN ISOTOPIC ANALYSES AND TEMPERATURES OF THE DANISH BELEMNITES

Specimen	$\delta(O^{18})$	t°C
1	-0.1_7	$12._8$
2	-0.4_3	$14._3$
3	-0.0_9	$12._3$

The *Belemnitella* guards are throughout oriented more or less horizontally, with occasional deviations ranging up to about 10° from the horizontal plane. Within the horizontal plane the belemnite rostra display random orientation as far as could be ascertained in the vertical exposure. *Exogyra costata* occurs sparingly distributed through the basal 7½ feet of the section, the individuals being generally small and thin shelled. Larger, but comparatively fragile individuals are abundant in the overlying 22 inches of the section which is conspicuously fossiliferous, consisting of a semicoquina of pelecypod shell debris. The specimens analyzed were taken *in situ*.

The North Carolina specimens were collected from a 6-inch calcareous sandstone ledge of the Peedee formation, exposed above water level, and 6 inches of soft marl below water level at the Jackson's Hole Landing, locality of Stephenson (1923, p. 25), Northeast Cape Fear River. A number of large, heavy-shelled *Exogyra costata* individuals, with strongly resorbed surfaces, and a single rostrum of *Belemnitella americana*, were secured *in situ* from the water-covered marly layer, which contrasts strongly with the rich mollusk assemblages of overlying calcareous sandstone ledge. Pectinidae and *Belemnitella americana*, originally calcitic skeletal types alone are well preserved; the originally aragonitic shells of the associated pelecypods is often represented by casts and molds. As the Peedee section lacks top and bottom it is not possible to determine the stratigraphic position of this section within the formational range.

TABLE 9.—OXYGEN ISOTOPIC ANALYSES AND TEMPERATURES FROM *Belemnitella americana* FROM THE SOUTHEASTERN UNITED STATES

Formation	Locality	Level	Analysis	Temp.	Av. Temp.
Prairie Bluff	Starkville, Miss. 3.6 miles N-NE. on Rocky Hill Church Road	Unknown	(1) -0.5_2	14.9	
			(2) -0.9_7	17.6	
			(3) -1.2_3	19.1	
			(4) -1.0_9	18.2	
			(5) -0.1_1	12.5	16.4
	Macon, Miss. A. Lindley place 4 miles SW. of Macon	13 feet above base of Prairie Bluff	(1) 0.0_0	11.9	11.9
		10 feet above base of Prairie Bluff	(1) -1.0_3	17.9	
			(2) -0.7_5	16.2	
			(3) -0.5_1	14.9	
			(4) -1.4_9	20.6	17.9
Peedee	Peedee River, S. C.	105 inches above base of formation	(1) -0.5_1	14.9	14.9
		57 inches to 68 inches above base of formation	(1) -0.4_4	14.5	
			(2) -0.3_0	13.8	
			(3) -0.2_8	13.4	
			(4) -0.3_1	13.7	
			(5) -0.2_7	13.4	
			(6) -0.6_7	15.8	
			(7) -0.5_5	15.1	
			(8) -0.4_6	14.6	
			(9) -0.2_8	13.5	
			(10) -0.6_6	15.8	
			(11) -0.6_1	15.5	14.4
	Cape Fear River	Unknown	(1) -0.5_4	15.1	
			(2) -0.8_9	17.1	16.1
Navesink	Mullica Hill, N. J.	Base of formation	(1) -1.2_1	19.1	
			(2) -1.1_8	18.8	
			(3) -0.9_0	17.2	
			(4) -0.8_1	16.7	
			(5) -1.0_9	18.8	
			(6) -0.9_8	17.6	18.0
	Hornerstown, N. J.	Base of formation	(1) -0.8_7	17.0	
	Crosswicks Creek		(2) -0.5_2	15.0	
			(3) -0.4_9	14.8	
			(4) -0.7_5	16.3	
			(5) -0.8_0	16.6	
			(6) -0.8_0	16.6	
			(7) -0.3_9	14.2	
			(8) -0.6_2	15.5	16.0
	Cream Ridge	Unknown	(1) -0.5_9	15.4	
			(2) -0.7_0	16.0	15.7

The New Jersey specimens analyzed were secured from the Navesink marl at the well-known fossil locality in the hillside just south of the railroad trestle at Mullica Hill (Weller, 1907, locality 169), in the cut of a tributary of

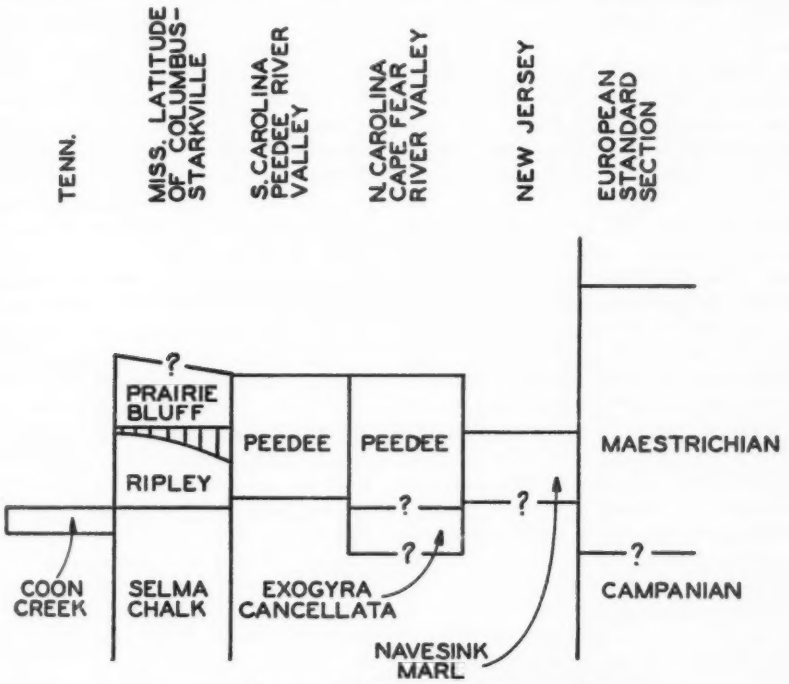

FIGURE 1.—CRETACEOUS SECTIONS FOR LOCALITIES STUDIED

Crosswicks Creek near Hornerstown, and from the dump piles of the abandoned "marl pit" on Edgar Schank's farm near Cream Ridge (Weller, 1907, locality 127). The Mullica Hill specimens were derived from a 4-inch shell bed, consisting of *Exogyra costata*, Pectinidae, and *Belemnitella americana* in a marly glauconitic sandy matrix about 12 feet above the base of the bluff exposure. The preservation of the pelecypods and belemnites is generally poor due to leaching and partial limonitic replacement, while conspecific forms occurring in shell beds, located 10 feet lower and about 3 feet higher up in the bluff section are represented only in the form of casts and molds. The Hornerstown specimens are derived from a shell bed, composed principally of *Exogyra costata*, *Gryphaea convexa*, and *Belemnitella americana*. The dense packing of the pelecypod shells with the randomly oriented, interwedged Belemnitellas indicates post mortem concentrations swept together in shallow agitated waters. Burial grounds foreign to the habitat are thus strongly implied for the Belemnitella element. According to Spengler and Peterson (1950), the shell beds mark the base of the Navesink member of the Monmouth formation, previously interpreted as a formation and group respectively. A basal position for the Mullica Hill and Hornerstown specimens in the Navesink is thus indicated, while the stratigraphic position of the Cream Ridge forms, secured loose from the dump piles, cannot be determined.

All the North American specimens included in the present study fall within the range of the *Exogyra costata* zone, as shown by the correlation of the formations from which they were derived (Fig. 1). In comparing the stratigraphic positions of the specimens secured from Tennes-

see, Mississippi, and South Carolina, and the Mullica Hill and Hornerstown localities in New Jersey within their respective formations and in relation to the formational ranges and their correlation, it will be seen that the Coon Creek forms, from southwestern Tennessee, occupy a lower; those from the Peedee formation of South Carolina and from the Navesink localities of New Jersey an intermediate, and the Prairie Bluff forms from northeastern Mississippi a higher position within the zonal range. Their stratigraphic relations to the North Carolina and Cream Ridge locality of New Jersey cannot be determined because of the unknown stratigraphic positions of the latter within their respective formations. To judge from the narrow range of the Navesink marl, the New Jersey specimens may be anywhere between the top of the Coon Creek formation of southwestern Tennessee and the base of the Prairie Bluff chalk in northeastern Mississippi, those from the Peedee formation of North Carolina a considerably wider interval.

The North American forms serve for an initial survey of the special paleotemperature range within the time interval occupied by the *Exogyra costata* zone, even though in some cases our specimens came from different levels within that zone and in other cases the relationships within the zone are uncertain.

Discussion of the North American Temperatures

The *Exogyra costata* zone is correlated with the Maestrichian of the European standard section (Stephenson and Reeside, 1938, p. 1637; Stephenson *et al.*, 1942, Chart No. 9). *Belemnitella mucronata* which occupies in the Upper Senonian of northern and central Europe a stratigraphic position similar to *Belemnitella americana* in southeastern North America, has been considered closely related to the North American species (Stephenson, 1923, p. 56). Approximate time equivalency of their enclosing strata is further indicated by other faunal and floral similarities. Keeping in mind the as-yet existing uncertainties in intercontinental correlation, particularly with reference to details in time equivalency and length of time intervals, it is nevertheless permissible to compare in general terms the Maestrichian paleotemperature data from both sides of the Atlantic that is, of the Gulf Coastal area in North America and of southern England and Denmark in northwestern Europe. There is surprisingly little difference in the temperatures recorded by the reliable forms from either side of the Atlantic despite the latitudinal range of the collecting localities, which extend from 33° to about 41°N. in North America to between about 52° and 56°N. in England and Denmark.

In surveying the meaning of the temperature records only those of the belemnites can be at present considered reliable. As the temperatures recorded constitute at best mean temperatures of skeletal growth periods, they do not necessarily represent annual mean temperatures of the waters in which they lived. This is clearly indicated by the temperature range recorded by the shell of a recent *Chama macerophylla* from the Bermuda inshore waters, which has been analyzed for seasonal effects. Shell material is laid down only after the surface waters reach 24°C and extends through the warm part of the year, which reaches a maximum at 29°C, while the yearly temperature range of the inshore waters covers a range from 18°C to 29°C. The mean temperature of 26½°C recorded by the *Chama mazerophylla* shell is thus 2½°C higher than that of the waters. Organisms with a narrow temperature range for skeletal growth, particularly with a growth period largely off the average with reference to the yearly range of their waters, would constitute unreliable data for climatic records unless forms from identical habitat with wider or overlapping skeletal growth periods are available for comparison. The *Inoceramus* lineage now under investigation may furnish a comparative element for correction at a future date.

Returning to the belemnites, preference for cooler waters is strongly implied by their geographic distribution. Dacqué (1915, p. 423–426), in discussing the paleoclimatology of the Cretaceous, pointed out that broad climatic zoning is introduced in the beginning of the Cretaceous and becomes sharply established by *Upper* Cretaceous time. Differentiation into a boreal and Mediterranean-aquaetorial zones is fairly well documented, the aquaetorial zone being characterized by prominent carbonate sediments, reef-forming corals and rudistids,

large Foraminifera, and heavy-shelled Nerineidae and actaeonellids. Most convincing is the appearance of dwarfed and crippled rudistids in the bordering boreal zones both to the north and south, as shown by Dacqué's distribution map for the rudistids. *Belemnitella* was shown to be confined to the northern boreal zone of the Upper Cretaceous seas. In comparing the size ranges of the collections of *Belemnitella americana* secured from the various localities of the Gulf Coastal area, an increase in maximum sizes attained is clearly noticeable from Mississippi northeastward to New Jersey. The Mississippi localities were apparently located in the southern border area, as Stephenson and Monroe record representatives of the rudistid genus *Durania* from the *Exogyra cancellata* subzone of the upper Selma Chalk in which *Belemnitella americana* makes its first appearance.

The northeastward trend of increasing sizes in *Belemnitella americana* could be correlated with cooler water preference, but their mean temperature records do not seem to support this view. Refinement in the sampling procedure contemplated for studies of seasonal variations may decide this question. Throughout our discussion we have neglected the possibility and even probability of some variation of the isotopic composition of the waters, and this may explain the nearly identical temperatures of the Carolina and Mississippi region as contrasted to New Jersey.

The depth range is another factor yet to be considered in the evaluation of the temperatures recorded by nectonic elements such as belemnites. The sediment character and the burial assemblages of the American representatives in the locations examined indicate that, though the bottoms were largely below effective wave base (except for New Jersey examples, which occur in wave concentrated shell beds), the abundant and varied mollusk forms point to comparatively shallow bottoms, well within the euphotic zone. This agrees with Naef's (1922) conclusions of prevalent shallow-water habitat for the belemnites in general as implied by functional morphology. Thus the temperature variation should be characteristic of a limited depth range. That *Belemnitella* lived in shallow cooler waters is further indicated by the absence of stray individuals in the southern Tethys waters.

The narrow gradient indicated by the mean temperatures of the Belemnitellas across the latitudinal width from Mississippi to Denmark is surprising. Unless the temperature tolerance of skeletal growth of the European and American species happens to coincide, rather uniform climatic conditions are suggested over most of the boreal zone during the Maestrichian. Gradual lowering of the temperatures through Upper Cretaceous time toward the Maestrichian are indicated in England and agree with the establishing of the climatic zones noted by Dacqué. Increased mixing of the oceans due to stronger current development should have resulted. North America and South America were probably separated by the circumequatorial Tethys, and the waters from the pole area previously connected with it via the western interior strait became separated at about the critical time that the lowering of the late Cretaceous temperatures is indicated to have taken place. Free mixing of the northern waters due to lack of the present existing north-south land barriers should have tended to equalize the temperatures toward the pole. Subtropical climatic conditions could have thus been maintained on the northern land masses where the dinosaurs continued to flourish.

Cowles (1939; 1940; 1945) has suggested extinction of the dinosaurs at the closing interval of the Cretaceous due to increased temperatures. On the other hand continued lowering of the temperatures as suggested by the English downward trend would have equally caused their extinction. We do not wish to emphasize this apparent downward trend since our temperatures depend on single samples in each zone and our experience indicates that a variation between a number of specimens of the same locality of as much as 5°C is possible. The investigation of more specimens from these zones and seasonal variations of such specimens may enable us to reach a definite conclusion. Longitudinal paleotemperature traverses for the entire Upper Cretaceous extending into early Tertiary, based on a large number of associated faunal elements and including benthonic forms should furnish a clearer trend of paleoclimatologic conditions as well as aid in quantitatively evaluating the temperature niches of the marine organisms.

References Cited

Colbert, E. H., Cowles, R. B., and Bogert, C. M. (1946) *Temperature tolerances in the American alligator and their bearing on the habits, evolution, and extinction of the dinosaurs*, Am. Mus. Nat. Hist., Bull., vol. 86, p. 333–373.

Cowles, R. B. (1939) *Possible implications of reptilian thermal tolerance*, Science, vol. 90, p. 465–466.

—— (1940) *Additional implications of reptilian sensitivity to high temperature*, Am. Nat., vol. 75, p. 542–561.

—— (1945) *Heat-induced sterility and its possible bearing on evolution*, Am. Nat., vol. 79, p. 160–175.

Curie, P. (1889) *Recherches sur le Pouvoir inducteur spécifique et le conductibilité des corps cristallisés*, Ann. Chim. Phys., vol. 17, p. 385.

Dacqué, E. (1915) *Grundlagen und Methoden der Palaeogeographie*, Gustav Fischer, Jena.

Dole, M. (1935) *Relative atomic weights of oxygen in water and air*, Am. Chem. Soc., Jour., vol. 57, p. 2731.

—— (1936) *Relative atomic weights of oxygen in water and air. Discussion of the atmospheric distribution of the oxygen isotopes and of the chemical standard of atomic weights*, Chem. Phys., Jour., vol. 4, p. 268.

—— (1949) *The history of oxygen*, Science, vol. 109, p. 77–81.

Epstein, S., Buchsbaum, R., Lowenstam, H. A., and Urey, H. C. (1951) *Carbonate-water isotopic temperature scale*, Geol. Soc. Am., Bull., vol. 62, p. 417–425.

Goldschmidt, V. M. (1933) *Grundlagen der quantitativen Geochemie*, Fortschritte Mineral., Kristal., Petrog. vol. 17, p. 112.

Joffe, A. (1923) *Elektrizitätsdurchgang durch Krystalle*, Ann. Phys., vol. 72, p. 461.

McCrea, J. M. (1949; 1950) *Isotopic chemistry of carbonates and paleotemperature*, Doctoral Dissertation, Univ. Chicago; Chem. Phys., Jour., vol. 18, p. 849 (1950).

Murphey, B. F., and Nier, A. O. C. (1941) *Variations in the relative abundance of the carbon isotopes*, Phys. Rev., vol. 59, p. 771.

Naef, A. (1922) *Die fossilen Tintenfische*, Gustav Fischer, Jena, p. 322.

Nier, A. O. C., and Gulbranson, E. A. (1939) *Variations in the relative abundance of the carbon isotopes*. Am. Chem. Soc., Jour., vol. 61, p. 697.

Spengler, W. B., and Peterson, J. J. (1950) *Geology of Atlantic Coastal Plain in New Jersey, Delaware, Maryland and Virginia*, Am. Assoc. Petrol. Geol., Bull., vol. 34, p. 40.

Stephenson, L. W. (1923) *The Cretaceous formations of North Carolina*, N. C. Geol. Econ. Survey, vol. V, pt. I.

—— and Monroe, W. H. (1940) *Upper Cretaceous deposits*, Miss. Geol. Survey, Bull. 40, 296 pages.

—— Reeside, J. B., Jr. (1938) *Comparison of Upper Cretaceous deposits of Gulf region and Western Interior region*, Am. Assoc. Petrol. Geol., Bull., vol. 22, p. 1629–1638.

——*et al.* (1942) *Correlation of the outcropping Cretaceous formations of the Atlantic and Gulf Coastal Plain and Trans-Pecos Texas*, Geol. Soc. Am., Bull., vol. 53, p. 435–448.

Thode, H. G., MacNamara, J., and Collins, C. B. (1949) *Natural variations in the isotopic content of sulfur, and their significance*, Canad. Jour. Research, vol. 27, p. 361.

——, ——, Lossing, F. P., and Collins, C. B. (1948) *Natural variations in the isotopic content of boron and its chemical atomic weight*, Am. Chem. Soc., Jour., vol. 70, p. 3008.

Urey, H. C. (1947) *The thermodynamic properties of isotopic substances*, Jour. Chem. Soc., p. 562.

—— and Greiff, L. J. (1935) *Isotopic exchange equilibria*, Am. Chem. Soc., Jour., vol. 57, p. 321.

Wade, B. (1926) *The fauna of the Ripley formation on Coon Creek, Tenn.*, U. S. Geol. Survey, Prof. Paper 137.

Weller, S. (1907) *Cretaceous paleontology of New Jersey*, Geol. Survey N. J., vol. IV, Paleont. Ser.

Institute of Nuclear Studies, University of Chicago, Chicago, Ill.

Manuscript Received by the Secretary of the Society, March 7, 1950.

Project Grant 517/47/S48.

Addendum

It is necessary to consider the possible effect of the changed temperature scale mentioned in the Addendum of the preceding paper on the temperatures recorded here. Repetition of the analyses using the modified method of preparation and the corrected temperature scale on 10 specimens reported in this paper changed their measured temperatures by an average of 1.1°C with a spread of −0.6° to +2.2°C. The temperatures remain remarkably uniform though systematically higher by about 1°C.

BULLETIN OF THE GEOLOGICAL SOCIETY OF AMERICA
VOL. 62, PP. 417–426, 5 FIGS. APRIL 1951

CARBONATE-WATER ISOTOPIC TEMPERATURE SCALE

BY SAMUEL EPSTEIN, RALPH BUCHSBAUM, HEINZ LOWENSTAM, AND HAROLD C. UREY

ABSTRACT

A relationship between temperature and relative O^{18} abundance in calcium carbonate in marine shells has been determined. If the relative O^{18} abundance of the water in which the shell grew is known, the temperature can be determined to an accuracy of $\pm 1.0°C$. The relative O^{18} contents of marine waters increase with salinity and, in the case of surface marine waters, with salinity and temperature.

CONTENTS

	Page
Introduction	417
Acknowledgments	417
Relative O^{18} contents of marine waters	418
Isotopic temperature scale	420
Marine shells selected and their growth temperatures	420
Extraction of carbon dioxide from marine shells, the problem of impurities, and results	422
Discussion	424
Conclusions	425
References cited	425
Addendum	425

ILLUSTRATIONS

Figure	Page
1. Plot of salinity vs. O^{18} content for ocean water	419
2. Plot of salinity vs. O^{18} content for surface ocean waters	419
3. Plot of temperature vs. O^{18} content for surface ocean waters	419
4. Plot of O^{18} concentration vs. temperature: calcium carbonate samples without heat treatment	423
5. Plot of O^{18} concentration vs. temperature; calcium carbonate samples with heat treatment	424

INTRODUCTION

Urey *et al.* (1951) discuss a method for measuring paleotemperatures that depends on a variation in the oxygen −18 abundances in calcium carbonate deposited in the sea. McCrea (1949; 1950, p. 849) investigated the isotopic composition of calcium carbonate precipitated inorganically from water and determined the temperature coefficient for the abundance of O^{18} in calcium carbonate relative to water as a function of temperature; he found a value of −5.4°C permil increase in the ratio of O^{18} to O^{16} in the calcium carbonate. McCrea gave a calculation for this quantity including estimates of the effect of the translational and hindered rotational degrees of freedom in the solid state on the distribution functions, and arrived at a value of 5.1. Assuming free rotation in the solid state Urey (1947, p. 562) calculated a value of −5.7 for the same quantity. This research aims to determine this quantity and to set up an equation relating temperature to the difference in isotopic composition of samples of carbon dioxide prepared from organically precipitated calcium carbonate and an arbitrarily selected reference sample of carbon dioxide.

The relationships between temperature and O^{18} abundance in calcium carbonate from marine shells and that from inorganic calcium carbonate precipitates are similar. But a number of special considerations must be taken into account in the case of marine shells to find the temperature of the sea water in which the marine animals lived: (1) the isotopic composition of the oxygen of the oceans; (2) the collection of marine shell-bearing animals which grow in water of constant and known temperatures; and (3) the problem of impurities in the carbon dioxide prepared from marine shells.

ACKNOWLEDGMENTS

We are indebted to The Geological Society of America and to the American Petroleum In-

stitute for grants which have made this work possible, and we wish to extend our most sincere thanks for this help. During recent months the work has also been supported under Task Order XXVIII, Contract N6ori-20 of the Office of Naval Research.

Relative O^{18} Contents of Marine Waters

Since the ratios of vapor pressures of H_2O^{16} to H_2O^{18} are 1.008 and 1.011 at 25°C and 0°C respectively (Riesenfeld and Chang, 1936, p. 127), evaporation and condensation continuously change the O^{18} contents of bodies of water. The magnitude of the variation of O^{18} in the oceans is important to the determination of a valid temperature scale and to the general problem of the determination of temperature of unknown samples, because this thermometer depends essentially on the magnitude of the difference between the O^{18} contents of the calcium carbonate and the water in which it was precipitated. Consequently a series of O^{18} determinations were made on samples of sea water, most of which were made available to us by H. Pettersson, who collected them on the Albatross expedition (1949, p. 182). The method of determining the relative O^{18} content of water samples involves the equilibration of carbon dioxide with the water at 25°C and analysis of an aliquot of the gas. The carbon dioxide so equilibrated is compared with our standard working sample of carbon dioxide prepared from the calcium carbonate of belemnites of the Peedee formation using a high-precision mass spectrometer (McKinney, McCrea, Epstein, Allen, and Urey, 1950). The analyses are relative only, but are correct within a probable error of about 0.2‰ of the isotope ratio. The results of these analyses are given in Table 1. The unit used in this table is defined by the following equation:

$$\delta(O^{18}) = \left(\frac{R_{sample}}{R_{standard}} - 1\right) 1000,$$

where R_{sample} and $R_{standard}$ are the ratios of $CO^{16}O^{18}$ to CO_2^{16} for the sample and standard reference gas, respectively.

Apparently, the isotopic composition of oxygen is not homogeneous throughout the oceans. Deviations from the mean isotopic composition of the oceans occur in the waters close to the mouth of a river, as is the case for the President Channel location. If water of fully marine composition is considered, then the maximum variation of O^{18} in ocean water is 1.7‰, which would represent about 10°C variation in temperature determination. Clearly, it is necessary to determine the O^{18} content of the water in which a marine shell grew if this particular shell is to be used in correlation of temperature with the O^{18} content of organically precipitated shell.

Table 1.—Relative O^{18} Content of Marine Waters

Location	Depth of point of collection (Meters)	Temperature (°C)	Salinity (‰)	$\delta(O^{18})$ (‰)
30°47′N. 25°25′W.	10	—	37.44	−0.0$_1$
	1000	—	35.43	−0.5$_9$
26°25′N. 34°00′W.	5000	—	34.9	−0.2$_1$
14°27′N. 66°13′W.	5000	4.2	34.9	−0.7$_4$
14°15′N. 71°02′W.	0	27.7	36.0	0.4$_2$
02°52′S. 88°20′W.	20	18.8	34.4	−0.3$_4$
	500	7.5	34.6	−0.5$_9$
	1000	4.5	34.6	−0.5$_6$
13°25′S. 149°30′W.	0	27.7	35.8	−0.2$_9$
	1000	4.3	34.6	−0.9$_3$
	4000	1.4	34.7	−0.6$_8$
07°45′S. 120°30′E.	10	29.5	34.5	0.5$_7$
10°06′N. 52°45′E.	20	29.3	35.5	0.0$_8$
	500	10.7	35.0	−0.2$_6$
	2000	2.9	34.8	−0.9$_0$
35°41′N. 21°50′E.	50	16.5	38.8	0.6$_9$
	2000	13.6	38.7	0.8$_4$
00°13′S. 18°26′W.	25	22.6	35.6	0.0$_4$
	500	7.1	34.7	−0.5$_0$
	2500	3.0	34.9	−0.3$_8$
	7500	1.4	34.8	−0.4$_4$
28°05′N. 60°49′W.	25	28.5	36.8	0.3$_8$
	500	16.3	36.3	−0.1$_8$
	2000	3.7	35.0	−0.5$_9$
43°04′N. 19°40′W.	2000	3.6	35.0	−0.6$_7$
President Channel, Puget Sound	171	9.4	31.4	−1.9$_4$
Middle Channel, Puget Sound	157	7.4	33.1	−0.9$_1$
Encenada, Mexico	~0	19	33.5	−0.8$_1$
St. Tomas, Mexico	~0	15	33	−0.7$_7$
Monterey Bay, California	~0	11	33.8	−0.8$_3$
La Jolla, California	~0	15	34.0	−0.7$_4$
Bermuda	~0	18–29	—	0.6$_4$

On further examination of the data an attempt was made to establish a correlation between the O^{18} content and the salinity of the water. Such a correlation is possible because processes which tend to increase or decrease the O^{18} of the water also tend to increase

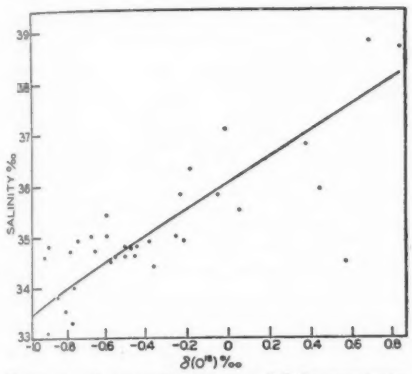

FIGURE 1.—PLOT OF SALINITY VS. O^{18} CONTENT FOR OCEAN WATERS

the salinity. The plot of salinity against relative O^{18} content is shown in Figure 1. The points scatter badly, but a regular trend is evident, and a straight-line relationship is assumed between salinity and O^{18} content of the water. The relationship is only approximate as was to be expected. Extrapolation of the line to zero salinity gives $-13.5‰$ as the relative O^{18} content of fresh water.

The approximate linear relationship between salinity and O^{18} abundances suggests that it might be more rigorously followed if limited to surface waters. Since surface salinity and surface temperature show some indication of being related linearly, we have plotted in Figures 2 and 3 salinity vs. O^{18} content and temperature vs. O^{18} content respectively for the waters of Table 1 coming from a depth of 25 meters or less. The plots indicate rather definite linear relations, but the data are too meager to justify any definite conclusion. We shall continue this investigation as we secure more water samples, particularly from higher latitudes.

The mean isotopic composition of the oceans will be close to that of the water of mean salinity, and we have selected this as having $-0.47‰$ relative to our standard gas and

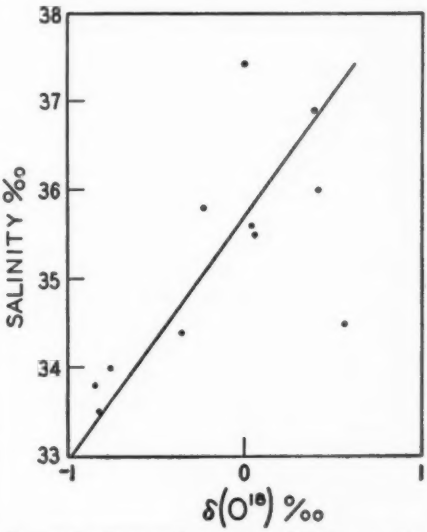

FIGURE 2.—PLOT OF SALINITY VS. O^{18} CONTENT FOR SURFACE OCEAN WATERS

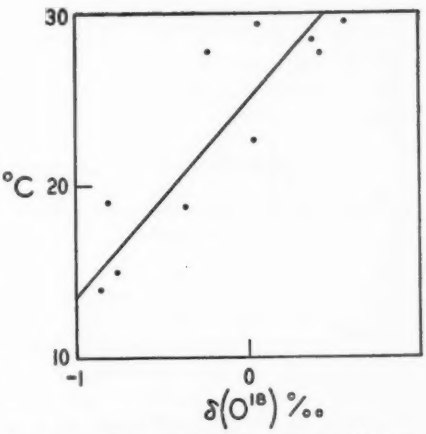

FIGURE 3.—PLOT OF TEMPERATURE VS. O^{18} CONTENT FOR SURFACE OCEAN WATERS

corresponding to $34.8‰$ salinity. This gives $-13.0‰$ as the isotopic composition of fresh water relative to that of sea water of $34.8‰$ mean salinity. This difference is larger than that expected for a fractionation equal to the ratio of vapor pressures, and substantially greater than that for any fresh-water samples investigated by us. Lake Michigan is representative and

analyzes as $-6.2‰$ relative to our mean sea water.

This large variation of isotopic composition of sea water decreases the reliability of temperature measurements by this method unless a sample of water is analyzed at the same time and a correction for the isotopic composition of the water is made on the carbon dioxide analyses. This error, some 2.5 times as large as expected, is disappointing, especially when paleotemperatures are considered. The melting ice of high latitudes must have a lower O^{18} content than has fresh water of the temperate zone. The whole problem of water evaporation from the oceans and its precipitation over the land and oceans is very complex, and our data are not sufficiently extensive to justify a more detailed discussion.

A correlation between salinity and O^{18} content is useful in that salinity data which are quite readily available for present-day oceans can give an approximate correction for the isotopic abundance if water samples are not available for mass spectrometric analyses. We hope the distribution of O^{18} between phosphate and water will give another thermometer with a different temperature coefficient, thus making possible the elimination of the water phase.[1]

Isotopic Temperature Scale

Marine Shells Selected and their Growth Temperatures

One problem in establishing a temperature scale using marine calcareous-shelled animals was to get shells which grew at known temperatures. To grow certain marine animals under controlled temperatures in the laboratory is a lengthy and difficult project. Nevertheless, constant-temperature baths were set up at three Pacific Coast marine laboratories,[2] and these were stocked with calcareous organisms with notched or drilled shells. It was thought that if repair occurred, the new shell, when analyzed, would yield reliable data which could be used to fix points on the temperature scale. Not all of the material is in, and some of the attempts were unsuccessful. However one of the experimental batches of animals has been analyzed and the results are presented later. Consequently, shell-bearing marine animals were collected from locations which have a minimum annual variation of temperature. The species of animals chosen were attached or sedentary forms which live in relatively confined areas so that the point at which collection was made would be representative of the condition under which the animals grew their shells. Animals were collected from marine locations which had records of maximum constancy and which had a minimum of contamination with freshwater drainage. Collections were made in the cooler waters of Puget Sound, intermediate conditions of Monterey Bay, and the warmer waters of certain areas along the coast of lower California in Mexico. In addition, shells from the still warmer waters of Bermuda were analyzed.

Particular care was taken to estimate carefully the temperature at which the particular fragment of shell used for analyses grew. For example, the samples analyzed from Santa Tomas, Mexico, included one large red abalone, *Haliotis rufescens*, and one large black abalone, *Haliotis cracherodii*, and two keyhole limpets, *Fissurella volcano*. The *Haliotis* were collected August 25, 1949, and thus the outer few millimeters of the rim of the shell grew within the months May to August. Dr. C. L. Hubbs measured temperatures at several stations in this region during September 1948, May, July, and August 1949, and also observed the daily variation on August 18, 1949. From these measurements we conclude that 15°C is a reasonable average temperature. The variations in temperature during these months is about the same as the daily variation from 14.4°C to 17.0°C. Thus a probable error of ±1°C seems a reasonable estimate. A complete cross section of the shell of the keyhole limpets was taken so that it was necessary to estimate the average annual temperature. The temperature in this location goes as low as 11°C and as high

[1] M. Steinberg is developing this possibility in our laboratory.

[2] Oceanographic Laboratory, University of Washington, Friday Harbor, Washington. We are indebted to Dr. Thomas G. Thompson and Dr. Emery Swan for assisting in this work, and also to Dr. C. Barnes for help in locating suitable areas for collecting. At the Hopkins Marine Station we are indebted to Dr. Rolf Bolin for help in looking after one of the experimental tanks. At Scripps Institution of Oceanograph, La Jolla, California, we are indebted to Dr. Carl Hubbs who assisted us in setting up one of the experimental tanks and in making collections in lower California.

TABLE 2.—DESCRIPTION OF SHELL SAMPLES USED FOR DETERMINATION OF TEMPERATURE SCALE

Location	Specimen No.	Specimen Name	Part of specimen used	Est. Temp. °C	Water analysis
Middle Channel, Puget Sound 48°22′30″N., 122°58′45″W., 130–157 meters, July 22, 1949.	1	Mussel *Volsella modiolus*	Cross section of complete half shell	7.4	-0.9_1
	2	Brachiopod *Terebratulina transversa*	Complete half shell		
President Channel, Puget Sound 48°41′50″N., 122°59′30″W., 171 meters July 16, 1949	3	Mussel *Volsella modiolus*	Cross section of complete half shell	9.4	-1.9_4
	4	Brachiopod *Terebratulina transversa*	Cross section of complete half shell		
Hopkins Marine Station, Pacific Grove, Calif.	5	Red abalone *Haliotis rufescens*. At low tide level May 14, 1949	At least a year's growth of shell	12.6	-0.8_8
	6	Giant keyhole limpet *Megathura crenulata* 50 m. off-shore, 3 m. Aug. 15, 1949	Cross section of complete shell	11.5	
Santa Tomas, Lower California, Mexico Aug. 27, 1949 3–6 meters	7	Red abalone *Haliotis rufescens*	Last ½ cm of large shell	15	-0.7_7
	8	Black abalone *Haliotis cracherodii*	Last ½ cm of large shell	15	
	9 10	Limpets *Fissurella volcano*	Cross section of 2 complete shells	14	
Between Encenada and Morro Points, Lower California, Mexico. 3 meters, Aug. 25, 1949	11	Red abalone *Haliotis rufescens*	Edge of shell	20	-0.8_1
Bermuda, Tank in laboratory	12	Snail (conch) *Strombus gigas*	Regenerated shell	31	0.6_4
	13	Bivalve, *Pinna* sp.	Regenerated shell (part)	29	

as 17°C. The average temperature of this sample of the shell was thus estimated to be 14°C within an error of less than 3°C and perhaps as close as ±1°C. Similar considerations of temperature data made available to us led to the assignment of other temperatures, and similar uncertainties exist in the estimate.

Table 2 describes the location at which the marine animals were found, the estimated temperature of the fragment of shell used for analyses, and the relative O^{18} of the water collected with the sample.

The carbon dioxide was prepared from the marine shells by reacting the calcium carbonate with approximately 100 per cent ortho phosphoric acid in an evacuated vessel. The carbon dioxide was trapped in a liquid nitrogen cooled trap and pumped free of the more volatile impurities, then passed through traps covered

by a solid CO_2-acetone bath to freeze out such less volatile impurities as water.

The samples of the shells described in Table 2 were then cleaned of obvious impurities and isotopes of the calcium carbonate during their deposition in their complex shell structure. But not enough information has been obtained to justify this conclusion regarding these groups

TABLE 3.—ISOTOPIC ANALYSES OF ORGANIC CALCIUM CARBONATE SAMPLES

Each isotopic analysis is a mean of at least four sample preparations. The measurements were all within the accuracy of $\pm 0.2‰$.

Number of specimen (Table 2)	Observed Temp. °C	Analysis (No heat treatment)	Analysis (With heat reatment)	Water correction	Corrected analysis (No heat treatment)	Corrected analysis (With heat treatment)
1	7.4	1.4_3	0.3_8	0.4_4	1.8_7	0.8_9
2	7.4	1.3_4	0.1_3	0.4_4	1.7_8	0.5_7
3	9.4	0.5_4	-1.2_7	1.4_7	2.0_1	0.2_0
4	9.4	-0.2_1	-1.1_4	1.4_7	1.2_6	0.3_3
5	12.6	0.5_9	-0.5_1	0.3_8	0.8_8	-0.1_3
6	11.5	1.0_8	-0.3_1	0.3_8	1.4_5	0.0_7
7	15	0.9_2	-0.9_7	0.3_0	1.2_2	-0.6_7
8	15	0.9_5	-0.8_1	0.3_0	1.2_5	-0.5_1
9	14	0.6_0	-0.4_3	0.3_0	0.9_0	-0.1_3
10	14	0.4_6	-0.5_0	0.3_0	0.7_6	-0.2_0
11	20	0.2_7	-1.8_0	0.3_4	0.6_1	-1.4_6
12	31	-0.5_8	-2.2_7	-1.1_1	-1.6_9	-3.3_8
13	29	—	-1.7_8	-1.1_1	—	-2.8_9

the carbon dioxide prepared. Table 3 gives the results of analyses when this method of preparation of carbon dioxide is used. The specimen numbers correspond to those in Table 2. The results of the sixth column are plotted in Figure 4.

The data show a correlation between temperature at which the marine animals grew and the relative abundance of O^{18} in the carbon dioxide prepared from the shells. But the deviations from a linear or nearly linear relationship are much larger than the expected experimental error. The difference in analyses for shells collected simultaneously from the same location eliminated the possibility that the poor correlation between temperature and relative O^{18} content was due to incorrect estimation of the temperature at which the animals grew.

The possibility that the animals did not lay down their shells in equilibrium with the surrounding water seemed to be unlikely because the relative O^{18} contents of calcium carbonate showed a definite correlation with temperature. Some preliminary results obtained during the investigation indicate that perhaps the echinoderms and corals fractionate the oxygen of invertebrates. In any case, the shells here used in the determination of the temperature scale were those which are deposited external to the animals' soft parts.

Comparison of results of McCrea with those of Table 3 indicated that the possible errors in the present work were of the order of magnitude of $1‰$ of the mass 46 to mass 44 ratio. Since impurities of mass 46 present to the extent of three parts per million would introduce an error equivalent to $1‰$ in the ratio, the usual chemical methods for analysis of impurities would be impractical in this case. Therefore, the criterion for valid analyses became the consistent correlation between temperature at which the shells were laid down and the measured change in relative abundance of mass 46 in the carbon dioxide.

Extraction of Carbon Dioxide, Problems of Impurities, and Results

The method of collecting the ion currents in the mass spectrometer gave measurements of the abundance ratio of mass 46 to the sum of masses 43, 44, 45, and 47. Consequently,

although the ratio of mass 46 to mass 44 would be relatively insensitive to small concentrations of impurities of masses 43, 45, and 47, these had to be considered. Purification of samples

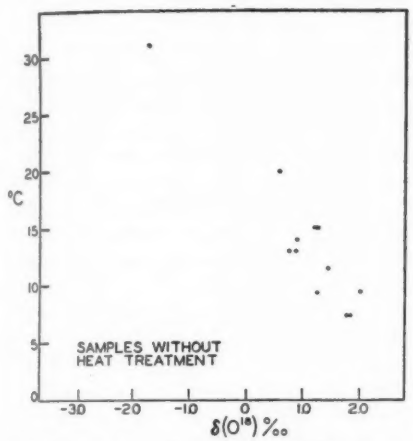

FIGURE 4.—PLOT OF O^{18} CONCENTRATION VS. TEMPERATURE: CALCIUM CARBONATE SAMPLES WITHOUT HEAT TREATMENT

could then either decrease or increase the value of the 46 to 44 ratio depending on whether purification eliminated impurities of mass 46 or of masses 43, 44, 45, and 47.

Many molecules or radicals formed in the ionizing chamber of the mass spectrometer, both organic and inorganic can contribute to the ions of mass 43 to 47. Some of these can be C_2H_5OH, CS, CH_3COOH, BCl, NO_2, N_2O, and propane. The first attempts were focussed on the possible impurities in the carbon dioxide gas. Several carbon dioxide samples from different marine shells were mixed with small volumes of bromine gas and irradiated by strong light, with the hope that bromination would shift the mass range of the impurities beyond the 43 to 47 range. Some samples of carbon dioxide were mixed with Van Slyke's (1940, p. 509) oxidizing solution or passed over hot CuO. Organic impurities would then be converted to carbon dioxide, and if present in trace amounts should not affect the 46 to 44 ratio of the carbon dioxide sample as a whole. Samples were also mixed with traces of ammonia and water to hydrolize compounds like boron trichloride, and passed over hot copper to reduce possible traces of nitrogen oxides.

In all these cases no appreciable effect on the isotopic analyses was observed.

Samples of carbon dioxide from the shells were also mixed with fluorine. Only where there was evidence of incomplete separation of the carbon dioxide and fluorine and subsequent contact with glass was there a change in O^{18} analysis. These changes were erratic for any one source of gas samples and varied from $-0.3‰$ to $-200‰$ of the 46 to 44 ratio. This was obviously due to SiF^+ of mass 47 adding to ion beam 44 and thus showing a decrease in the ratio of 46 to 44.

A more successful approach to the purification problem involved treatment of the powdered calcium carbonate before preparation of the carbon dioxide. The powder was heated at 400°C for 60 minutes with a slow stream of helium passing over the powder. The helium was first purified by passing it over copper oxide at 750°C and then through a liquid nitrogen cooled trap. With this treatment the relative O^{18} contents of the calcium carbonate from shells was decreased in most cases, and in a reproducible manner.

Experiments to determine the length of time necessary for heating the calcium carbonate powder to attain constancy of O^{18} analysis with further heating showed that heating at 400°C for 15–30 minutes was necessary to "purify" the samples tried. A safety factor of two was adopted, and the samples were heated for an hour. Since the equilibrium pressure of carbon dioxide over calcium carbonate is 10^{-6} atmospheres at 400°C, it was necessary to test this treatment for possible loss of carbon dioxide and fractionation of the oxygen isotopes. Two samples of calcium carbonate, one normal in O^{18} and the other enriched by $100‰$, were precipitated inorganically (using sodium carbonate and calcium chloride). Samples of each were analyzed without the heat treatment and with heat treatment. The analyses of each variety of calcium carbonate checked, showing that heat treatment did not change the analyses of such samples. Clearly, it was the organically precipitated calcium carbonate alone which was affected by the heat treatment. To shorten the time for the experiments the powdered

samples were heated for 15 minutes at 475°C with the attainment of the identical results observed for the longer heating times. We do not understand the mechanism of purification of the marine shell samples by the heating process. In most cases it is obvious that charring of organic matter occurs.

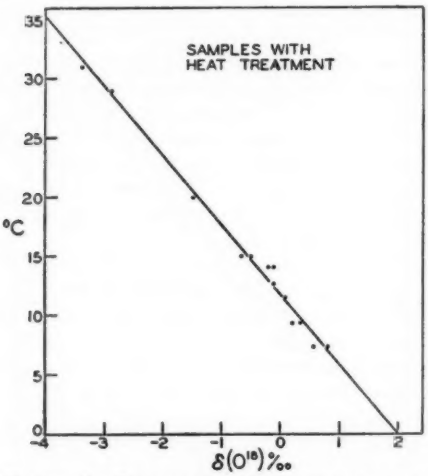

FIGURE 5.—PLOT OF O^{18} CONCENTRATIONS VS. TEMPERATURE: CALCIUM CARBONATE SAMPLES WITH HEAT TREATMENT

Calcium carbonate samples from specimens listed in Table 2 were heated before the carbon dioxide was prepared, and then analyzed. The results are given in Table 3, last column, and plotted in Figure 5.

Comparisons of Figures 4 and 5 indicate that the heat treatment of the organically precipitated calcium carbonate lowered the apparent O^{18} contents of the carbon dioxide prepared from all these samples. Apparently the marine shells contained variable amounts of some impurity, causing the inconsistency in the relationship between temperature and O^{18} content when unheated samples were used.

Least-squares calculations of the data for the heat-treated samples in Table 3 gave a straight-line relationship

$$t = 11.88 - 5.91\delta(O^{18}),$$

where t equals the temperature in °C, $\delta(O^{18})$ is the per mil difference between the ratios of masses 46 and 44 for the sample and standard gas. The constant 11.88 is characteristic of our standard gas, while the constant 5.91 should be independent of this gas.

DISCUSSION

Our constant, 5.91, for the slope of the curve differs from that secured by McCrea (5.4). The deviation is in the direction expected for incomplete equilibrium between solid calcium carbonate and dissolved carbonate ion as found by him. We do not believe this is the cause of the disagreement since a considerable variety of organisms all give analyses lying so closely on our curve.[3] The measurements of these small quantities are very difficult and, though we do not understand the reasons for the disagreement, it is only 10 per cent in the slope of the curve. Rather than regarding this as disagreement, we believe it shows that these living organisms approximate equilibrium conditions rather closely. Analyses at present are more reproducible than they were when McCrea completed his work, and this may have significance in regard to the discrepancy.

The possible effects of the difference in crystal structure of calcite and aragonite have not been explored. It is hardly to be expected that any large effects will be present, but, as our techniques improve, they should be investigated. Not only may the isotopic composition of aragonite and calcite crystals grown under similar conditions differ, but our heating procedure may convert aragonite to calcite and thus modify fractionation effects in the liberation of carbon dioxide by phosphoric acid.

The presence of a physiological effect in the case of certain groups of animals such as the echinoderms and corals, and plants such as a coralline algae, has seemed probable at some points in our work, but we do not feel it is certainly established. These specimens are difficult to investigate because of the large amounts of organic matter present, but, since we have established a rather secure basis for our work on the mollusks and brachiopods, it now seems feasible to investigate these groups. The echino-

[3] As this is written an analysis of a sample of regenerated shell from *Haliotis cracherodii* grown in a bath at a controlled temperature of 18.9 ± 0.1°C. shows agreement with our curve within 0.3°C.

derms and corals are not particularly useful in relation to the paleotemperature scale because of extensive infiltration of the fossils. The Foraminifera should be investigated for, even if not useful over long periods of time, they may be of interest for the investigation of more recent temperatures.

The variation of O^{18} content in marine and fresh waters, together with precise methods of measurement of the small quantities involved, makes possible an investigation of meteorological effects of considerable interest. The fractionation of the oxygen isotopes in evaporation and precipitation of water should give some information in regard to these processes as they occur in nature. We intend to continue our studies on the isotopic composition of water since the problem bears so directly on the measurements of paleotemperatures.

Conclusions

The variation in isotopic composition of marine waters is appreciable in terms of the isotopic temperature scale. When corrections are made for the isotopic composition of sea water in which mollusks and brachiopods have lived, a linear relationship between temperature and the O^{18} concentration exists. The slope of the curve agrees approximately with calculated values and with that secured when inorganically precipitated calcium carbonate samples crystallized at known temperatures are used. Organically precipitated calcium carbonate gives reproducible analyses if it is first heated to 475°C for 15 minutes and then reacted with phosphoric acid to prepare carbon dioxide, the gas used in the mass spectrometer.

References Cited

McCrea, J. M. (1949; 1950) *Isotopic chemistry of carbonates and paleotemperature*, Doctoral Dissertation, Univ. Chicago; Chem. Phys., Jour. vol. 18, p. 849 (1950).

McKinney, C. R., McCrea, J. M., Epstein, S., Allen, H. A., and Urey, H. C. (1950) *Improvements in mass spectrometers for the measurement of small differences in isotope abundance ratios*, Rev. Sci. Inst., vol. 21, p. 724.

Pettersson, H. (1949) *The floor of the ocean*, Endeavor, vol. 8, p. 182.

Riesenfeld, E. H., and Chang, T. L. (1936) *Vapor pressure, boiling point, and heat of vaporization of HDO and H_2O^{18}*, Z. Phys. Chem., vol. B33, p. 127.

Urey, H. C. (1947) *The thermodynamic properties of isotopic substances*, Jour. Chem. Soc., April, p. 562.

——, Lowenstan, H. A., Epstein, S., and McKinney, C. R. (1951) *Measurement of paleotemperatures and temperatures of the Upper Cretaceous of England, Denmark, and the Southeastern United States*, Geol. Soc. Am., Bull., vol. 62, p. 399–426.

Van Slyke, D. D., Folch, J., and Plazin, J. (1940) *Manometric carbon determination*, Biol. Chem., Jour., vol. 136, p. 509.

Institute for Nuclear Studies, University of Chicago, Chicago, Illinois.

Manuscript Received by the Secretary of the Society, March 8, 1950.

Project Grant 517/47/S48.

Addendum

We have delayed publication of this paper while it was in galley proof because we discovered disturbing variations in our temperature determination. We traced this to the use of heated copper oxide to remove impurities from helium gas passed over our samples during the heating process. Small amounts of oxygen from the copper oxide were present in the helium, and the carbon dioxide formed apparently exchanged in some cases with the calcium carbonate of the samples. Removal of all oxygen by means of a charcoal trap at liquid nitrogen temperature corrected these difficulties. Our tentative corrected temperature equation becomes $t = 14.8 - 5.41\delta$. The slope now agrees with McCrea's value. We will publish details of this temperature scale shortly.